ANTIPROTON DEUTERON INTERACTIONS FROM 1.60 TO 2.90 GeV/c

Thesis for the Degree of Ph. D. MICHIGAN STATE UNIVERSITY PAUL STANLEY EASTMAN 1972

LIBRAI Michigan Sale
University

ABSTRACT

ANTIPROTON DEUTERON INTERACTIONS

FROM 1.60 TO 2.90 GeV/c

By

Paul Stanley Eastman

In a bubble chamber experiment, the cross sections for zero- and two- through eight-prong topologies, along with the reaction cross sections within the two through six prong topologies for antiproton momenta from 1.60 to 2.90 GeV/c have been determined. Resonance production cross sections in antiproton-neutron multipion annihilations for multiplicities of three through six pions and their angular and momentum distributions are presented with comparisons of the predictions of a multiperipheral model and a statistical model. Particular emphasis has been given to investigating the isospin-one structure at center-of-mass energy of 2350 MeV derived from the total cross section measurements of antiproton-proton and antiproton deuteron interactions. The momentum to momentum dependence of the cross sections shows a possible enhancement in the ω production channels from the four and six pion annihilations, however further data at lower energies is necessary to confirm this enhancement.

ANTIPROTON DEUTERON INTERACTIONS

FROM 1.60 TO 2.90 GeV/c

Ву

Paul Stanley Eastman

A THESIS

Submitted to
Michigan State University
in partial fulfillment of the requirements
for the degree of

DOCTOR OF PHILOSOPHY

Department of Physics

1972

678868

ACKNOWLEDGMENTS

I wish to express my appreciation to Professor Gerald A. Smith for his help and guidance throughout the preparation of this thesis.

I would especially like to thank Professor Robert J. Sprafka for his confidence, his advice, his friendship, and his beer.

I wish also to thank Professor Z. Ming Ma and Dr. Benedict Y. Oh for help and advice throughout the analysis of this experiment and for the many helpful suggestions which have been given to me; and to thank Dr. Donald L. Parker for preceding me and smoothing the obstacles of analysis.

I also wish to acknowledge the programming efforts of Mr.

Sherwood K. Haynes II who many times has helped me to find the obvious.

I am grateful to our scanning and measuring staff for all their efforts; and also to the Michigan State University Computing Center staff without whose special help this thesis would still be many months from completion.

Last but not least, I would like to thank my wife, Sheila, for putting up with my research for the last three years.

This research was supported in part by the National Science Foundation.

TABLE OF CONTENTS

			Page
ACKNOWI	LEDGM	ENTS	ii
LIST O	F TAB	LES	v
LIST O	F FIG	URES	vii
Chapte	r		
1.	INTR	ODUCTION	1
2.	EXPE	RIMENTAL PROCEDURES	5
3.	TOPO	LOGICAL CROSS SECTIONS	
	3.1	Experimental Methods	10
	3.2	Cross Sections	11
	3.3	Conclusions	11
4.	REAC	TION CROSS SECTIONS	
	4.1	Experimental Methods	14
	4.2	Two Prong Cross Sections	17
	4.3	Three and Four Prong Cross Sections	20
	4.4	Five and Six Prong Cross Sections	30
	4.5	Conclusions	33
5.		NANCE PRODUCTION IN THE MULTIPION HILATIONS	
	5.1	Experimental Methods	38
	5.2	Three Pion Final States	41
	5.3	Four Pion Final States	41
	5.4	Five Pion Final States	46

Chapter		
	5.5 Six Pion Final States	46
	5.6 Conclusions	59
6.	UPPER LIMIT ON THE DECAY $\omega \rightarrow 2\pi$	64
7.	ANGULAR AND MOMENTUM DISTRIBUTIONS	69
8.	MODELS FOR NUCLEON-ANTINUCLEON ANNIHILATIONS	120
9.	SUMMARY AND CONCLUSIONS	128
LIST O	F REFERENCES	130

LIST OF TABLES

Table		Page
1.	Topological Event Statistics	7
2.	Topological Cross Sections in mb	12
3.	Reaction Cross Sections (mb) in the Two Prong Topology Corrected for One Prong Losses	19
4.	Reaction Cross Sections (mb) in the Three and Four Prong Topologies	27
5.	Reaction Cross Sections (mb) in the Five and Six Prong Topologies	34
6.	Reaction Cross Sections (mb) for Multipion Fits with Spectator Cuts	40
7.	Resonance production cross sections for the $\pi^+2\pi^-$ channel	43
8.	Resonance production cross sections in mb for the $\pi^+2\pi^-\pi^\circ$ channel	48
9.	Resonance production cross sections in mb for the $2\pi^+3\pi^-$ channel	53
10.	Resonance production cross sections in mb for the $2\pi^+3\pi^-\pi^\circ$ channel	58
11.	Legendre polynomial coefficients	
	11.1 Legendre Polynomial Coefficients from the three pion final state	79
	11.2 Legendre Polynomial Coefficients from the four pion final state	80
	11.3 Legendre Polynomial Coefficients from the five pion final state	81
	11.4 Legendre Polynomial Coefficients from	82

Table			Page
12.	Asymme	etry and Collimation parameters	
	12.1	Parameters for π^+ from the three pion final state	94
	12.2	Parameters for π^- from the three pion final state	95
	12.3	Parameters for π^{+} from the four pion final state	96
	12.4	Parameters for π^- from the four pion final state	97
	12.5	Parameters for π^o from the four pion final state	98
	12.6	Parameters for π^+ from the five pion final state	99
	12.7	Parameters for π^- from the five pion final state	100
	12.8	Parameters for π^+ from the six pion final state	101
	12.9	Parameters for π^- from the six pion final state	102
	12.10	Parameters for π° from the six pion final state	103

LIST OF FIGURES

Figure		Page
1.	Topological cross sections in mb	13
2.	Spectator momentum distributions in the multipion annihilations. The solid curves are the prediction of the deuteron wave function assuming an impulse model	
	2.1 Distribution for $\bar{p}d \rightarrow p\pi^+2\pi^-$	16 16 16 16 16
3.	Distributions from the analysis of events fitting the hypothesis $\bar{p}d \rightarrow pn\bar{p}\pi^+\pi^-$	
	3.1 Missing mass distribution of events classified as belonging to $\bar{p}d \rightarrow pn\bar{p}\pi^{+}\pi^{-}$. Shaded events also fit the hypothesis of multipion annihilation	23
	3.2 Angular distribution of the outgoing antiproton from events classified as belonging to pd → pnpπ ⁺ π ⁻ . Shaded events also fit the hypothesis of multipion annihilation	23
	3.3 Neutral particle mass distribution for events fitting $\bar{p}d \rightarrow p\bar{p}\pi^{+}\pi^{-}X^{\circ}$. Shaded events are those classified as belonging to	
	the hypothesis $\bar{p}d \rightarrow pn\bar{p}\pi^+\pi^-$	23
4.	multipion annihilation	23
	4.1 Missing mass squared distribution for events between 1.60 and 2.00 GeV/c	26

Figure		Page
	 4.2 Confidence level distribution for events between 1.60 and 2.00 GeV/c 4.3 Missing mass squared distribution for events between 2.15 and 2.90 GeV/c 4.4 Confidence level distribution for events between 2.15 and 2.90 GeV/c 	26 26 26
5.	Reaction cross sections for single and double pion production without annihilation in the three and four prong topologies. Other experiments shown are: (1) 1.96 GeV/c, ref. 19; (2) 2.8 GeV/c, ref. 20, 21; (3) 5.55 GeV/c, ref. 22; (4) 1.0 - 1.6 GeV/c, ref. 44	28
6.	Reaction cross sections for annihilation channels in the three and four prong topologies. pp data is from ref. ll	29
7.	Missing mass squared and confidence level distributions for events fitting the multipion annihilation hypothesis $\bar{p}d \rightarrow p \pi^+ \pi^+ \pi^- \pi^- \pi^- \pi^0$	
	 7.1 Missing mass squared distribution for events between 1.60 and 2.00 GeV/c 7.2 Confidence level distribution for events between 1.60 and 2.00 GeV/c 7.3 Missing mass squared distribution for events between 2.15 and 2.90 GeV/c 7.4 Confidence level distribution for events between 2.15 and 2.90 GeV/c 	32 32 32 32
8.	Reaction cross sections for annihilation channels in the five and six prong topologies. pp data is from ref. ll	36
9.	Resonance production cross sections for the $\pi^+2\pi^-$ channel	42
10.	Invariant mass distributions for the $\pi^+2\pi^-$ channel	45
11.	Resonance production cross sections for the $\pi^+2\pi^-\pi^\circ$ channel	47
12.	Invariant mass distribution for the $\pi^+2\pi^-\pi^\circ$	50

Figure		Page
13.	Resonance production cross sections for the $2\pi^+3\pi^-$ channel. Open points are $\bar{p}p_{I=1} \to \rho^\circ \rho^\circ \pi^\circ$ from reference 4	52
14.	Invariant mass distributions for the $2\pi^+3\pi^-$ channel	55
15.	Resonance production cross sections for the $2\pi^+3\pi^-\pi^\circ$ channel	57
16.	Invariant mass distributions for the $2\pi^+3\pi^-\pi^\circ$ channel	61
17.	Resolution ideogram of the error from invariant mass combinations between 0.7 $\rm GeV/c^2$ and 0.8 $\rm GeV/c^2$ with the mass fixed at 0.75 $\rm GeV/c^2$	
	17.1 Ideogram for events fitting $\bar{p}d \rightarrow p\pi^{+}2\pi^{-}$ for the momentum range 1.60 to 2.00 GeV/c 17.2 Ideogram for events fitting $\bar{p}d \rightarrow p2\pi^{+}3\pi^{-}$	67
	in the momentum range 1.60 to 2.00 GeV/c 17.3 Ideogram for events fitting $\bar{p}d \rightarrow p\pi^+2\pi^-$	67
	in the momentum range 2.15 to 2.90 GeV/c 17.4 Ideogram for events fitting $\bar{p}d \rightarrow p2\pi^{+}3\pi^{-}$	67
	in the momentum range 2.15 to 2.90 GeV/c	67
18.	Angular distributions for the three pion final state. The solid curves are fits to the Legendre polynomials	71
19.	Angular distributions for the four pion final state. The solid curves are fits to the Legendre polynomials	73
20.	Angular distributions for the five pion final state. The solid curves are fits to the Legendre polynomials	75
21.	Angular distributions for the six pion final state. The solid curves are fits to the Legendre polynomials	77
22.	Legendre polynomial coefficients	
	22.1 Legendre polynomial coefficients for π^+ from the four pion final state	84

Figure			Page
	22.2		0.5
	22.3	from the four pion final state Legendre polynomial coefficients for π°	85
	00.4	from the four pion final state	86
	22.4	Legendre polynomial coefficients for π^+ from the five pion final state	87
	22.5	Legendre polynomial coefficients for π^-	
	22.6	from the five pion final state Legendre polynomial coefficients for π^+	88
		from the six pion final state	89
	22.7	Legendre polynomial coefficients for π^- from the six pion final state	90
	22.8	Legendre polynomial coefficients for π°	
		from the six pion final state	91
23.	Asymm	etry and collimation parameters	
	23.1	Parameters for π^+ from the three pion final	
	23.2	state	94
	23.2	final state	95
	23.3		96
	23.4	final state	90
	00 5	final state	97
	23.5	Parameters for π° from the four pion final state	98
	23.6	Parameters for π^+ from the five pion	00
	23.7	final state	99
		final state	100
	23.8	Parameters for π^+ from the six pion final state	101
	23.9	Parameters for π^- from the six pion	
	23 10	final state	102
	20110	final state	103
24.	Cente	r-of-mass longitudinal and transverse momentum	
		ibutions. The solid curves are fits to stical model predictions	
		·	
	24.1	Longitudinal momentum distributions from three pion final states between 1.60 and	
		2.00 GeV/c	106

Figure			Page
	24.2	Transverse momentum distributions from three pion final states between 1.60 and	
	24.3	2.00 GeV/c	107
	24.4	2.00 GeV/c	108
	24.5	and 2.00 GeV/c	109
	24.6		110
	24.7		111
	24.8	five pion final states between 1.60 and 2.00 GeV/c	112
	24.9	five pion final states between 1.60 and 2.00 GeV/c	113
		five pion final states between 2.15 and 2.90 GeV/c	114
	24.10	Transverse momentum distributions from five pion final states between 2.15 and 2.90 GeV/c	115
	24.11	Longitudinal momentum distributions from six pion final states between 1.60 and 2.00 GeV/c	116
	24.12	Transverse momentum distributions from six pion final states between 1.60 and	
	24.13	six pion final states between 2.15 and	117
	24.14	2.90 GeV/c	118
25.	Regge	2.90 GeV/c	119
	CLA mo		
	25.2 25.3	Three pion final state	122 122 122 122

Figure		Page
26.	Comparison of the multipion annihilations with the multiperipheral and statistical models. Solid (dashed) curves are predictions of the multiperipheral (statistical) model	125

CHAPTER 1

INTRODUCTION

Antiproton-deuteron interactions are interesting as a means for studying antiproton-neutron interactions. There is no available source of free neutrons for use as a target; however the deuteron with its low binding energy of 2.2 MeV provides a source of almost free neutrons which may be used as a target. When the range of interaction and the wavelength of the incident particle are short compared with the separation of the individual nuclei within the nucleus, the incident particle can interact with a single nucleon. Thus, in deuterium the beam particle can interact with one of the nucleons leaving the "spectator" nucleon with the same momentum it had before the interaction. This is called the "impulse model" and is the basic assumption in using deuterons as a source of neutron targets.

In a high statistics counter experiment in 1967, Abrams et.al. 1 measured the total cross section for antiprotons on hydrogen and deuterium and found structure in both total cross sections. This structure in itself is not unique since structure has been found in the total cross sections for π 's and K's in both hydrogen and deuterium 2 . One possible interpretation for the structure is that some final state is rising sharply from its threshold value causing an inflection in the total cross section. An example of this is seen in both K-p and K-d interactions where there is a rapid increase of the

total cross section starting at the threshold for the production of the K*(890). Another possible interpretation for such structure is the formation of a direct channel resonance such as occurs in the π^+ p interactions wherein the total cross section peaks strongly as the total center-of-mass energy passes through the region of the Δ^{++} (1236) resonance.

The antiproton-neutron system is an eigenstate of isospin with an eigenvalue of one, I=1, while the antiproton-proton system is a superposition of two such eigenstates with eigenvalues I=1 and I=0. Thus by combining the total cross sections for antiprotons on protons and deuterons, the experimenters of reference I were able to determine the isospin component cross sections of antiproton-nucleon interactions. By fitting the I=1 total cross sections to a smooth polynomial background, they found two "bumps" which, assuming Breit-Wigner descriptions, were referred to as the π_1^* (2190, 85) and the π_1^* (2350, 140), where the subscript is the isospin and (E_0, Γ) are the center-of-mass energies and full center-of-mass widths in MeV. The corresponding incident momentum and height for these structures are 1.32 GeV/c and 5.5 mb for the π_1^* (2190) and 1.77 GeV/c and 3.2 mb for the π_1^* (2350). Several experiments have been performed to attempt to determine the origin of these structures. One such study 3 , tried to explain the π_1^* (2190) as a threshold effect from single pion production without annihilation and concluded that an excitation curve sufficient to explain the structure was inconsistent with the data. A formation experiment⁴ has reported an enhancement in the $\rho\rho\pi$ cross section at 2190 MeV with a width 20 MeV $\leq \Gamma \leq 80$ MeV which the experimenters

associate with the $\pi_1^*(2190)$. Similarly, missing mass experiments $^{5-7}$ in π^-p gave evidence for narrow boson resonances with I=1 or 2 at energies of 2195 MeV, the T meson(width less than 13 MeV), and 2375 MeV, the U meson (width of about 30 MeV); however the reported widths are much narrower than those reported in the $\bar{p}p$ and $\bar{p}d$ total cross sections.

In this thesis, a comprehensive study of inelastic antiproton-deuteron interactions between 1.60 GeV/c and 2.90 GeV/c is presented. Emphasis has been placed on the topological, reaction, and resonance production cross sections with particular regard to searching for the origins of the I=l structures in the total cross section using the antiproton-neutron annihilations. An earlier study in the 1.60 GeV/c to 2.00 GeV/c momentum region as well as a $\bar{p}p$ exposure in the same energy range has led to a published report⁸ of an I=l enhancement in the K*K $\pi\pi$ final state centered at 2360 ± 25 MeV but with a width, Γ < 60 MeV. Both the mass and the width of this enhancement agree with those of the U meson, however, the narrow width is inconsistent with that observed for the $\pi_1^*(2350)$.

A study of the angular and momentum dependence of the multipion annihilations is also presented. The angular dependence is analyzed in terms of both Legendre polynomials and collimation and asymmetry parameters. Furthermore, the collimation and asymmetry parameters are discussed in relation to the general features of a multiperipheral multi-Regge pole model. The center-of-mass longitudinal momentum distributions and transverse momentum distributions of the individual pion charge states are compared with predictions of a statistical model, with quite good agreement. In addition, the general features

of the multipion annihilations are discussed in terms of both a multiperipheral model and a statistical model.

CHAPTER 2

EXPERIMENTAL PROCEDURES

The data used in this thesis was obtained from two separate exposures of deuterium to antiproton beams from the Zero Gradient Synchroton at the Argonne National Laboratory. The exposures, taken in the 30-inch MURA bubble chamber, consisted of (1) 130,000 stereo triads at incident momenta 1.60, 1.75, 1.85 and 2.00 GeV/c (total center-of-mass energies of 2289, 2342, 2378 and 2430 MeV) and (2) 126,000 stereo triads at 2.15, 2.30, 2.45, 2.60 and 2.90 GeV/c (total center-of-mass energies of 2483, 2534, 2586, 2636, and 2736 MeV.).

The 1.60 - 2.00 GeV/c film was scanned for all 2-8 prong events (events with 2-8 charged tracks leaving the interaction vertex) and for all events with neutral vee decays (decays where an unseen neutral particle decays into two charged particles which leave tracks in the bubble chamber) and one-sixth of the film was rescanned. A list was made of all events on which the two scans disagreed as to the existence of an event or its event type and these events were looked at again to resolve the differences. From the overlap of the two independent scans, it was possible to determine the efficiency (the number of events found on a single scan divided by the calculated total number of events in the fiducial volume) for each topology at each momentum. Typical single scan efficiencies for this film were 92% for events without neutral vee

decays and are listed in Table 1.

The combined antiproton-proton, antiproton-neutron, and antiproton-deuteron elastic cross sections are a large fraction of the total antiproton-deuteron cross section 1,10 and are dominated by interactions with very low momentum transfer from the antiproton beam to the target. The principle characteristic of these events is that the elastically scattered antiprotons in the low momentum transfer region cannot be distinguished from the antiprotons which do not interact. Thus for this and other reasons one prong events were not looked at in this experiment since the scanning losses would be too great and there would be little justification for the amount of effort expended.

The 2.15 - 2.90 GeV/c film was scanned for events with neutral vee decays and in two independent scans was simultaneously scanned and measured for 3- and 4-prong events, 5- and 6-prong events. In addition, an interaction count was made on 0-, 7-, and 8-prong events on a limited sample of the film at selected momenta. One-third of this film was second scanned for 3- and 4-prong, and 5- and 6-prong events and typical scan efficiencies found were 87% and 83% respectively. Since a similar investigation of the antiproton-proton system was being conducted in the same momentum range in two separate bubble chamber exposures, only one-sixth of the 2.15 - 2.90 GeV/c film was scanned for 4-prong and 6-prong events. The results of the study of the antiproton-proton system are described elsewhere. 10

Approximately 80% of the 1.60 - 2.00 GeV/c film was scanned and measured at Lawrence Berkeley Laboratory. The remainder of this exposure and the 2.15 - 2.90 GeV/c exposure was measured using image

Table 1. Topological Event Statistics

		Measuring and	Scanning Stati	stics
D		Number of		Number of
PL	Event type	events found	Scanning	events used
(GeV/c)		on complete	efficiency	in the final
		first scan	(%)	physics analysis
1.60	2 pmonas	22600	00.0	26724
1.00	2-prongs	32680	90.9	26724
	3-prongs	9158	92.9	7831
	4-prongs	20271	92.9	16949
	5-prongs	4411	97.6	2885
	6-prongs	5290	97.6	3611
1.75	2-prongs	19720	93.3	16348
	3-prongs	5850	90.3	5091
	4-prongs	11793	90.3	10107
	5-prongs	2713	96.0	1846
	6-prongs	3258	96.0	2353
1.85	2-prongs	20281	93.8	17259
	3-prongs	6003	94.2	524 0
	4-prongs	12405	94.2	10751
	5-prongs	2952	95.7	1946
	6-prongs	3534	95.7	2547
2.00	2-prongs	11246	92.8	9363
	3-prongs	5252	92.3	4663
	4-prongs	11851	92.3	9844
	5-prongs	2518	96.1	1835
	6-prongs	2842	96.1	2378
2.15	3-prongs	3466	83.1	3087
2	4-prongs	5030	82.2	4243
	5-prongs	182 4	83.7	1504
		389	79.1	328
2.30	6-prongs			
2.30	3-prongs	3527	78.0	3309
	4-prongs	1599	84.5	1729
	5-prongs	1948	83.4	1612
0.45	6-prongs	450	83.4	374
2.45	3-prongs	3360	77.8	2992
	4-prongs	1528	83.9	1451
	5-prongs	1841	83.4	1550
	6-prongs	449	83.4	370
2.60	3-prongs	4099	77.5	3886
	4-prongs	1457	86.1	1354
	5-prongs	2428	83.4	2056
	6-prongs	510	83.4	417
2.90	3-prongs	3417	77.6	3110
	4-prongs	1384	86.2	1312
	5-prongs	1959	83.2	1682
	6-prongs	496	85.0	424

Conflict Scanning Statistics

Event type	P _L (GeV/c)	Number of good events found on first scan	Number of good events found on second scan	Number of good events found on both scans
3- and 4-prongs	1.60	1389	1259	1170
	1.75	1337	1322	1194
	1.85	1111	1161	1094
	2.00	1070	1060	978
	2.15	976	1048	900
	2.30	1041	1143	937
	2.45	1186	1252	1094
	2.60	1003	995	921
	2.90	920	963	864
5- and 6-prongs	1.60	468	410	376
	1.75	441	441	403
	1.85	404	391	357
	2.00	392	369	339
	2.15	1214	1355	1102
	2.90	1362	1472	1240

plane digitizers at Michigan State University. The measured events were processed through the three-dimensional geometric reconstruction program, $TVGP^{11}$, and the kinematic fitting program, $SQUAW^{12}$ using the Michigan State University CDC 3600. Events which failed reconstruction on the first attempt were remeasured resulting in an overall passing rate (percentage of scanned events for which one or more of the attempted hypotheses was successfully fitted) of between 90% and 95%. In order to reduce bias in the final sample, the acceptance criteria for fits of measured events was made deliberately loose (i.e., successful fits correspond to confidence levels greater than 10^{-5} .) This procedure resulted in many events successfully fitting more than one hypotheses.

CHAPTER 3

TOPOLOGICAL CROSS SECTIONS

3.1 Experimental Methods

The antiproton-deuteron cross section in the 1.60 - 2.90 GeV/c momentum range is sufficiently large that several interactions occur in each frame. The calculation of σ/N , the cross section per event, was based on a track count and an attenuation factor determined from the mean interaction length

$$\ell = \frac{2}{\sigma_t \rho A_0} \tag{1}$$

where $\sigma_{\mathbf{t}}$ is the total antiproton-deuteron cross section from reference 1, ρ is the density of liquid deuterium, and A_0 is Avagodro's number. The total number of tracks at each momentum, $N_{\mathbf{tks}}$, was determined by counting the number of tracks entering the fiducial volume (the volume of the bubble chamber common to all three views) on every 50th frame. The cross section per event was then calculated from

$$\frac{\sigma}{N} = \frac{\sigma t}{N_{tks}(1-e)}$$
 (2)

where the effective length of the bubble chamber, λ , was determined from the limits of the interaction vertex positions of events and the paths of tracks in the chamber.

3.2 Cross Sections

Table 2 and Figure 1 show the topological cross sections which were obtained from multiplying σ/N at each momentum by the number of events of a given topology found in the scanning and corrected by the efficiency for that scan. To determine whether or not any of the $\pi_1^*(2350)$ was present in the data, both the three and the five prong cross sections were individually subtracted from the total I=1 cross section. The remaining I=1 cross section was then fitted to a six parameter function.

$$\sigma_{1} = \left[\sum_{i=0}^{4} \frac{a_{i+1}}{E^{i}}\right] + a_{6} \left[\sum_{p^{*}} \frac{\pi N}{[(E-E_{0}) \frac{2}{F}]^{2} + 1}\right]$$
(3)

where p* is the \bar{p} c.m. momentum, E the \bar{p} n total c.m. energy and N a normalization factor which is adjusted to give a value of 3.2 mb for the $\pi_1^*(2350)$ in the total I=1 cross section.

3.3 Conclusions

The fits showed that the three prong events could account for $a_6(E=E_0) \times 3.2 \text{ mb} = 0.34 \pm 3.67 \text{ mb}$ of the enhancement while the five prong events showed a contribution of $a_6(E=E_0) \times 3.2 \text{ mb} = -0.80\pm3.03 \text{ mb}$ where $E_0 = 2350 \text{ MeV}$. Obviously, these results neither support nor rule out any association of these channels with the $\pi_1^*(2350)$. For an accurate determination of the contribution to the enhancement cross section, this method of fitting a subtracted background requires many closely spaced points with small relative errors neither condition being met by the present data.

Table 2. Topological Cross Sections in mb

MOM TOPOLOGY	1.60	1.75	1.85	2.00	2.15	2.30	2.45	2.60	2.90
0 Prong	5.9±.05	1	•	5.19±0.6	1	1	5.1±0.5	1	5.2 ±0.6
2 Prong	54.8±1.7	52.6±1.6	53.3±1.6	52.0±1.5	•	ı	ı		•
3 Prong	16.76±0.50	17.10±0.51	51 16.23±0.49 15.69±0.47	15.69±0.47	12.70±0.38	14.20±0.49	13.04±0.45	12.87±0.44	12.60±0.44
4 Prong	37.4±1.1	35.0±1.1	34.4±1.0	34.3±1.0	31.9±0.9	31.7±1.2	32.9±1.3	28.9±1.2	29.4±1.2
5 Prong	7.73±0.40	7.54±0.40	7.97±0.40	7.47±0.40	6.66±0.40	7.34±0.40	6.67±0.40	7.09±0.40	6.72±0.40
6 Prong	9.28±0.50	9.05±0.50	9.55±0.50	9.55 ± 0.50	9.41±1.0	9.04+0.9	9.74±1.0	10.26±1.0	10.71±1.1
7 Prong	.344±.043	.400±.053	.420±.055	.458±.066	ı	ı	.75±0.2	ı	.89±0.12
8 Prong	.331±.042	.335±.046	.400±.052	.458±.066	•	ı	.75±0.2		.92±0.12
Observed vee decay events	2.38±0.08	2.39±0.08	2.55±0.07	2.45±0.08	2.38±0.09	2.43±0.09	2.44±0.09	2.51±0.08	2.50±0.09
Sum	135±4	130±4	130±4	128±4	ı	ı	ı	•	•
Estimated* 1 Prong	42±4	42±4	38±4	35±4					

* The estimated one prong cross section was obtained by subtracting the sum of the observed cross section from the total cross sections of reference 1.

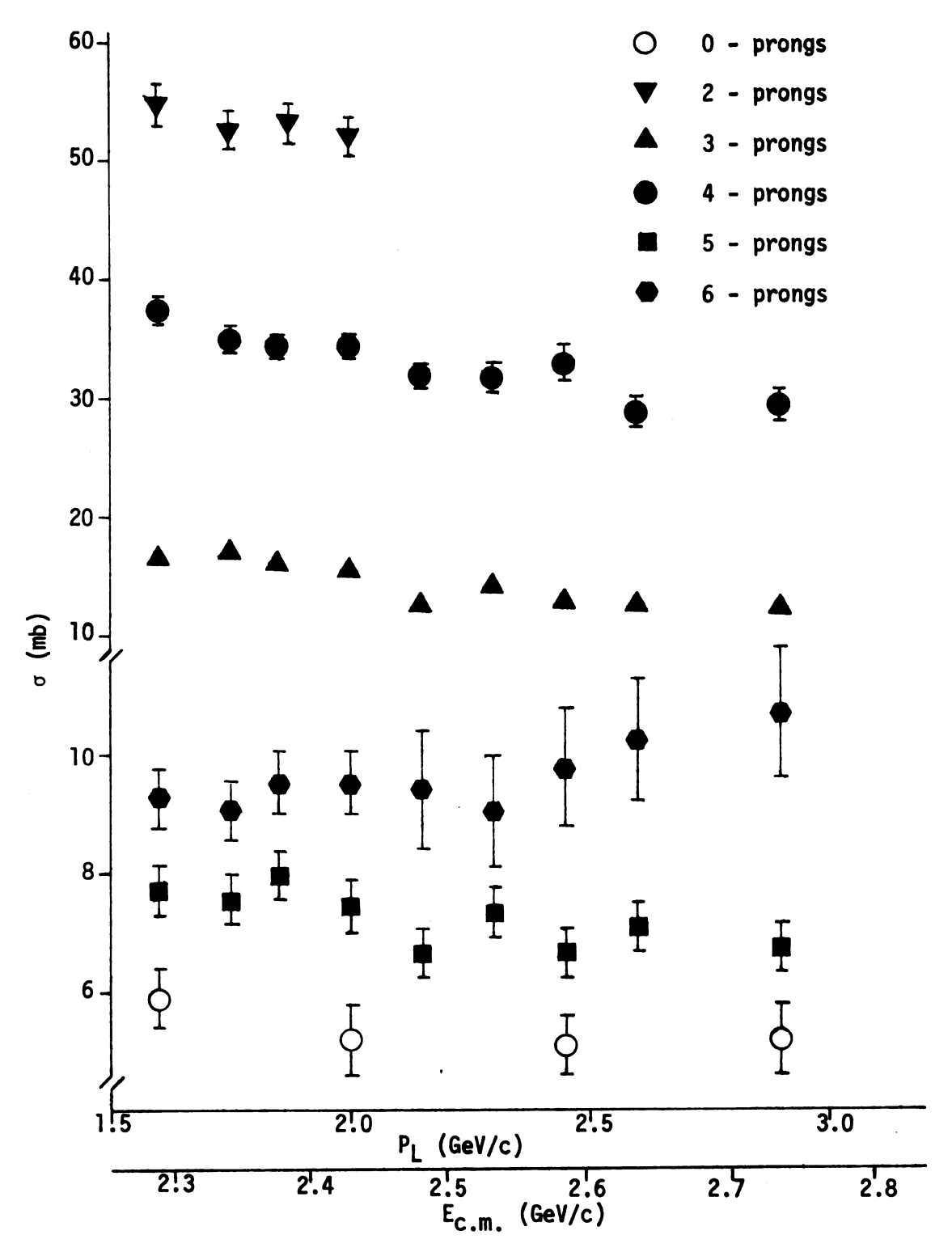


Figure 1. Topological cross sections in mb

CHAPTER 4

REACTION CROSS SECTIONS

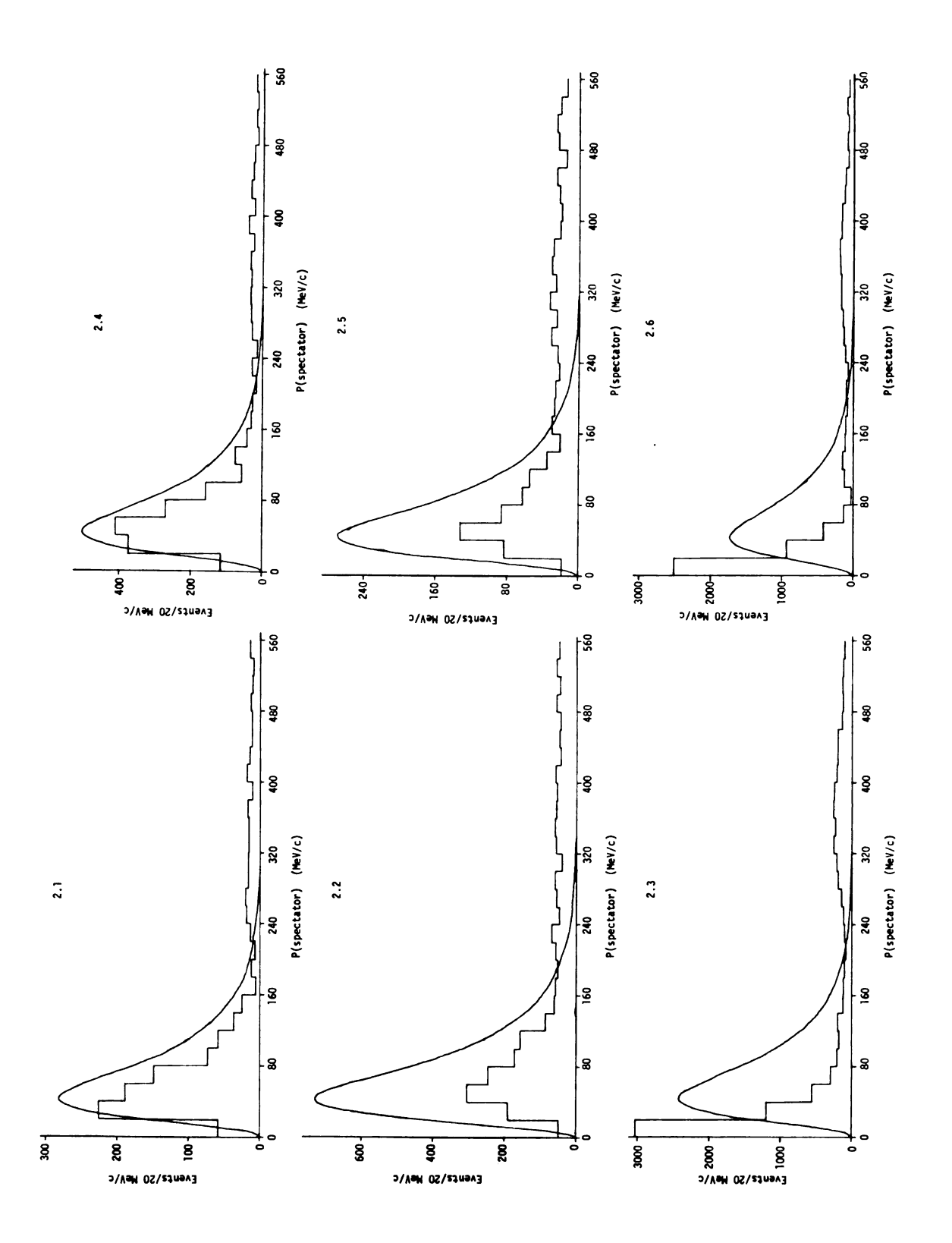
4.1 Experimental Methods

Since the fitting criteria were made deliberately loose (i.e., successful fits correspond to confidence levels greater than 10^{-5}), additional cuts, which will be explained later, were made on the confidence levels and missing mass values. The individual reaction cross sections were corrected for events lost through failure of the reconstruction programs by normalizing to the topological cross sections, using the total available sample after reconstruction. This procedure eliminates any bias of the reconstruction programs toward any individual topology and eliminates a second renormalization in topologies where only a partial sample of the film was measured.

The momentum distribution of the spectator nucleon in the annihilation channels showed a large excess of events in the high momentum tail. This excess of events, which appears to come from throughout the undistorted distribution, is attributed to secondary scattering of the spectator nucleon by the pions 13. This effect resulted in a larger contribution to the cross sections from even prong events than would be expected if the spectator momentum was that predicted by the impulse model. Figure 2 shows the spectator momentum distributions

Figure 2. Spectator momentum distributions in the multipion annihilations. The solid curves are the prediction of the deuteron wave function assuming an impulse model

- 2.1 Distribution for $\bar{p}d \rightarrow p\pi^+2\pi^-$ 2.2. Distribution for $\bar{p}d \rightarrow n2\pi^+2\pi^-$ 2.3 Distribution for $\bar{p}d \rightarrow p\pi^+2\pi^-\pi^\circ$ 2.4 Distribution for $\bar{p}d \rightarrow p2\pi^+3\pi^-$ 2.5 Distribution for $\bar{p}d \rightarrow n3\pi^+3\pi^-$ 2.6 Distribution for $\bar{p}d \rightarrow p2\pi^+3\pi^-\pi^\circ$



for six different annihilation reactions within the three through six prong topologies compared with the Moravcsik III wave function 14 normalized to the same area under the curves. Figures 2.1 and 2.4 are the nucleon spectator momentum distributions for the four constraint fits $\bar{p}d \rightarrow p\pi^+2\pi^-$ and $\bar{p}d \rightarrow p2\pi^+3\pi^-$. Figures 2.2, 2.3, 2.5 and 2.6 show the spectator distributions for the one constraint fits $pd \rightarrow n2\pi^{+}2\pi^{-}$, $\bar{p}d \rightarrow p\pi^+2\pi^-\pi^\circ$, $\bar{p}d \rightarrow n3\pi^+3\pi^-$, and $\bar{p}d \rightarrow p2\pi^+3\pi^-\pi^\circ$ respectively. In the fits with a π° , the large distortion of the lower momentum data arises from the odd (three and five) prong events. When the spectator is not seen in the bubble chamber its momentum is set to zero with errors of 30 MeV, 30 MeV, and 40 MeV in the x, y and z directions. These errors allow the fitted momentum of the spectator to be adjusted properly when all other particles involved in the final reaction are directly accounted for, however, when there is another unseen particle such as in the case of the π° , the errors in the momentum of the unseen particle do not allow sufficient adjustment of the spectator momentum. Thus the momentum of the spectator is held close to the initial assumption in the optimized fit.

All errors in the reaction cross sections are statistical with a minimum of 3%. All the cross sections are observed cross sections with no cuts on the momentum of the spectator nucleon and no corrections for the shadowing of one nucleon by another as described by Glauber¹⁵ and Franco and Glauber¹⁶.

4.2 <u>Two-Prong Cross Sections</u>

Measurements of 76,000 two-prong events in the 1.60 GeV/c to 2.90 GeV/c momentum range have been completed with each event fitted

to the following hypotheses:

$$\vec{p}d \rightarrow pn\vec{p}$$
 (4a)
 $\rightarrow p\pi^{-}$ (4b)
 $\rightarrow p\pi^{-}\pi^{\circ}$ (4c)
 $\rightarrow d\vec{n}\pi^{-}$ (4d)
 $\rightarrow d\vec{p}$ (4e)
 $\rightarrow d\vec{p}\pi^{\circ}$ (4f)
 $\rightarrow n\pi^{+}\pi^{-}$ (4g)

and the corresponding zero-constraint "missing mass fits." One other zero-constraint fit:

$$\bar{p}d \rightarrow \bar{p}\pi^{+}MM$$
 (4h)

was also tried. Both reactions (4b) and (4e) were four constraint fits and were accepted into the hypothesis if the confidence level exceeded 10^{-4} . Antiproton-deuteron elastic scattering, reaction (4e), has been previously published⁹. Reactions (4c) and (4g) have extremely small cross sections, on the order of one hundred μ b, and the latter hydrogen like reaction can best be described elsewhere 10,17,18, thus no attempt has been made to separate these reactions from the missing mass channels. No events were found which fit hypothesis (4b) and an upper limit is listed in Table 3. Most of the data reduction in the two-prong topology has been done and is included with the permission of Dr. Z. Ming Ma. The reaction cross sections from the two-prong events corrected for losses in the one-prong events are shown in Table 3.

Table 3. Reaction Cross Sections (mb) in the Two Prong Topology Corrected for One Prong Losses

MOM REACTION	1.60	1.75	1.85	2.00	
pd → pnp	29.3 ± 1.7				
→ p̄d	37.9 ± 1.6	37.3 ± 2.7	32.7 ± 2.5	32.4 ± 3.2	
→ p̄dπ°	1.21 ± 0.05	1.65 ± 0.07	1.83 ± 0.08	1.82 ± 0.10	
→ ndπ	1.34 ± 0.05	1.51 ± 0.07	1.67 ± 0.07	1.87 ± 0.10	
→ pπ ⁻	< 2 μb	< 3 μb	< 3 μb	< 5 μb	

4.3 Three and Four Prong Cross Sections

Measurements have been made of 24,000 3-prong and 49,000 4-prong events in the 1.60 - 2.90 GeV/c film and 16,000 3-prong and 9,700 4-prong events in the 2.15 - 2.90 GeV/c film. Each measured event was fitted to the following hypotheses:

$$\bar{p}d \rightarrow pp\bar{p}\pi^{-} \qquad (5a)$$

$$\rightarrow pp\bar{p}\pi^{-}\pi^{\circ} \qquad (5b)$$

$$\rightarrow pp\bar{n}\pi^{-}\pi^{-} \qquad (5c)$$

$$\rightarrow pn\bar{p}\pi^{+}\pi^{-} \qquad (5d)$$

$$\rightarrow p\pi^{+}\pi^{-}\pi^{-} \qquad (5e)$$

$$\rightarrow p\pi^{+}\pi^{-}\pi^{-}\pi^{\circ} \qquad (5f)$$

and the corresponding zero-constraint missing mass fits. The fourprong events were also fitted to the hypotheses:

 \rightarrow pK⁺K⁻ π ⁻

$$\bar{p}d \rightarrow d\bar{n}\pi^{+}\pi^{-}\pi^{-} \tag{5h}$$

$$\rightarrow d\bar{p}\pi^{+}\pi^{-} \tag{5i}$$

(5g)

$$\rightarrow d\bar{p}\pi^{\dagger}\pi^{-}\pi^{\circ} \tag{5j}$$

$$\rightarrow n\pi^{+}\pi^{+}\pi^{-}\pi^{-} \tag{5k}$$

and their corresponding missing mass fits.

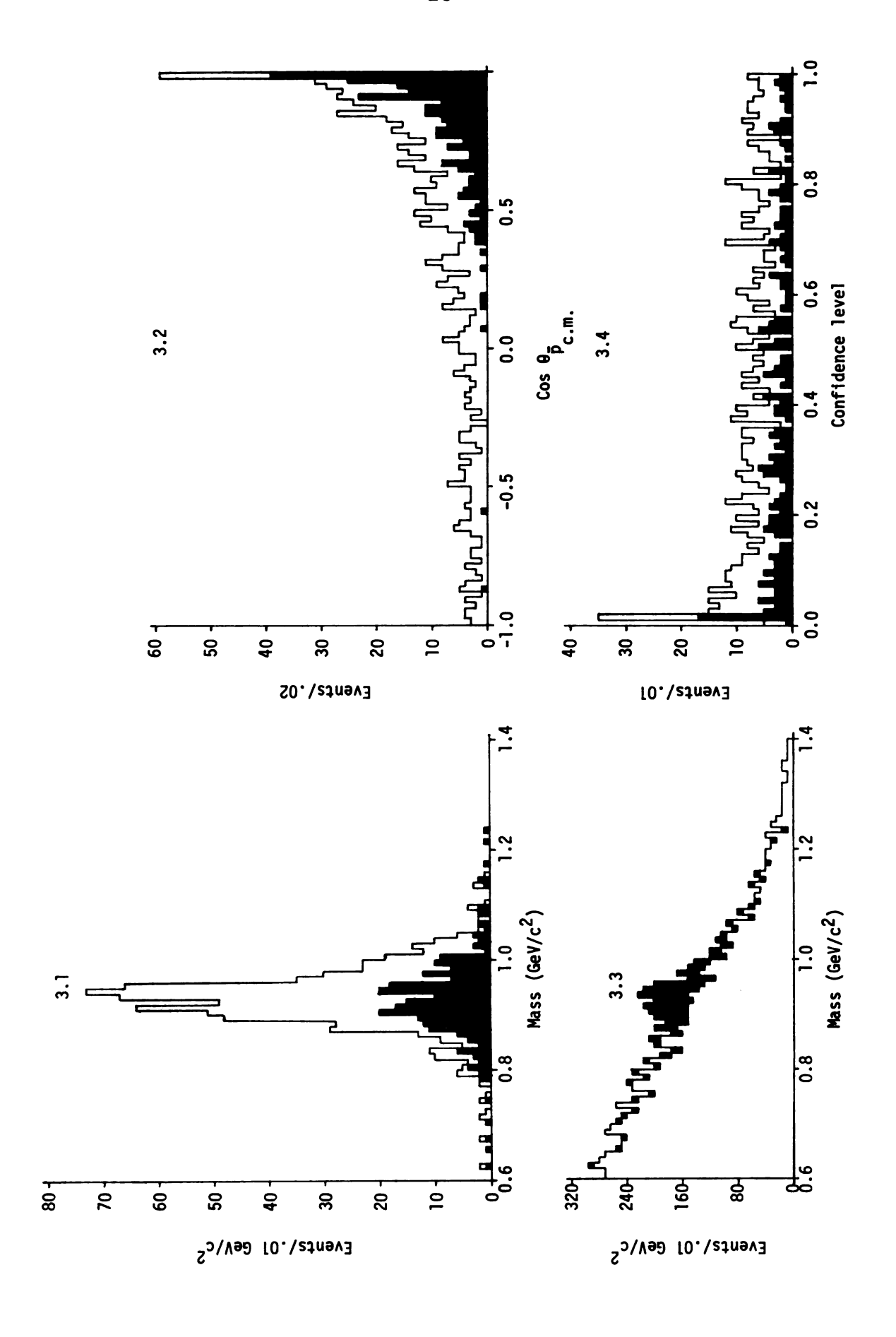
The three double pion production channels (5b) - (5d) rise sharply from the $\Delta\bar{\Delta}$ threshold and therefore were only analyzed in the 2.15 - 2.90 GeV/c data. An ionization study (a comparison of the predicted bubble density with that observed in the film) allowed the complete separation of (5b) and (5c) due to the presence of at least two slow charged nucleons in the laboratory system. About one-half the events classified as belonging to hypothesis (5d) had antiprotons with

a momentum greater than 1.2 GeV/c in the lab (relative ionization of less than 1.5) and thus were ambiguous with the missing mass class pd $\rightarrow p\pi^{+}\pi^{-}\pi^{-}_{MM}$ even after the ionization analysis.

Figure 3.1 shows the missing mass distribution of the events classified as belonging to hypothesis (5d) with the shaded events representing those events which were ambiguous between reaction (5d) and $pd \rightarrow p\pi^{+}\pi^{-}\pi^{-}MM$. The confidence level distribution for events classified as belonging to (5d) is shown in Figure 3.4 with the shaded regions representing the ambiguous events. Similarly, Figure 3.2 shows the angular distribution of the outgoing antiproton from the events belonging to reaction (5d). All three of these figures indicate that those events which were ambiguous with the reaction $pd \rightarrow p\pi^{+}\pi^{-}\pi^{-}MM$ (the shaded events) belong to hypothesis (5d). Thus, unless the ionization ruled out the nucleon hypothesis, the event was determined to belong to (5d). This is further justified by Figure 3.3 where all events from the three and four prong topologies that had at least one of their fits corresponding to $\bar{p}d \rightarrow \bar{p}p\pi^{+}\pi^{-}X^{\circ}$ (where X° represents any neutral particle or any combination of neutral particles) are plotted with the shaded portions representing those events classified as belonging to hypothesis (5d).

Both reactions (5a) and (5e) were four-constraint hypotheses and were accepted if their confidence levels for the fits were greater than 10^{-3} . Events fitting reaction (5f) were accepted if their confidence level was greater than 10^{-3} and the missing mass squared was within 2.5 standard deviations of the nominal value of the π° mass

- Figure 3. Distributions from the analysis of events fitting the hypothesis $\bar{p}d \rightarrow pn\bar{p}\pi^+\pi^-$
 - 3.1 Missing mass distribution of events classified as belonging to $\bar{p}d \rightarrow pn\bar{p}\pi^{\dagger}\pi^{-}$. Shaded events also fit the hypothesis of multipion annihilation.
 - 3.2 Angular distribution of the outgoing antiproton from events classified as belonging to $\bar{p}d \rightarrow pn\bar{p}\pi^{\dagger}\pi^{-}$. Shaded events also fit the hypothesis of multipion annihilation.
 - 3.3. Neutral particle mass distribution for events fitting $\bar{p}d \rightarrow p\bar{p}\pi^+\pi^-X^\circ$. Shaded events are those classified as belonging to the hypothesis $\bar{p}d \rightarrow pn\bar{p}\pi^+\pi^-$
 - 3.4 Confidence level distribution of events classified as belonging to $\bar{p}d \rightarrow pn\bar{p}\pi^{T}\pi^{T}$. Shaded events also fit the hypothesis of multipion annihilation.



squared and with an upper limit of mass squared of 0.3 GeV². Analysis of these events showed a significant amount of contamination on the high side of the π° mass.

By requiring the confidence level to be greater than 10^{-1} , the contamination was significantly reduced. The missing mass squared distributions for events fitting reaction (5f) are shown in Figure 4.1 for events in the 1.60 GeV/c to 2.00 GeV/c and Figure 4.3 for events in the 2.15 GeV/c to 2.90 GeV/c incident momentum ranges. The confidence level distributions for reaction (5f) for the 1.60 GeV/c to 2.00 GeV/c and 2.15 GeV/c to 2.90 GeV/c incident momentum ranges are shown in Figures 4.2 and 4.4 respectively. The shaded regions represent those events excluded by the 10^{-1} confidence level cut. The total reaction cross section was then calculated by fitting the remaining (i.e. unshaded) missing mass squared distributions to a Breit-Wigner line shape centered around the π° mass squared value to obtain the true number of events and then correcting this number for those events excluded by the cut by multiplying by 10/9.

The hydrogen-like reaction (5k) also was contaminated on the high side of the neutron mass. The analysis was treated similarly, but since the mass of the neutron is much greater than that of the pion it was necessary to fit the missing mass squared spectrum to a Gaussian rather than a Breit-Wigner.

The four-constraint reaction (5g) was accepted if the confidence level of the fit was greater than 10^{-3} . However, an additional requirement that the ionization be consistent with the kaon interpretations was imposed on the final sample. Table 4 and Figures 5 and 6 show the

- Figure 4. Missing mass squared and confidence level distributions for events fitting the multipion annihilation hypothesis $\bar{p}d \rightarrow p\pi^+\pi^-\pi^-\pi^\circ$
 - 4.1 Missing mass squared distribution for events between 1.60 and 2.00 GeV/c
 - 4.2 Confidence level distribution for events between 1.60 and 2.00 GeV/c
 - 4.3 Missing mass squared distribution for events between 2.15 and 2.90 GeV/c
 - 4.4 Confidence level distribution for events between 2.15 and 2.90 GeV/c

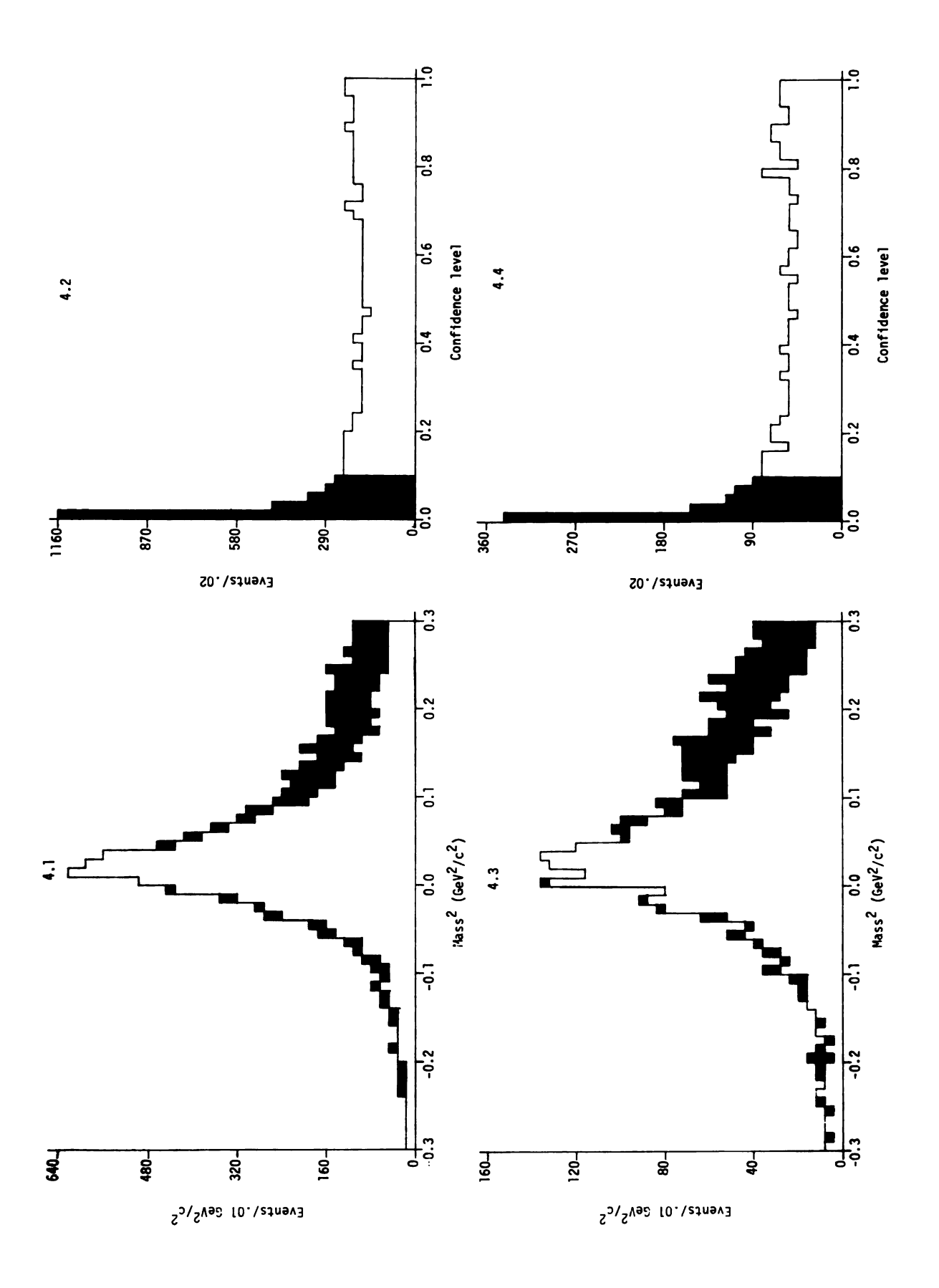


Table 4. Reaction Cross Sections (mb) in the Three and Four Prong Topologies

P _L REACTION	1.60	1.75	1.85	2.00	2.15	2.30	2.45	2.60	2.90
_π₫qq+b₫	3.08±.08	3.76±.11	3.75±.11	4.53±.11	4.21±.16	4.54±.21	4.84±.23	4.36±.18	4.01±.20
→pppπ-π°	ı	ı	ı	•	.158±0.60	.337±.052	.442±.069	.550±.069	.769±.077
-#_##dd+	ı	ı	ı	ı	.068±.055	.061±.037	.156±.045	.193±.043	.324±.059
- # #dud+	1	•	ı	1	.773±.122	1.377±.136	1.672±.172	1.468±.143	2.67±.21
-#-#-#d+	1.112±.049	.857±.054	.819±.051	.692±.048	.562±.056	.342±.052	.549±.088	.294±.051	.228±.049
• # _ # _ # d ←	6.64±.13	6.12±.14	5.71±.13	4.83±.13	3.75±.15	3.37±.20	3.18±.22	2.87±.20	2.41±.19
-#-#+##+	2.15±.07	1.91±.08	1.74±.07	1.57±.07	1.26±.10	1.11±.14	1.11±.16	.87±.14	.87±.14
+pK ⁺ K ⁻ "	.257±.032	.202±.030	.181±.026	.238±.025	.128±.032	.200±.040	.155±.044	.114±.030	.133±.40
Sum	13.24±.18	12.85±.20	12.20±.19	12.20±.19 11.86±.19	10.91±.29	11.34±.36	12.10±.35	10.72±.35	11.41±.39
3 prong missing mass	10.45±.32	10.61±.33	10.02±.31 9.63±.30	9.63±.30	7.59±.25	8.70±.27	7.89±.24	7.44±.23	7.24±.22
4 prong missing mass	30.47±.92	28.64±.86	28.42±.86	28.42±.86 28.49±.86	26.08±.81	25.88±.78	25.94±.79	21.75±.67	23.34±.73

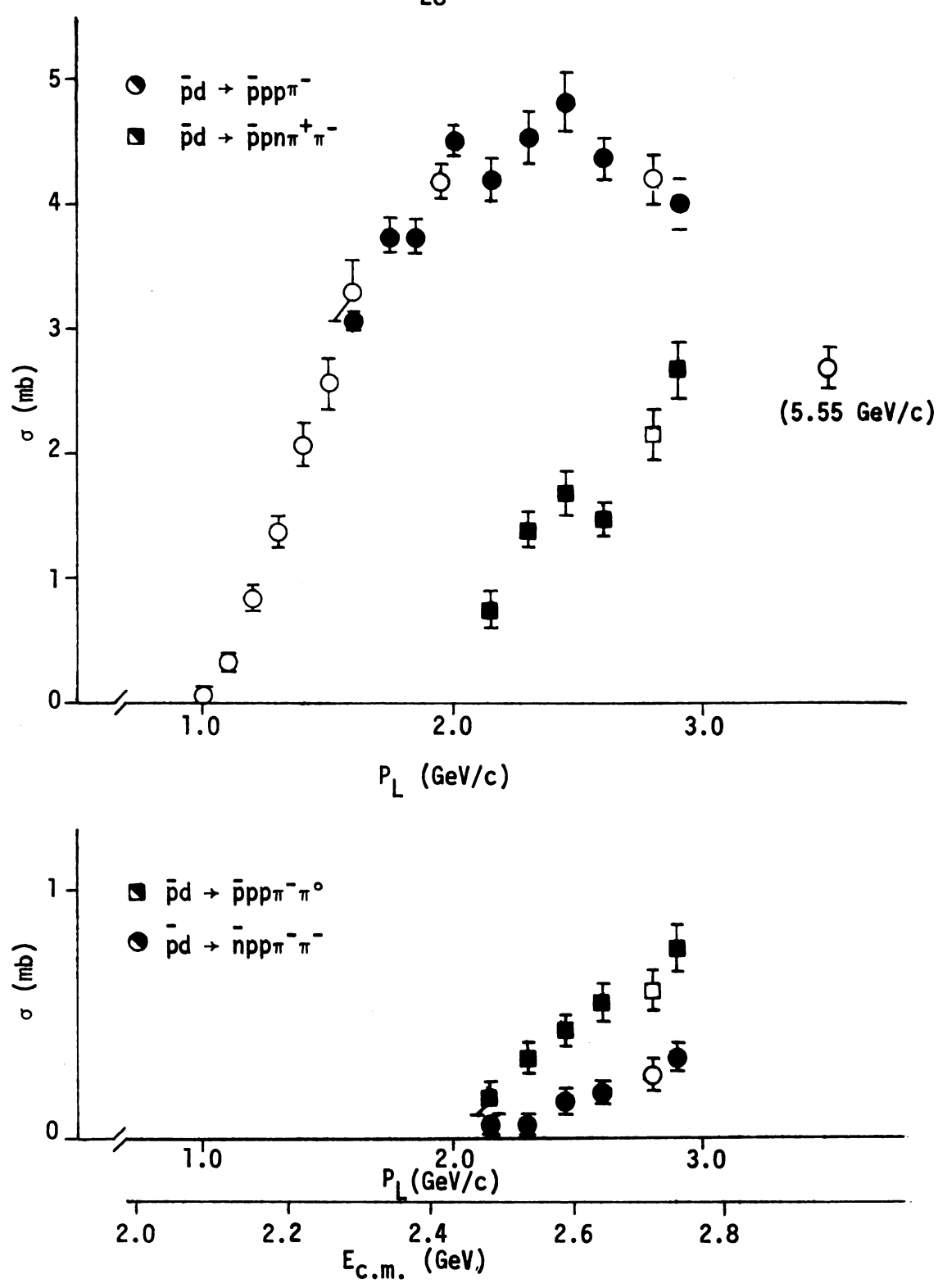


Figure 5. Reaction cross sections for single and double pion production without annihilation in the three and four prong topologies. Other experiments shown are: (1) 1.96 GeV/c, ref. 19; (2) 2.8 GeV/c, ref. 20,21; (3) 5.55 GeV/c, ref. 22; (4) 1.0-1.6 GeV/c, ref. 44.

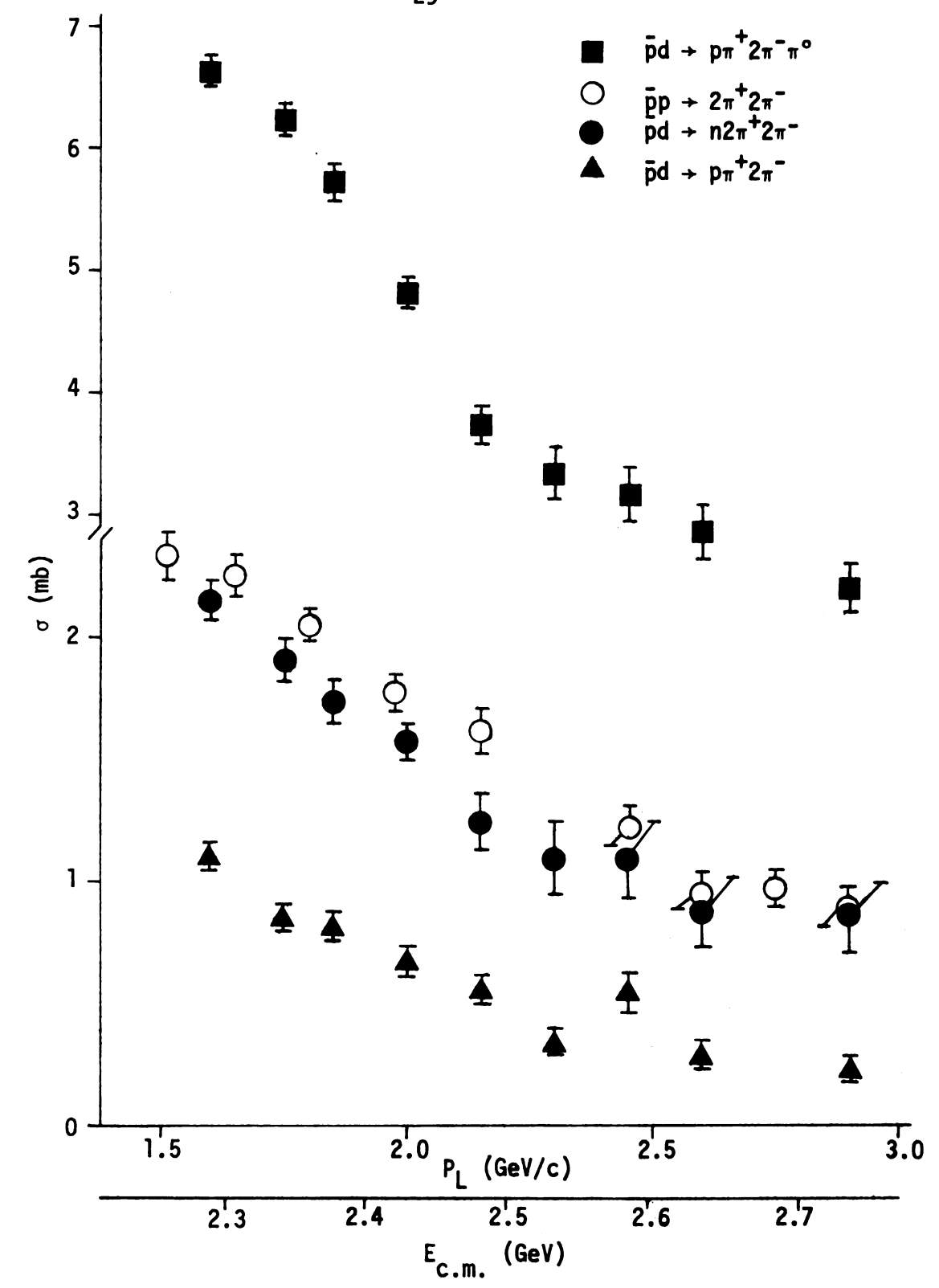


Figure 6. Reaction cross sections for annihilation channels in the three and four prong topologies. $\bar{p}p$ data is from ref. 11

reaction cross sections for the combined 3-prong and 4-prong data. A further study of reaction (5g), as well as $\bar{p}d \rightarrow pK^+K^-\pi^+\pi^-\pi^-$ and similar antiproton-proton reactions, appears elsewhere 8. Since the cross sections for reactions with a deuteron in the final state (hypotheses (5h), (5i) and (5j)) were extremely small, no attempt was made to extract the events fitting these hypotheses.

4.4 Five and Six Prong Cross Sections

Measurements of 8,500 5-prong and 11,000 6-prong events in the 1.60 - 2.00 GeV/c film and 8,400 5-prong and 1,900 6-prong events in the 2.15 - 2.90 GeV/c film have been completed. Each event was fitted to the following final states:

$$\bar{p}d \rightarrow p\pi^{+}\pi^{+}\pi^{-}\pi^{-}\pi^{-}$$
 (6a)

$$\rightarrow p\pi^{+}\pi^{+}\pi^{-}\pi^{-}\pi^{-}\pi^{\circ}$$
 (6b)

$$\rightarrow pK^{+}K^{-}\pi^{+}\pi^{-}\pi^{-}$$
 (6c)

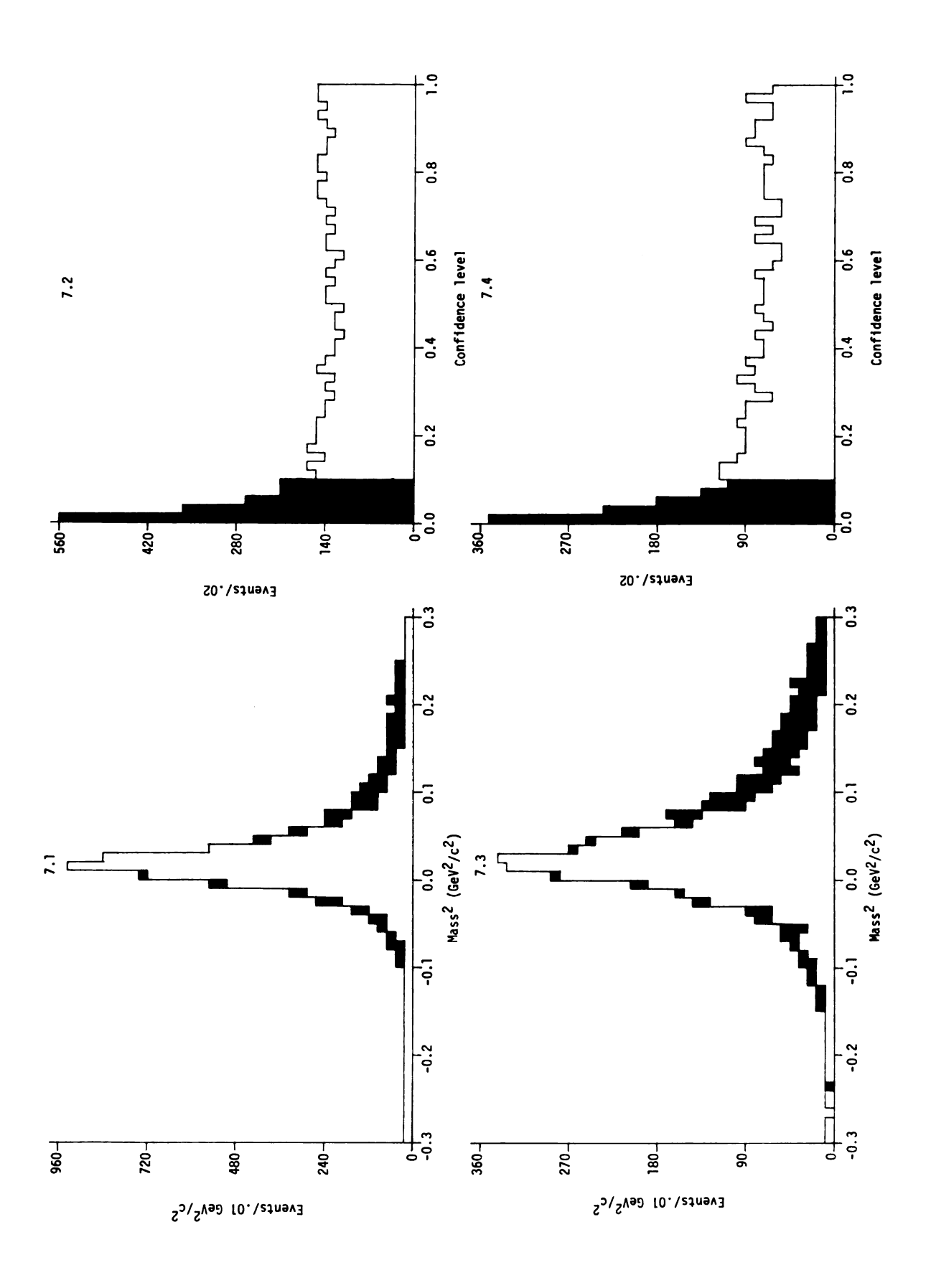
and the missing mass hypothesis $pd \rightarrow p\pi^{+}\pi^{+}\pi^{-}\pi^{-}\pi^{-}MM$. The six prong events were also fitted to

$$\bar{p}d \rightarrow n\pi^{+}\pi^{+}\pi^{+}\pi^{-}\pi^{-}\pi^{-}$$
 (6d)

as well as the corresponding missing mass fit.

As in the three prong and four prong events, reaction (6a) was accepted if the confidence level was greater than 10^{-3} . Hypotheses (6b) and (6d) showed contamination similar to that of hypotheses (5g) and (5k). Again by requiring that the confidence level be greater than 10^{-1} the contamination was reduced significantly. The missing mass squared distributions for events fitting reaction (6b) are shown in Figure 7.1 for events in the 1.60 GeV/c to 2.00 GeV/c and Figure 7.3 for events in 2.15 GeV/c to 2.90 GeV/c incident momentum ranges. The confidence level

- Figure 7. Missing mass squared and confidence level distributions for events fitting the multipion annihilation hypothesis $\bar{p}d \rightarrow p\pi^+\pi^+\pi^-\pi^-\pi^-\pi^-$
 - 7.1 Missing mass squared distribution for events between 1.60 and 2.00 GeV/c
 - 7.2 Confidence level distribution for events between 1.60 and 2.00 GeV/c
 - 7.3 Missing mass squared distribution for events between 2.15 and 2.90 GeV/c
 - 7.4 Confidence level distribution for events between 2.15 and 2.90 GeV/c



distributions for reaction (6b) in the two momentum ranges are shown in Figure 7.2 and Figure 7.4 respectively. The shaded events again represent those events excluded by the 10^{-1} confidence level cut. Fitting the remaining missing mass squared distributions of (6b) to a Breit-Wigner line shape and (6d) to a Gaussian line shape was used to obtain the true number of events in each hypothesis for use in calculating the total reaction cross sections. A correction factor of 10/9 was again used to compensate for the confidence level cut. The analysis of (5c) was done in a similar manner as reaction (5g), again requiring a confidence level of greater than 10^{-3} and a film ionization of the kaon pair consistent with that predicted by the fit. The reaction cross sections for the combined 5-prong and 6-prong events are shown in Table 5 and Figure 8.

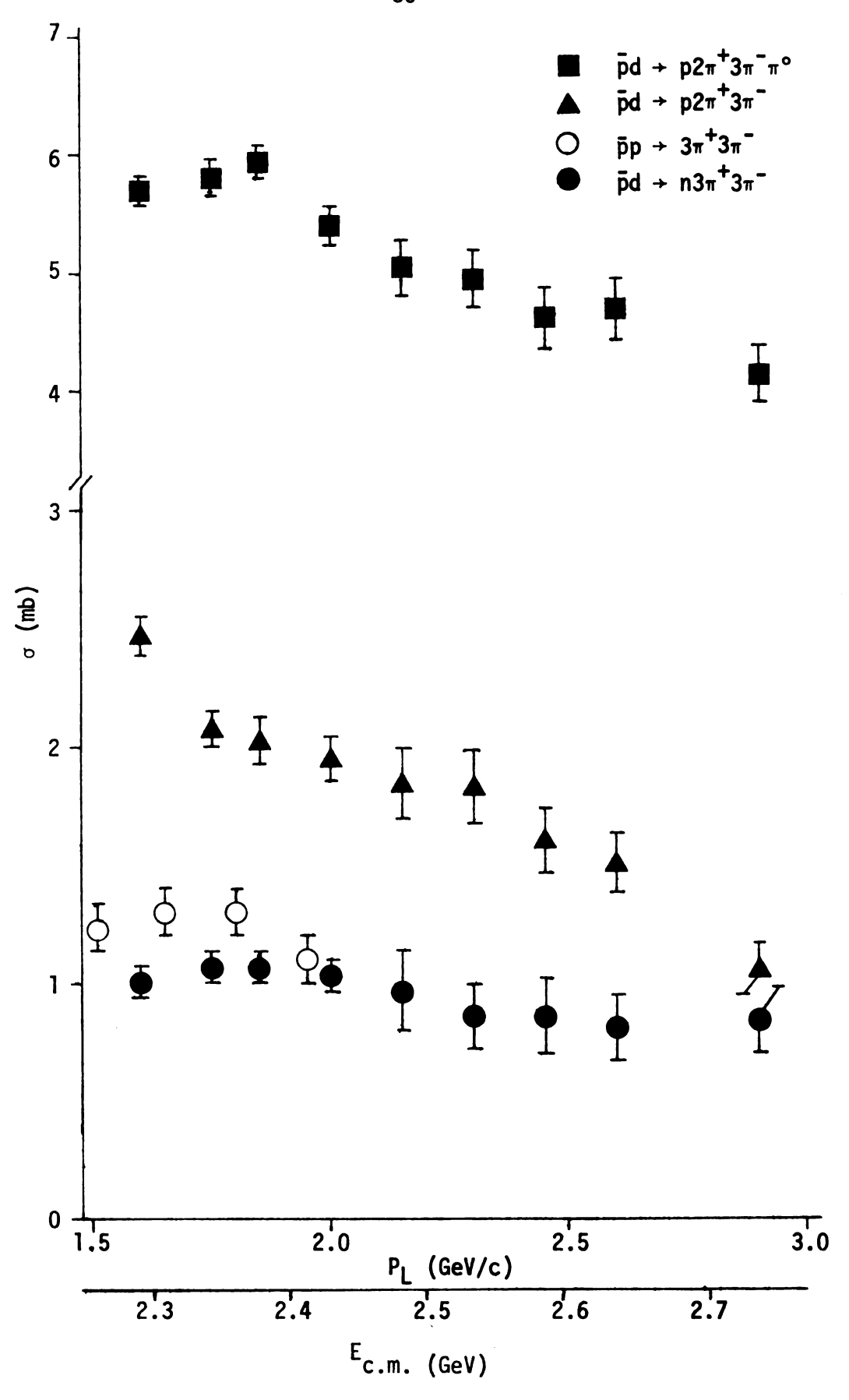
4.5 Conclusions

The reaction cross sections from the two- through six-prong to-pologies have been determined for incident momenta between 1.60 and 2.90 GeV/c. Whereas any structure in the total cross sections may be more noticeable in the reaction cross sections, there is little evidence pointing to such structure. Single pion production without annihilation has already been investigated and would require an excitation curve inconsistent with the data. The double pion production reactions without annihilation cannot contribute since their cross sections rise rapidly from the $\Delta\bar{\Delta}$ threshold which is too great a center-of-mass energy (2470 MeV) to be associated with any of the enhancements observed in the total cross sections. The annihilation reactions $\bar{p}d \to p\pi^+2\pi^-$.

Table 5. Reaction Cross Sections (mb) in the Five and Six Prong Topologies

P _L REACTION	1.60	1.75	1.85	2.00	2.15	2.30	2.45	2.60	2.90
pd+p2π ⁺ 3π ⁻	2.46±.08	2.07±.08	2.02±.09	1.95±.09	1.84±.15	1.82±.15	1.60±.14	1.50±.13	1.06±.10
+p2π ⁺ 3π ⁻ π°	5.70±.13	5.81±.15	5.94±.15	5.30±.15	5.04±.24	4.95±.23	4.62±.25	4.70±.25	4.14±.24
÷n3π ⁺ 3π ⁻	1.02±.05	1.07±.06	1.08±.06	1.04±.06	.959±.166	.856±.144	.862±.151	.806±.141	.844±.146
→pK ⁺ K ⁻ " ⁺ " .184±.030	184±.030	.160±.036	.219±.042	.141±.033	.246±.048	.191±.040	.280±.047	.169±.034	$.285\pm.048$
Sum	9.36±.16	9.11±.18	9.26±.19	8.43±.19	8.09±.33	7.82±.31	7.36±.33	7.18±.32	6.33±.30
5 Prong Missing Mass	3.05±.09	3.08±.11	3.33±.12	3.27±.11	2.80±.12	3.38±.13	3.07±.12	3.64±.12	3.60±.12
6 Prong Missing Mass	4.60±.14	4.40±.14	4.93±.15	5.36±.16	5.19±.37	5.18±.36	5.98±.41	6.52±.41	7.50±.48

Figure 8. Reaction cross sections for annihilation channels in the five and six prong topologies. pp data is from ref. 11



and $\bar{p}d \rightarrow p2\pi^+3\pi^-$ both have smoothly decreasing cross sections and fail to show evidence for any significant structure. The reactions $\bar{p}d \rightarrow p\pi^+2\pi^-\pi^\circ$ and $\bar{p}d \rightarrow p2\pi^+3\pi^-\pi^\circ$ exhibit turnovers in the region of the $\pi_1^*(2350)$. This turnover, however, appears at the low energy end of the data and no definite conclusions can be drawn without further investigation at lower energies. As will be seen in the next chapter, this turnover may be reflected in the resonance production cross section channels stemming from the reaction $pd \rightarrow \bar{p}2\pi^+3\pi^-\pi^\circ$.

CHAPTER 5

RESONANCE PRODUCTION IN THE MULTIPION ANNIHILATIONS

5.1 Experimental Methods

Inspection of the invariant mass distributions $M(\pi^+, \pi^-)$, $M(\pi^\pm, \pi^\circ)$, and $M(\pi^+, \pi^\circ, \pi^-)$ shows that $\rho^\circ(765)$, $f^\circ(1260)$, $\rho^\pm(765)$, and $\omega^\circ(784)$ are present in the data. Fitting by the method of maximum likelihood²³ showed that the multi-pion annihilations are dominated by resonance production. The model used assumes that the data can be described by the incoherent sum of phase space and any resonant processes apparent in the invariant mass distributions. In addition, associated resonance production was included where there was evidence from the Dalitz plots that such production was possible and where the inclusion of the associated resonances improved the overall fits.

In the analysis, an approximate matrix element was constructed assuming that each resonance is represented by a simple Breit-Wigner shape of the form proposed by Jackson²⁴. The Breit-Wigner intensity is

$$BW(\mu) = \frac{\mu\Gamma(\mu)}{(E^2 - \mu^2)^2 + E^2\Gamma^2(\mu)}$$
 (7)

where E is the mass of the resonance, Γ is the full width and μ is the effective mass of the decay products. The matrix element is written

$$|M|^2 = (1 - \sum_{i=1}^{n} \alpha_i) + \sum_{i=1}^{n} \alpha_i R_i/N_i$$
 (8)

where α_i is the fraction of the ith resonant process R_i , N_i is the normalization for the ith process, and n is the number of channels with resonances. The R_i are taken to be the sums of possible Breit-Wigner line shapes for a particular resonant process or the sums of products of two such line shapes in the case of associated resonance production. The normalization, N_i , is simply the integral of the function R_i over phase space.

The masses and widths of the resonances were obtained visually from the data and were adjusted slightly where there was a significant improvement in the overall X^2 values of the fitted invariant mass distributions for a particular final state. Although the Bose-Einstein symmetrization suggested by Goldhaber et al. 25 was observed (approximately a 5% effect) no attempt was made to include it in the model.

The model of phase space plus resonances proved inadequate to describe the reactions where events involved in the secondary scattering of the spectator proton by one of the pions were included in the final sample. An upper limit of 200 MeV/c on the momentum of the spectator proton was imposed and reasonable fits were obtained. This limit reduced the effective cross sections by 30% to 40%. The remaining cross sections are shown in Table 6. In all references to the resonance production cross sections any contributions from associated resonance production have been removed and shown separately (i.e. $\rho^{\circ}\pi^{+}\pi^{-}$ does not contain any contribution from $\rho^{\circ}\rho^{\circ}$).

Table 6. Reaction Cross Sections (mb) for Multipion Fits with Spectator Cuts

PL	_pd→(p)π ⁺ π ⁻ π ⁻	$pd \rightarrow (p) \pi^{+} \pi^{-}$		
1.60	.746 ± .049	4.25 ± .13	1.75 ± .08	3.71 ± .13
1.75	$.573 \pm .054$	3.80 ± .14	1.48 ± .08	3.60 ± .15
1.85	.553 ± .051	3.65 ± .13	1.41 ± .09	3.93 ± .15
2.00	.469 ± .048	3.19 ± .13	1.41 ± .09	3.59 ± .15
2.15*	.389 ± .054	2.23 ± .15	1.30 ± .15	3.32 ± .24
2.30*	.250 ± .045	2.12 ± .20	1.20 ± .15	3.38 ± .23
2.45*	.277 ± .043	1.83 ± .22	1.10 ± .14	3.05 ± .25
2.60*	.177 ± .041	1.81 ± .20	.983 ± .130	3.08 ± .25
2.90*	.183 ± .045	1.46 ± .19	.813 ± .100	2.72 ± .24

^{*} A value of .261 \pm .055 mb was used for the averaged cross section in the 2.15 GeV/c to 2.90 GeV/c incident momentum range for the reaction pd \rightarrow (p) $\pi^+\pi^-\pi^-$.

5.2 Three Pion Final States

The three pion annihilation channel prominantly exhibits both ρ° and f° production. The cross sections for the quasi-two-body final states fall much more rapidly than the three pion cross section. Resonant production decreases from about 45% of the total cross section at 1.60 GeV/c to well below 20% at the highest momenta. The resonance parameters used were (M, Γ)_{ρ} = (740, 120)* and (M Γ)_f = (1250, 150) where M and Γ are the mass and full width of the resonance in MeV. Since the three pion cross section is so small at the higher momenta, the number of events at each momenta (approximately 60) is too small to fit; hence, only a fit to the combined data was possible in the 2.15 to 2.90 GeV/c momentum range. The resonance cross sections and histogram χ^2 values (root mean square deviation of the experimental values from the fitted values calculated for a particular mass combination) are shown in Figure 9 and Table 7. Figure 10 shows the fits to the invariant mass distributions from the three pion annihilations.

5.3 Four Pion Final States

Resonance production in the four pion annihilation channel consists primarily of ω° , ρ° , ρ^{\pm} , and f° . A small fraction of the quasitwo-body associated resonance production, $\rho^{\circ}\rho^{-}$, is also present. The resonance production cross sections fall only slightly faster than the total four pion cross section. The resonance parameters (M, Γ) = (765, 120), (M, Γ) $_{\omega}$ = (785, 60), and (M, Γ) $_{f}$ = (1260, 150) were used to

^{*}The resonance parameters differ slightly from the accepted values. The parameters used were those which gave the best overall fits to the data within a given topology.

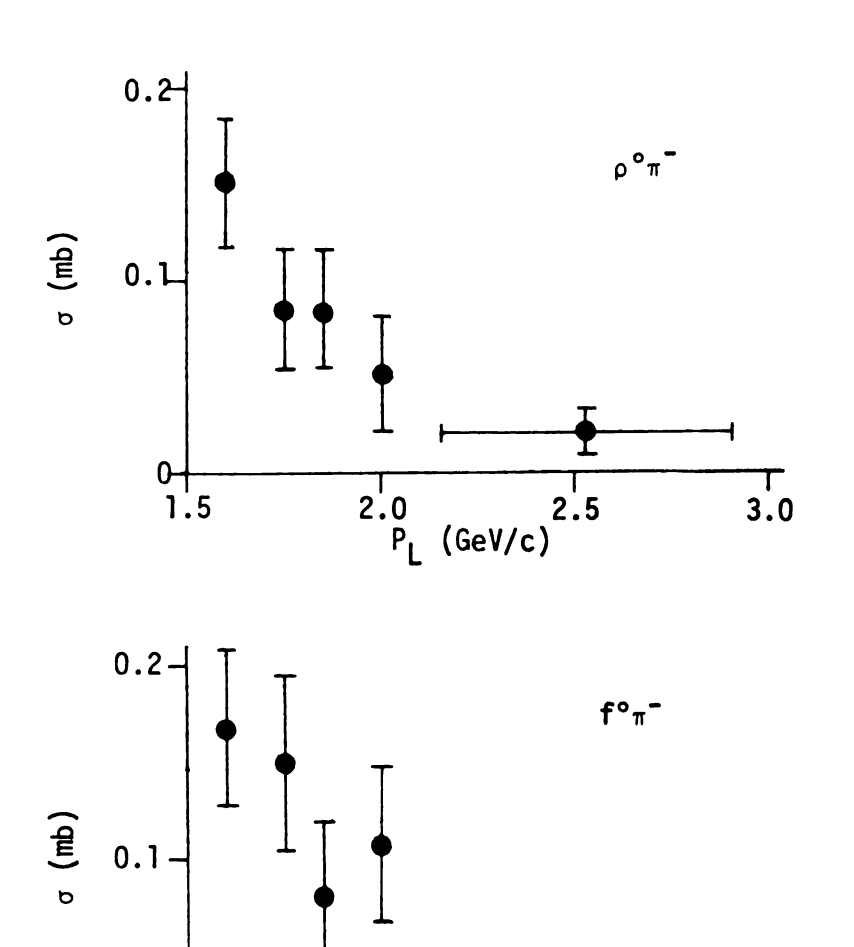


Figure 9. Resonance production cross sections for the $\pi^+2\pi^-$ channel

(GeV/c)

2.5

E_{c.m.} (GeV)

2.5

3.0

2.0 P L

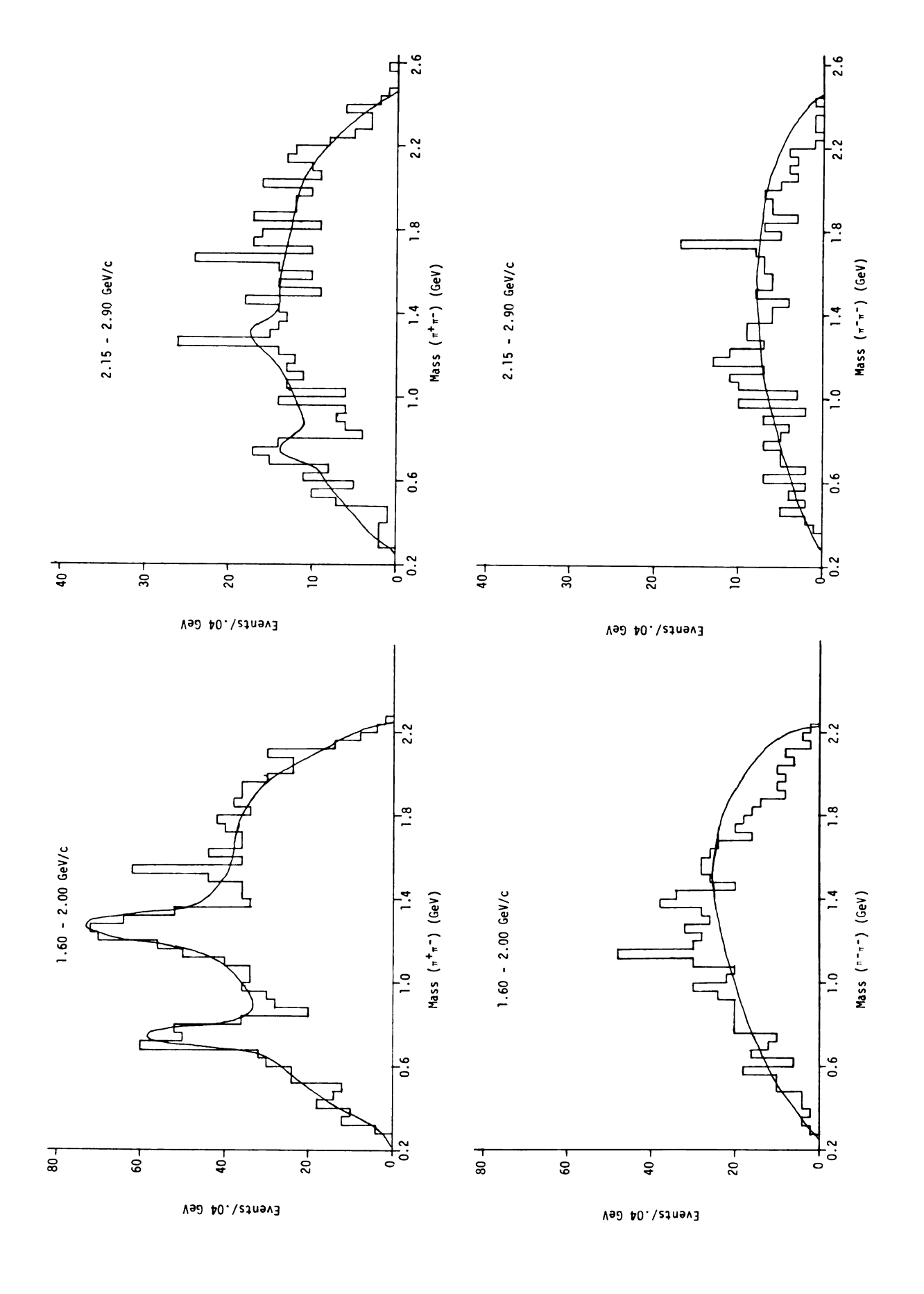
0 +

2.3

Table 7. Resonance production cross sections for the $_{\pi}^{+}2_{\pi}^{-}$ channel

P _L	ρ°π¯	f°π¯	Histogra π ⁺ π-	am X ² /Bins π-π-
1.60	.151±.033	.169±.040	68/58	71/58
1.75	.085±.031	.150±.045	54/57	51/56
1.85	.085±.031	.080±.040	56/56	52/56
2.00	.051±.030	.108±.040	63/56	60/56
2.15-2.90	.021±.010	.025±.014	75/56	53/56

Figure 10. Invariant mass distributions for the $\pi^+2\pi^-$ channel



obtain the resonance cross sections and histogram χ^2 values shown in Figure 11 and Table 8. Although the A_2 was not used in the maximum likelihood fitting, it was investigated independently. The combined cross sections for A_2° and A_2^{-} was calculated to be approximately $150 \pm 50 \, \mu b$ at 1.60 GeV/c falling to an upper limit of 40 μb at 2.00 GeV/c. There was no significant evidence for A_2 production at any of the higher momenta. The fits to the invariant mass distributions from the four pion annihilations are shown in Figure 12.

5.4 Five Pion Final States

In the five pion annihilation channel, the only clear resonance production was the ρ° and the associated $\rho^{\circ}\rho^{\circ}$. While the fraction of resonance production increased from 55% at the lowest momentum to 80% at the higher momenta, the amount of associated production decreased markedly. There is a negative correlation between $\rho^{\circ}\pi^{+}\pi^{-}\pi^{-}$ and $\rho^{\circ}\rho^{\circ}\pi^{-}$ which leads to the large errors in the cross sections. The invariant mass distribution, $M(\pi^{+},\pi^{-})$, characterizes the ρ° as a shoulder on the high effective mass side of the peak of phase space making fitting difficult and contributing to the large errors. The mass and FWHM of the ρ used in the fitting were 760 MeV/c² and 120 MeV/c² respectively. The ρ° and $\rho^{\circ}\rho^{\circ}$ cross sections and the histogram χ^{2} are shown in Figure 13 and Table 9. Figure 14 shows the fits to the invariant mass distributions from the five pion annihilations.

5.5 Six Pion Final States

Resonance production in this channel was very difficult to analyze due to the large number of combinations for each process. The

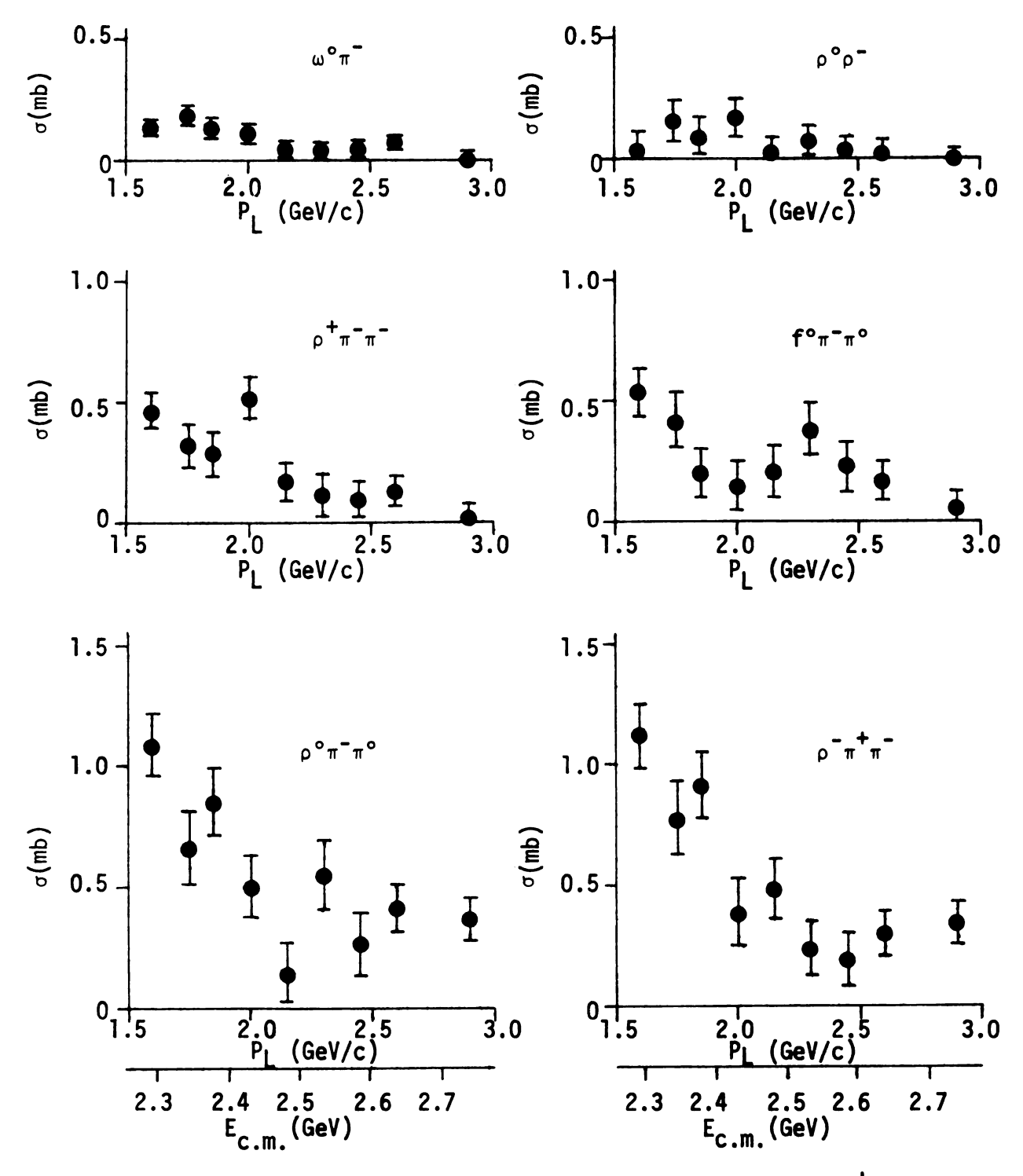
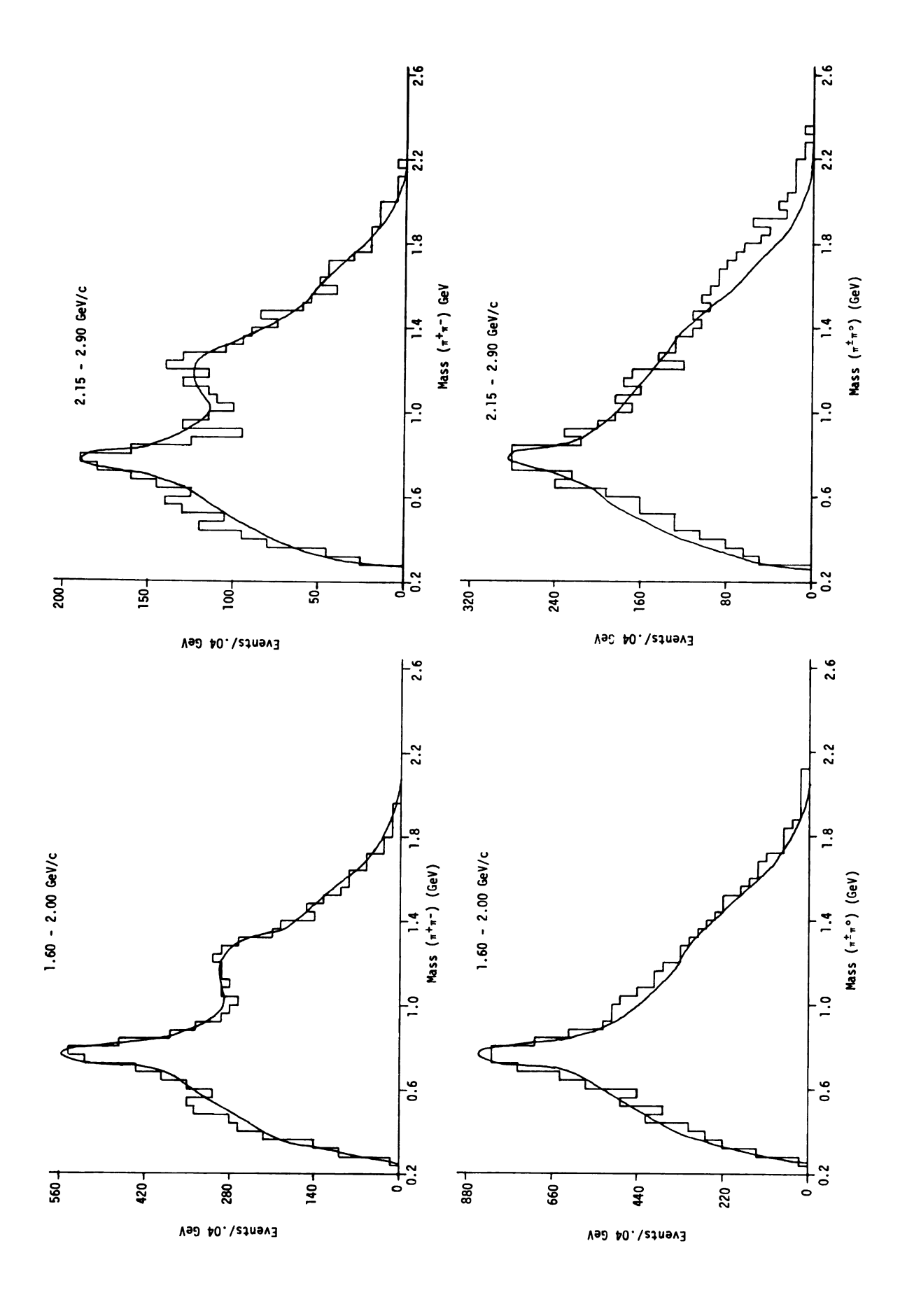


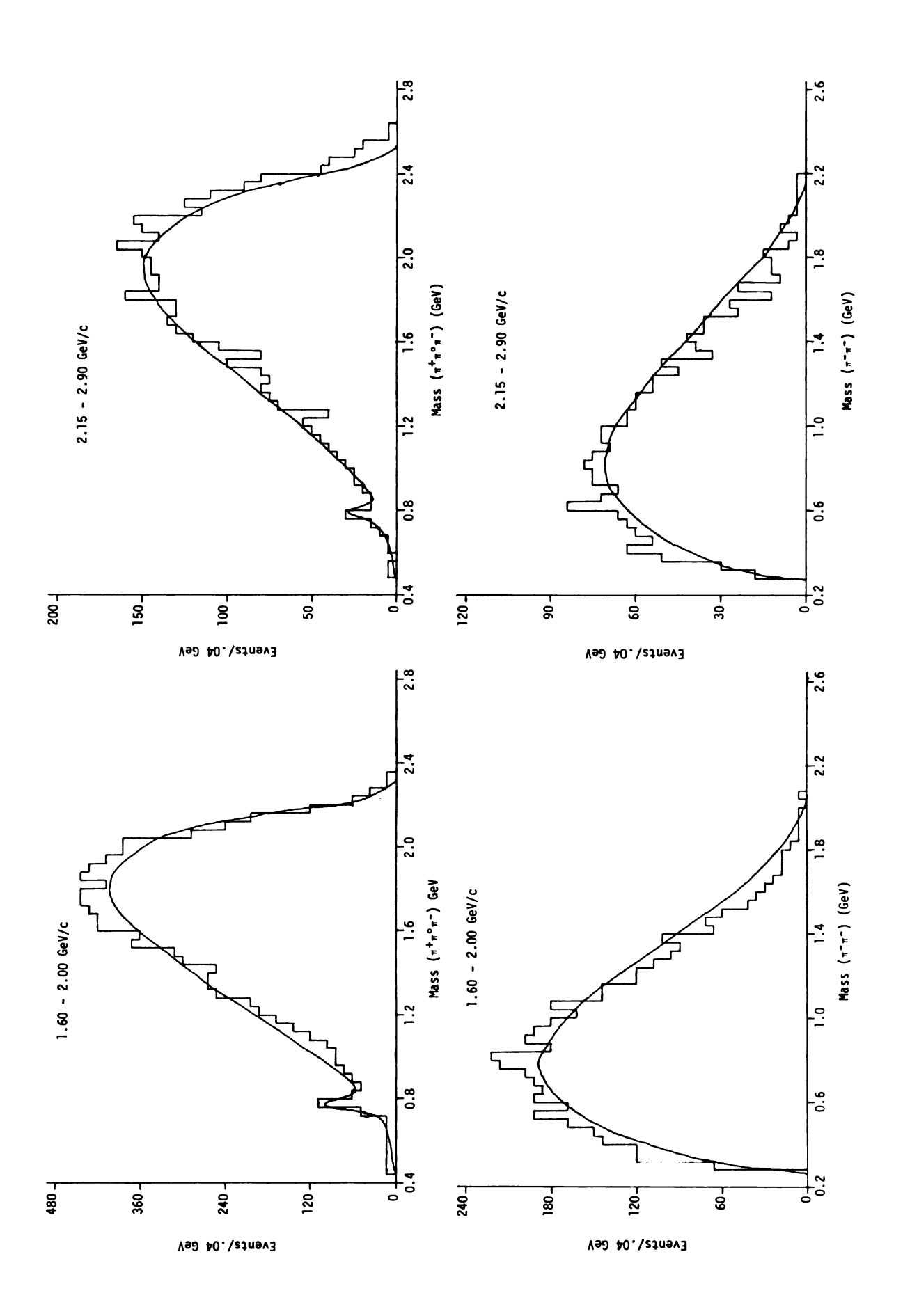
Figure 11. Resonance production cross sections for the $\pi^+2\pi^-\pi^\circ$ channel

Resonance production cross sections in mb for the $_{\pi}^{+}2_{\pi}^{-}{}_{\pi}^{\circ}$ channel Table 8.

P _L	— [™] o ai	ρ ^ο π ^ο π ⁻	f°π°π-	ρ-π + π-	_ d _o d	p+#+a-	
1.60 1.75 1.85 2.00 2.30 2.45 2.90	.130±.026 .183±.034 .135±.030 .122±.030 .040±.024 .053±.028 .080±.023	1.093±.127 .665±.148 .856±.140 .499±.132 .144±.121 .554±.128 .265±.124 .416±.095	.544±.096 .421±.116 .202±.099 .153±.103 .207±.106 .377±.106 .223±.103 .171±.079	1.115±.133 .776±.152 .911±.135 .383±.134 .482±.125 .240±.111 .194±.108 .301±.087	.043±.081 .155±.092 .089±.083 .171±.080 .022±.069 .071±.067 .040±.059	.46æ.075 .317±.085 .29æ.082 .517±.083 .17æ.078 .107±.082 .092±.070 .13æ.058	
		Histogra	Histogram X ² /Bins				
٦ -	π+π-	π ⁺ πο	_π ⁺ π°π	Щ	_ =		
1.60 1.75 1.85 2.30 2.30 2.60	63/56 66/56 55/56 49/56 62/57 71/55 71/55	93/56 63/56 75/56 75/56 61/56 66/57 74/56	95/55 54/54 62/54 47/49 37/47 31/47	5 4 4 60/ 9 9 7 7 7 52/ 0 77/ 4	55 55 55 55 55 55 55 55 55 55 55 55 55		

Figure 12. Invariant mass distribution for the $\pi^+2\pi^-\pi^\circ$ channel





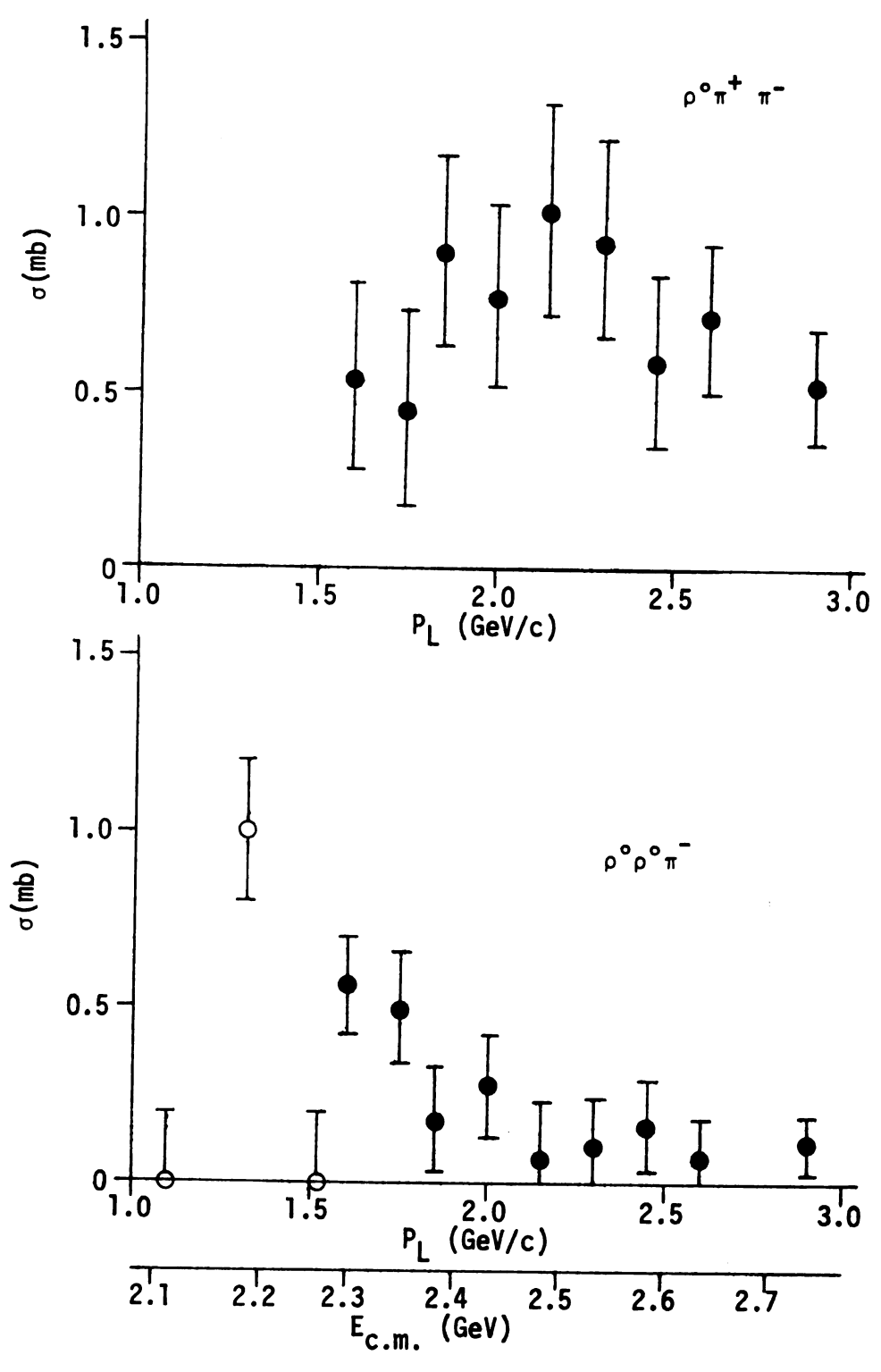
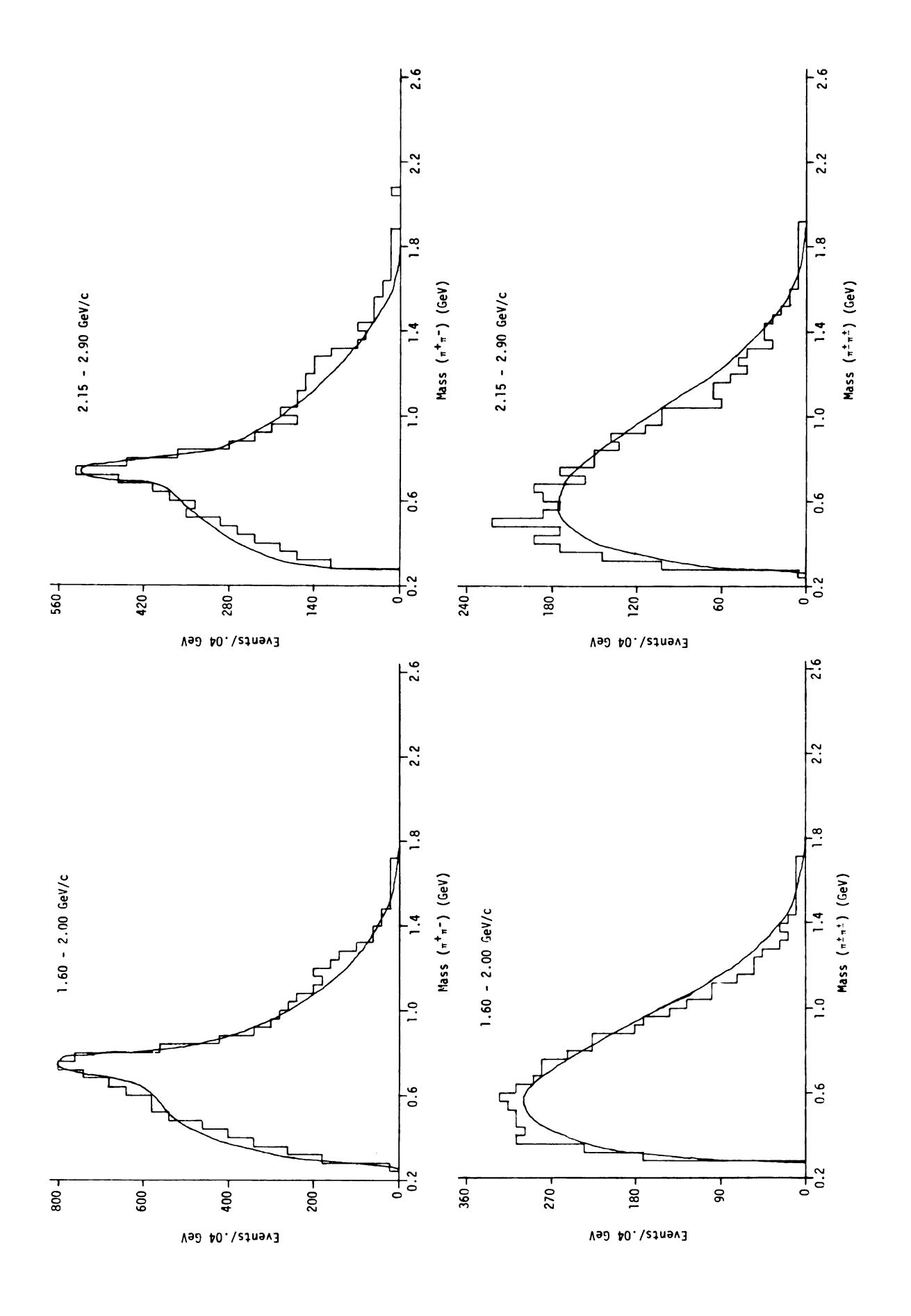


Figure 13. Resonance production cross sections for the $2\pi^+3\pi^-$ channel. Open points are $pp_{I=1}^{+} \rightarrow \rho^{\circ} \rho^{\circ} \pi^{\circ}$ from reference 4.

Table 9. Resonance production cross sections in mb for the $2\pi^{+}3\pi^{-}$ channel

P_L	^ ^	o o =		stogram_X ² ,	
L	ρ° 3π	ρ°ρ°π¯	π ⁺ π ⁻	ππ	π+π+
1.60	.546±.264	.561±.140	100/56	65/56	64/56
1.75	.451±.287	.498±.153	101/56	54/56	67/54
1.85	.897±.267	.179±.148	98/56	42/56	64/53
2.00	.773±.260	.280±.142	96/56	102/55	52/56
2.15	1.016±.300	.067±.163	65/56	70/54	52/53
2.30	.935±.278	.103±.144	54/56	71/56	68/52
2.45	.593±.243	.168±.127	76/56	63/56	48/54
2.60	.710±.210	.069±.114	63/56	60/55	40/55
2.90	.523±.164	.110±.087	50/56	59/56	64/56

Figure 14. Invariant mass distributions for the $2\pi^{+}3\pi^{-}$ channel



only clear resonance in the invariant mass histograms was the ω° . The ρ region appeared only as a slight shoulder on a phase space distribution and a prediction of 20% ρ looks only slightly different from a prediction of 80% ρ production. An attempt was made to determine the parameters of the ρ , however, variations of as much as 45 MeV/c² in the central value did not significantly change either the cross sections or the histogram χ^2 values. The resonance parameters used, $(M, \Gamma)_{\rho} = (765, 120)$ and $(M, \Gamma)_{\omega} = (785, 40)$ are those which gave the best overall χ^2 values.

There was no evidence for the production of f° and only a small contribution from η° . Neither resonance was used in the maximum likelihood fitting. The cross section for η° production was less than 50 μb at all momenta.

Initially, the maximum likelihood method was used to fit only the single resonance ω° , ρ° , and ρ^{\pm} . At the three lowest momenta, it was necessary to include associated production of $\omega^{\circ}\rho^{\circ}$ and $\rho^{\circ}\rho^{\pm}$. Production of $\rho^{\circ}\rho^{+}$ decreased rapidly in the lowest four momenta and its inclusion was unnecessary above 2.00 GeV/c. The channel $\rho^{\circ}\rho^{\circ}\pi^{-}\pi^{\circ}$ was also tried and found to be unnecessary.

The cross section from ω° as well as the associated productions $\rho^{\circ}\rho^{-}$ and $\omega^{\circ}\rho^{\circ}$ at first fall more rapidly than the six pion cross sections then level out to a constant percentage at higher center-of-mass energies. The percentage of ρ production increases at first to compensate for the decrease in associated production, then remains essentially constant at higher energies. The resonance cross sections and histograms χ^2 values are shown in Figure 15 and Table 10. The fits to

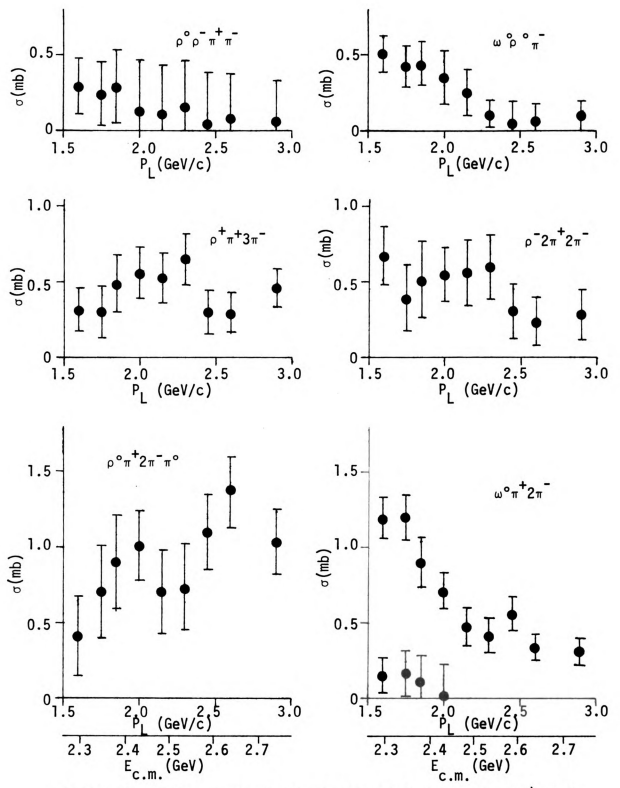


Figure 15. Resonance production cross sections for the $2\pi^+3\pi^-\pi^\circ$ channel

Resonance production cross sections in mb for the $2\pi^{+}3\pi^{-}\pi^{\circ}$ channel Table 10.

PL	ρ°4π	ρ ⁺ 4π	ρ-4π	ω°3π	ρ°ρ ⁺ 2π	ρ°ρ-2π	ພິດິສີ
1.60 1.75 1.85 2.00 2.15 2.45 2.60	.415±.260 .707±.303 .901±.352 1.018±.227 .709±.278 .730±.218 1.098±.248 1.393±.207	.320±.139 .302±.164 .481±.184 .555±.149 .531±.163 .649±.168 .301±.142 .296±.131	.6734.197 .3924.216 .5124.253 .5534.165 .5704.219 .6014.206 .3134.177 .2434.159	1.189±.134 1.197±.148 .904±.158 .710±.115 .478±.122 .410±.113 .564±.109 .332±.085	.156±.119 .167±.150 .115±.166 .011±.207 	.296±.182 .243±.206 .289±.239 .137±.324 .111±.326 .155±.299 .050±.320	.506±.120 .423±.134 .445±.147 .354±.174 .252±.154 .109±.095 .051±.145
٦	-# + #	o + +	Histogram X	χ ² /Bins π ⁺ π°π-	 =	Ë	+ + + =
1.60 1.75 1.75 2.00 2.30 2.45 2.90	87/57 68/55 90/57 57/56 63/57 61/57 65/56	50/54 53/54 55/57 52/57 73/56 64/56 59/56	82/55 49/54 60/56 47/56 60/56 78/56 90/56	103/59 70/57 78/58 93/57 70/59 73/57 53/58 54/56	59/54 57/56 77/54 64/56 57/54 65/55 46/56	39/ 42/ 48/ 45/ 75/ 75/	/50 /55 /55 /56 /56 /56

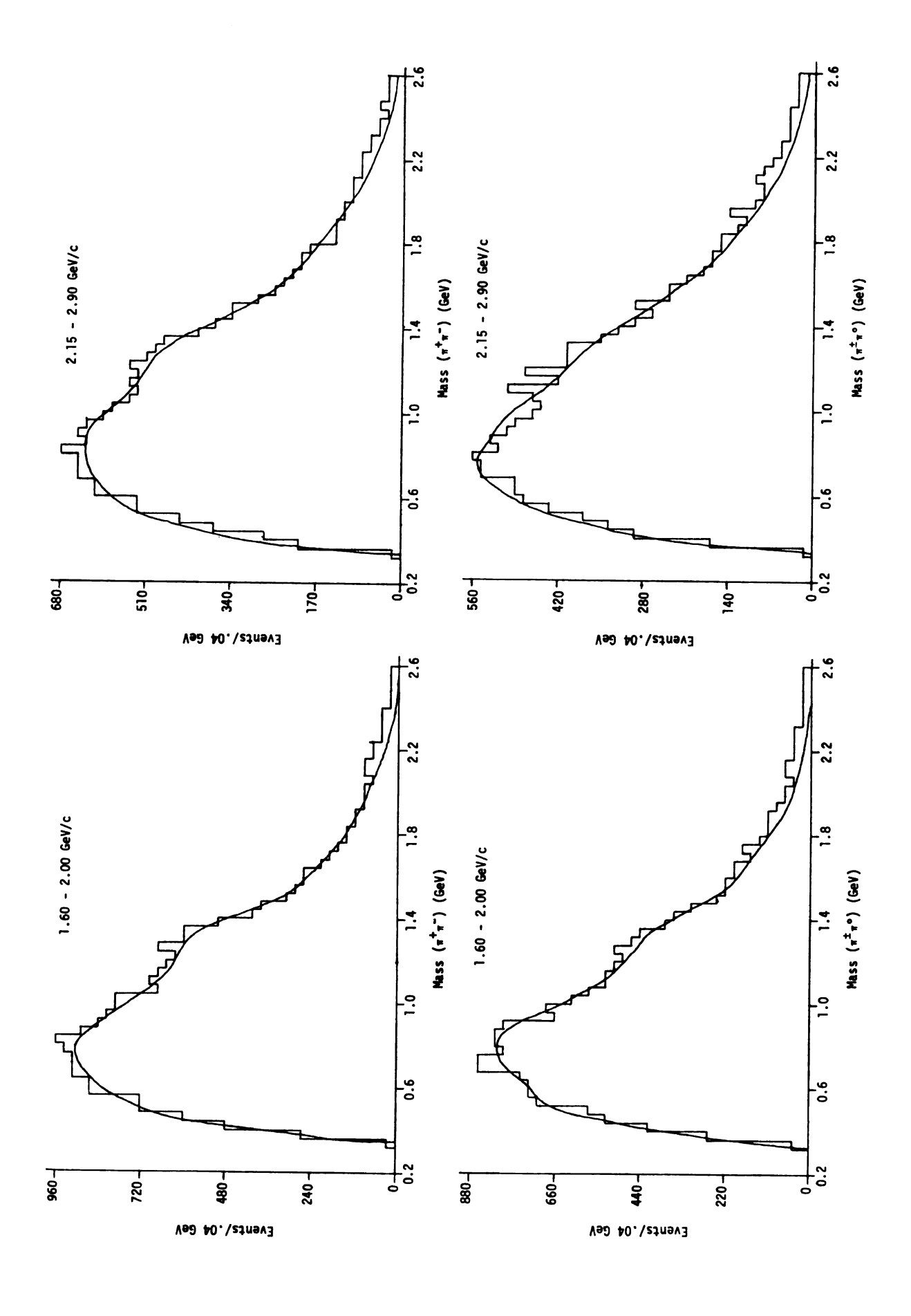
the invariant mass distributions from the six pion annihilations are shown in Figure 16.

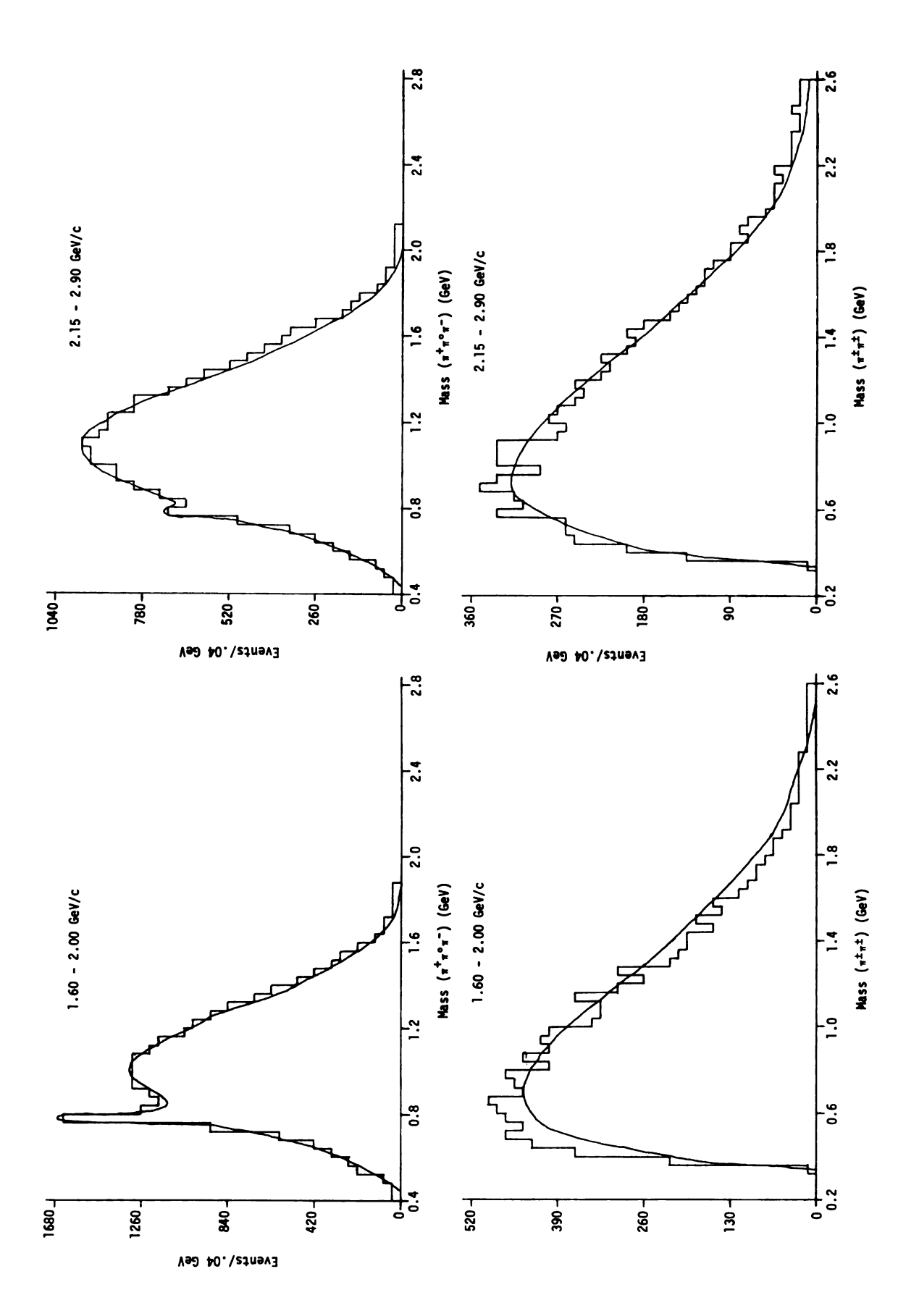
5.6 Conclusions

Investigation of the resonance production cross sections in the annihilation channels has yielded little evidence for contributions to the I=1 structures. The only significant channels are the K*K $\pi\pi$ which shows an enhancement at 2360 MeV seen both in this experiment and in a $\bar{p}p$ experiment⁸ and the $\omega^{\circ}\pi^{-}$, the $\omega^{\circ}\pi^{+}\pi^{-}\pi^{-}$ and remotely the $\omega^{\circ}\rho^{\circ}\pi^{-}$ channels which exhibit possible turnovers in the low energy regions of the data. All other resonance production cross sections appear to have a smooth energy dependence and give little evidence for structure. Most of the resonance production cross sections are decreasing with increasing incident momentum and those channels which do not decrease are consistent with smoothly falling cross sections when they are combined with their corresponding associated resonance production channels.

An enhancement in the $\rho^{\circ}\rho^{\circ}\pi^{\circ}$ channel from $\bar{p}p$ annihilations at 1.32 GeV/c (2190 MeV center-of-mass energy) was reported in the formation experiment of Kalbfleisch et al.⁴. They determined that this enhancement has a cross section of 0.5 \pm 0.1 mb and a width 20 MeV/c² < Γ < 80 MeV/c². Their observation of essentially zero cross section for $\rho^{\circ}\rho^{\circ}\pi^{\circ}$ at 1.52 GeV/c (no events were observed at either 1.11 GeV/c or 1.52 GeV/c) is confirmed by Parker¹⁰ in the momentum range from 1.51 GeV/c to 2.90 GeV/c ($\rho^{\circ}\rho^{\circ}\pi^{\circ}$ cross section of 0.19 \pm 0.19 mb at 1.51 GeV/c.). If the $\rho^{\circ}\rho^{\circ}\pi^{\circ}$ channel is isospin one as indicated by the authors of reference 4, it should be reflected in the $\rho^{\circ}\rho^{\circ}\pi^{-}$

Figure 16. Invariant mass distributions for the $2\pi^{+}3\pi^{-}\pi^{\circ}$ channel





channel from the five pion annihilations in $\bar{p}n$ which must be I=1. Since $\bar{p}p$ is an equal mixture of I=1 and I=0, the $\bar{p}p$ I=1 cross section is half the $\bar{p}n$ cross section. Thus, if the $\rho^{\circ}\rho^{\circ}\pi^{\circ}$ channel is isospin one, it should contribute 1.0 ± 0.2 mb to the total I=1 cross section at 1.32 GeV/c incident momentum. Assuming that the $\bar{p}p \rightarrow \rho^{\circ}\rho^{\circ}\pi^{\circ}$ cross section of Parker at 1.51 GeV/c is a mixture of I=1 and I=0 and represents solely background for the $\rho\rho\pi$ channel, the 0.6 ± 0.2 mb observed for $\bar{p}n \rightarrow \rho^{\circ}\rho^{\circ}\pi^{-}$ at 1.60 GeV/c would indicate a width for the $\rho\rho\pi$ enhancement much larger than that reported by the authors of reference 4 (see Figure 13). Further data at lower energies is necessary to confirm an I=1 $\rho^{\circ}\rho^{\circ}\pi^{-}$ enhancement in $\bar{p}n$ at 2190 MeV.

CHAPTER 6

UPPER LIMIT ON THE DECAY RATE $\omega \rightarrow 2\pi$

Recently, experimental results $^{26-31}$ have been reported indicating the existence of the G-parity violating decay $\omega \to 2\pi$. This decay has been seen as an interference effect between $\omega \to 2\pi$ and $\rho \to 2\pi$ in the $\pi^+\pi^-$ invariant mass distributions. A knowledge of the coherence between the ρ and the ω amplitudes is necessary to obtain the branching ratio

$$R = (\omega \rightarrow \pi^{+}\pi^{-})/(\omega \rightarrow \pi^{+}\pi^{\circ}\pi^{-})$$
 (9)

In an e⁺e⁻ colliding beam experiment at Orsay³², the ω and ρ production amplitudes are known to be completely coherent and a value of R = 3.5 $^{+3.0}_{-2.1}$ % has been obtained. Groups at Daresbury³³ and M.I.T.³⁴ from coherent photo-production of pion pairs off nuclei, have obtained R = 0.80 $^{+0.28}_{-0.22}$ % and R = 1.22 \pm 0.30% respectively. Their results rely on the ratio of photon- ρ and photon- ω coupling constants which each group determined independently. In most strong interaction experiments, the degree of coherence between the ρ and ω production amplitudes is unknown and only a lower limit on R has been determined. A unique exception to this case in the strong interactions is the \bar{p} n interaction where the ρ and ω production amplitudes are completely incoherent.

Nucleon-antinucleon states of total isospin I, total spin S, and parity $(-1)^{L+1}$ are eigenstates of G-parity with eigenvalues³⁵

$$G = (-1)^{L+S+I}$$
 (10)

Since $\bar{p}n$ is a pure I=1 state, $G=(-1)^{L+S+1}$; therefore, states of opposite total G-parity proceed from states of different spin or different parity. G-parity is multiplicative in all mesonic states and the ρ and ω have opposite G-parity. Thus if G-parity is conserved in the production process, for a given pion multiplicity, ρ and ω can proceed only from different states of G-parity which cannot interfere.

In the search for the $\pi^+\pi^-$ decay of the ω in the three and five pion annihilation channels, the experimental mass resolution was determined by taking events which fit the three and five pion hypotheses and reprocessing them through TVGP-SQUAW, fitting them to the hypothesis

$$pd \Rightarrow p\pi^{-}(\pi^{+}\pi^{-})X^{\circ}$$

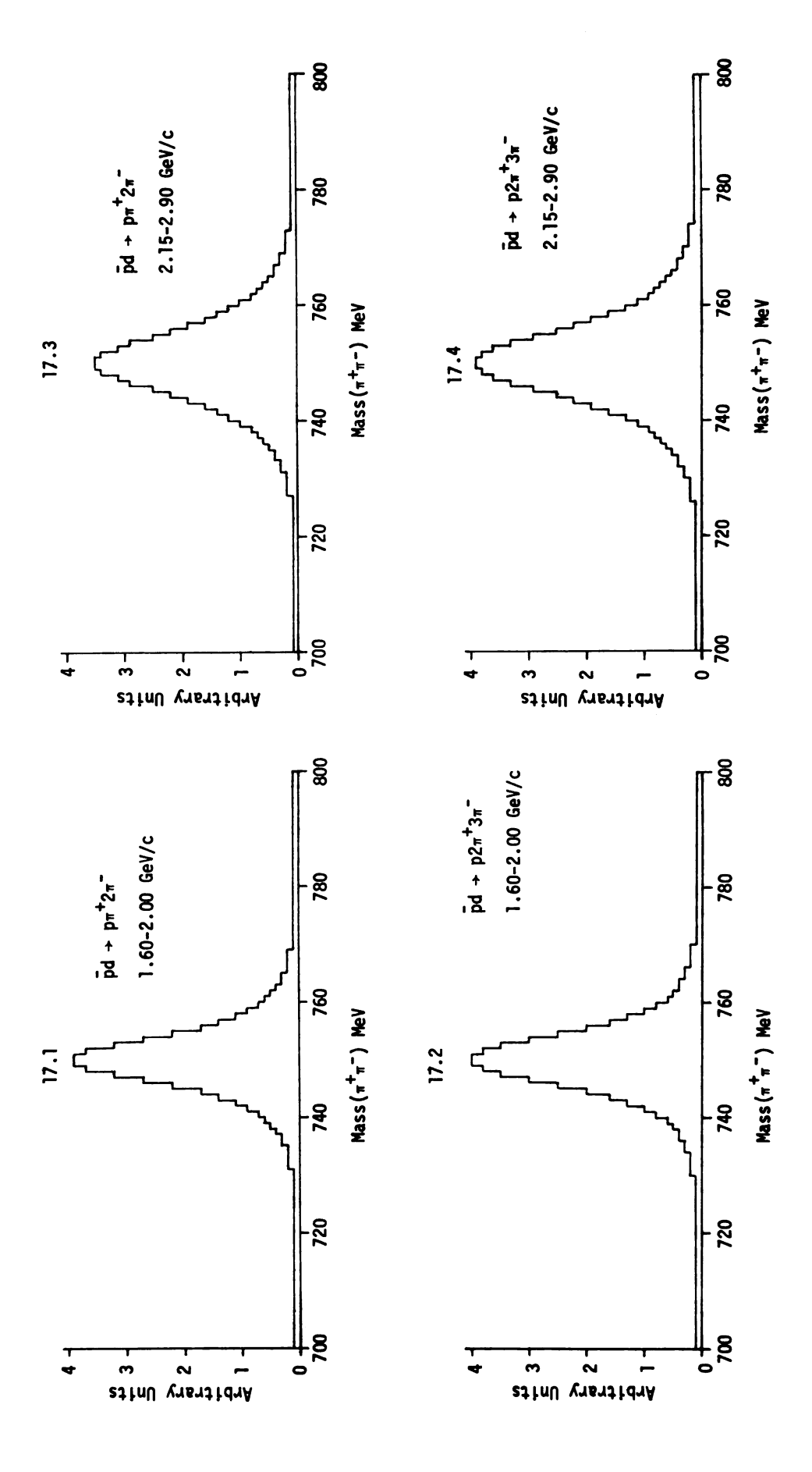
$$\downarrow_{\rightarrow}\pi^{+}\pi^{-}$$
(11)

The resolution for two pion invariant mass combinations between 0.7 GeV/c^2 and 0.8 GeV/c^2 from the three and five pion annihilations was found to be 11 MeV/c^2 , FWHM, in the 1.60 - 2.00 GeV/c incident momentum range and 14 MeV/c^2 in the 2.15 - 2.90 GeV/c range. Figure 17 shows the ideogramed mass resolution where the invariant masses have been fixed at 750 MeV/c. The resolution for $\omega \to 3\pi$ was determined by the width of the ω distributions in the four and six pion final states since the natural decay width of the ω is much smaller than the three pion resolution. Values of 60 MeV/c^2 and 40 MeV/c^2 , FWHM, were obtained for the four and six pion final states respectively.

In the interest of maximum statistics, the data from the four lowest momenta and the five highest momenta were combined into two groups for both the three and five pion channels. The amount of

- Figure 17. Resolution ideogram of the error from invariant mass combinations between 0.7 GeV/c^2 and 0.8 GeV/c^2 with the mass fixed at 0.75 GeV/c^2
 - 17.1 Ideogram for events fitting $\bar{p}d \rightarrow p\pi^+2\pi^-$ for the momentum range 1.60 to 2.00 GeV/c
 - 17.2 Ideogram for events fitting $\bar{p}d \rightarrow p2\pi^{+}3\pi^{-}$ in the momentum range 1.60 to 2.00 GeV/c
 - 17.3 Ideogram for events fitting $\bar{p}d \rightarrow p\pi^+2\pi^-$ in the momentum range 2.15 to 2.90 GeV/c
 - 17.4 Ideogram for events fitting $\bar{p}d \rightarrow p2\pi^{+}3\pi^{-}$ in the momentum range 2.15 to 2.90 GeV/c





 $\omega \to \pi^+\pi^-$ was fitted employing the maximum likelihood method with the mass and width for the ω set at 784 MeV/c² and 15 MeV/c² respectively. All other resonance parameters were the same as those found to give the best overall results in the determination of the resonant production cross sections. The amounts of resonant production other than $\omega \to 2\pi$ were checked and found to be very nearly the same as those without the inclusion of $\omega \to 2\pi$.

In the low momentum data, the branching ratio was determined to be $R = 2.89 \pm 6.19\%$ from the three pion channel and $R = 0.62 \pm 2.58\%$ from the five pion channel. There was no eivdence for $\omega \to 2\pi$ in the high momentum data in either the three or five pion channels with branching ratios of $R = 0.0 \pm 9.92\%$ and $R = 0.0 \pm 5.11\%$ respectively, however the large errors do not rule out the possibility for a small amount of $\omega \to 2\pi$. On the basis of the most significant channel, namely the five pion annihilations at the lowest momenta, an upper limit of 5.78% can be placed on the value of R at the 95% confidence level.

CHAPTER 7

ANGULAR AND MOMENTUM DISTRIBUTIONS

Recently there has been a great deal of interest in single particle distributions as a means for understanding various reaction processes. The results from nucleon-anti-nucleon annihilation studies have been reported in various journals, however, almost all the data published is from proton-antiproton reactions.

The center-of-mass angular distributions, relative to the beam direction, for events fitting the reaction hypotheses $\bar{p}n \rightarrow m\pi$, where m=3, 4, 5 and 6, and where the number of neutral pions is less than or equal to one, are shown in Figures 18, 19, 20 and 21 respectively. The distributions for the three pion annihilations have been combined into the two momentum groups for greater statistics. The solid curves are fits of the data to the first five Legendre polynomials of the form

$$P_{\Omega}(x) = 1 \tag{12}$$

$$P_1(x) = x \tag{13}$$

$$P_2(x) = 1/2(3x^2 - 1)$$
 (14)

$$P_3(x) = 1/2(5x^3 - 3x) \tag{15}$$

$$P_4(x) = 1/8(35x^4 - 30x^2 + 3)$$
 (16)

where x is cos $\theta_{\pi c.m.}$. The fitted coefficients for the Legendre polynomials are shown in Table 11 and Figure 22.

Figure 18. Angular distributions for the three pion final state. The solid curves are fits to the Legendre polynomials

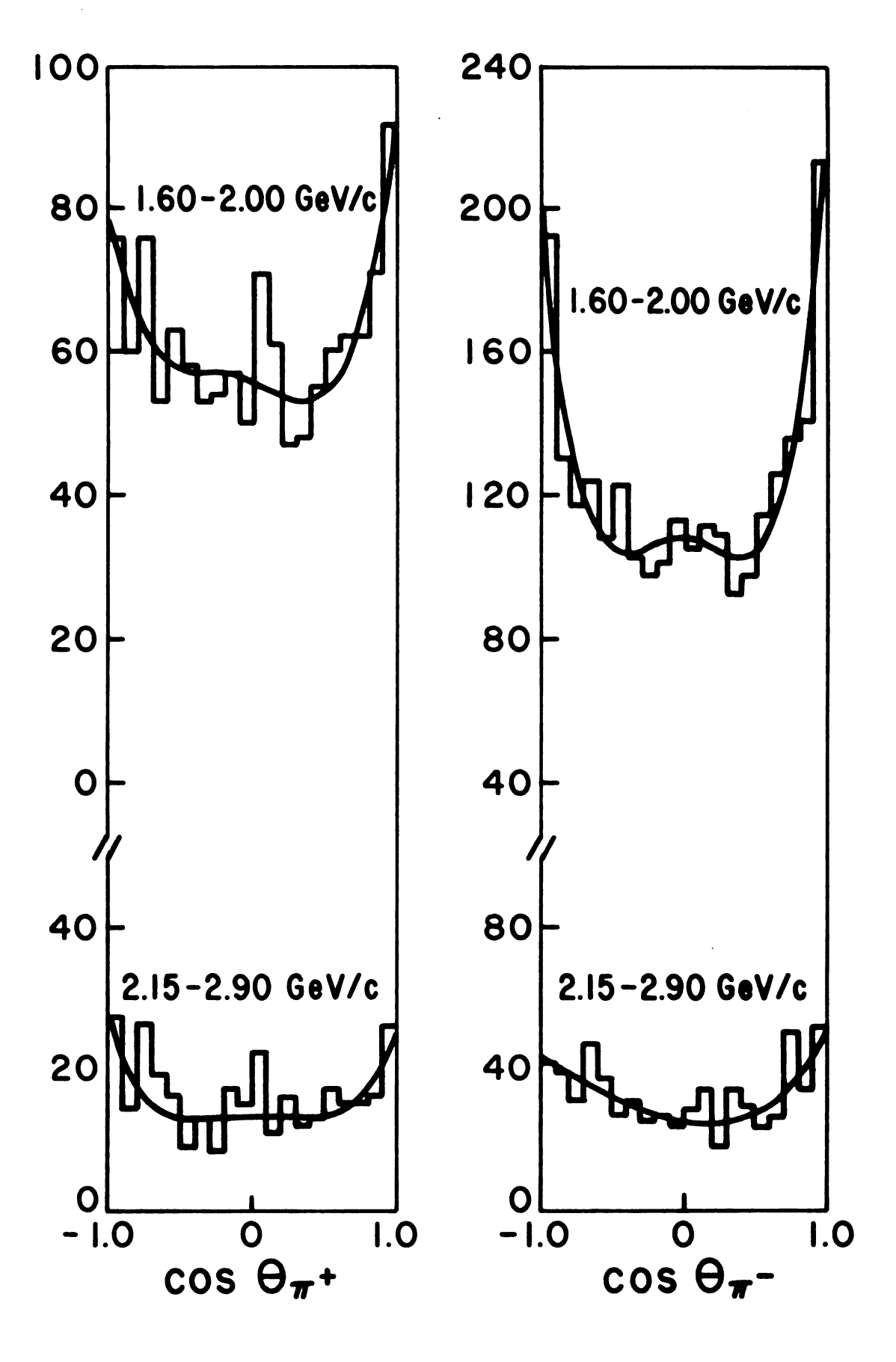


Figure 19. Angular distributions for the four pion final state. The solid curves are fits to the Legendre polynomials

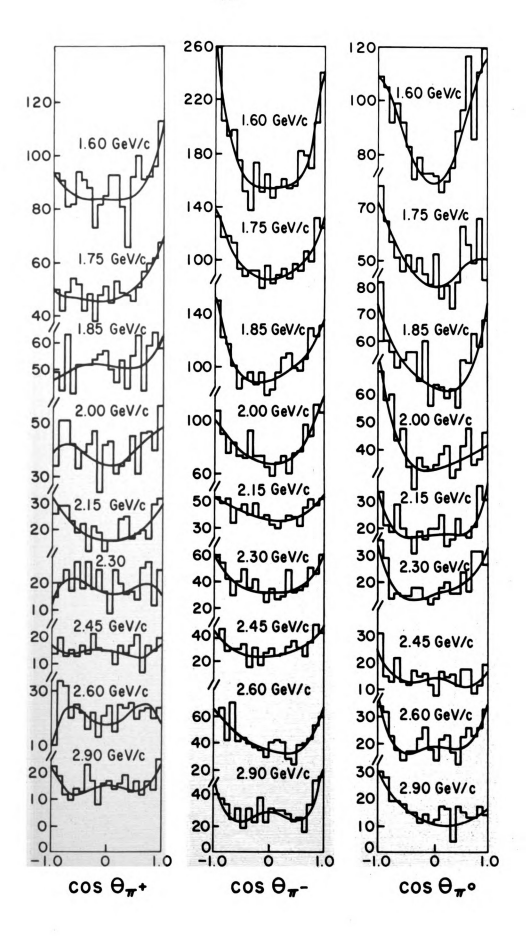


Figure 20. Angular distributions for the five pion final state. The solid curves are fits to the Legendre polynomials

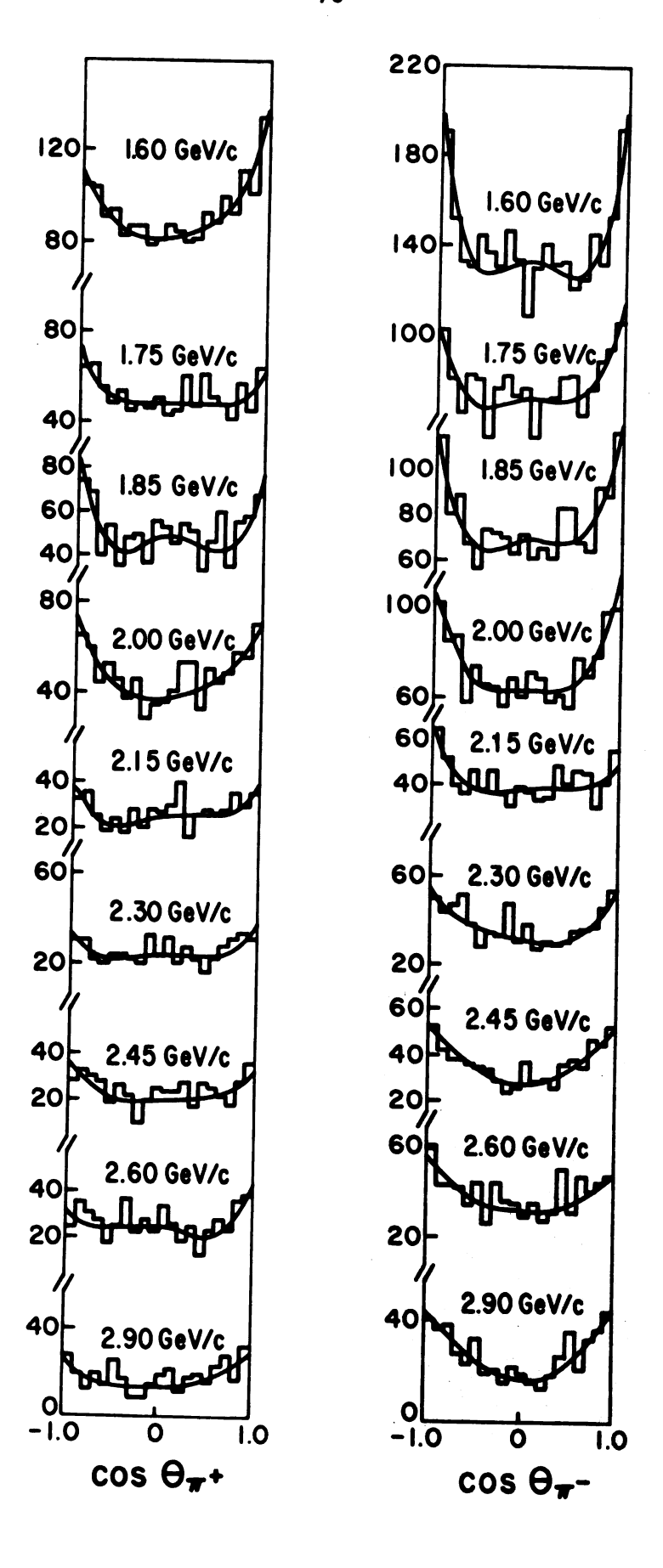


Figure 21. Angular distributions for the six pion final state.
The solid curves are fits to the Legendre polynomials

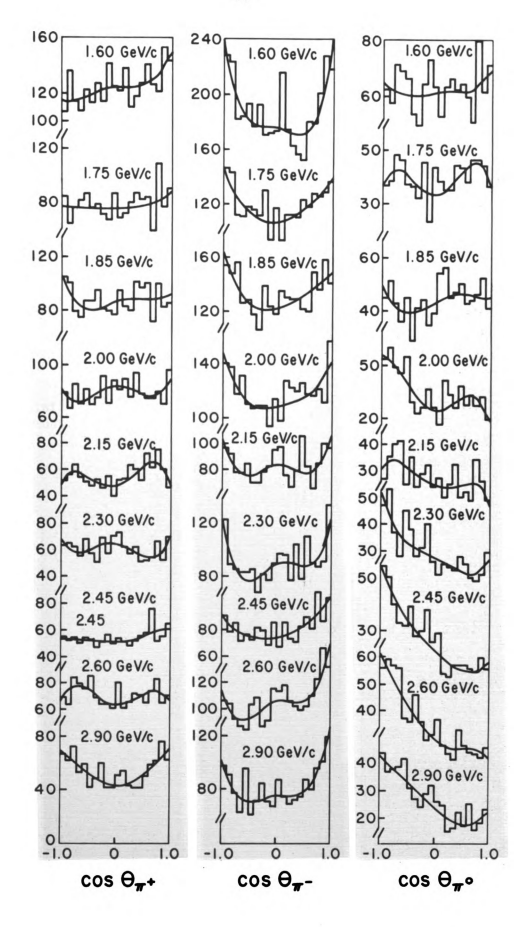


Table 11. Legendre polynomial coefficients

- 11.1 Legendre Polynomial Coefficients from the three pion final state
- 11.2 Legendre Polynomial Coefficients from the four pion final state.
- 11.3 Legendre Polynomial Coefficients from the five pion final state
- 11.4 Legendre Polynomial Coefficients from the six pion final state

Table 11.1 Legendre Polynomial Coefficients from the three pion final state.

	P _L (GeV/c)	P _o (x)	P ₁ (x)	P ₂ (x)	P ₃ (x)	P _{4} (x)	x ₂
. μ θ soc	(1.60-2.00)	.991±.028	.042±.052	.291±.068 .435±.133	.103±.079	.160±.093	12.43
_πθ so⊃	(1.60-2.00)	.995±.020	.048±.038 012±.072	.454±.050	.073±.058	.283±.067 .058±.126	15.63

Table 11.2 Legendre Polynomial Coefficients from the four pion final state.

P _L (GeV/c)	P _o (x)	P _] (x)	P ₂ (x)	P3(x)	P4(x)	χ ²
1.60 1.75 1.85 + 2.00 0 2.15 80 2.45 2.60 2.90	.993±.024 .994±.031 .985±.031 .971±.035 .965±.048 .924±.048 .948±.055 .946±.046	.061±.042 .151±.056 .078±.053 .045±.062 020±.090 059±.084 026±.097 .077±.081 .051±.099	.135±.055 .167±.072 .030±.070 .206±.079 .450±.115 .048±.105 .062±.129 .018±.099 .250±.134	.062±.065 .074±.086 .104±.083 .132±.094 002±.135 .202±.130 .175±.154 .077±.120	.051±.076 .118±.101 .043±.095 067±.109 .059±.152 213±.150 .196±.169 380±.141 .349±.176	13.48 6.49 15.63 23.95 15.44 30.13 16.36 23.17 15.79
1.60 1.75 1.85 2.00 0 2.15 2.30 2.45 2.60 2.90	.997±.017 .997±.022 .996±.025 .992±.025 .986±.034 .975±.035 .971±.040 .978±.033	032±.031 017±.041 .022±.040 .051±.046 024±.062 .001±.066 .090±.074 122±.063 .058±.073	.348± .040 .301± .053 .339± .052 .341± .059 .282± .080 .456± .085 .402± .095 .435± .081	036±.047 013±.062 123±.061 .071±.069 .105±.094 .053±.100 065±.111 .136±.093 .133±.111	.135± .055 .046± .071 .085± .069 .039± .079 .037± .107 .130± .111 .070± .126 .114± .108	14.18 7.98 10.18 14.66 12.17 21.30 18.44 20.26 28.09
1.60 1.75 1.85 ° ≥ 2.00 ⊕ 2.15 ∞ 2.30 ⊗ 2.45 2.60 2.90	.994±.024 .979±.031 .987±.031 .984±.035 .962±.047 .968±.049 .937±.055 .974±.047	.036±.044138±.057071±.057219±.065 .057±.090 .104±.095152±.100 .010±.089394±.105	.384± .074 .430± .084 .469± .118 .577± .123 .267± .134 .487± .118	.023± .066096± .085 .087± .087233± .097008± .134160± .142161± .163067± .133048± .151	083±.077 049±.099 .095±.100 .089±.114 .291±.158 .240±.157 .220±.184 .355±.152	11.50 21.76 14.92 13.96 17.21 13.48 19.86 12.36 20.59

Table 11.3 Legendre Polynomial Coefficients from the five pion final state.

	PL GeV/c)	P _o (x)	P ₁ (x)	P ₂ (x)	P ₃ (x)	P ₄ (x)	χ ²
Cos 0 "	1.60 1.75 1.85 2.00 2.15 2.30 2.45 2.60 2.90	.998±.023 .990±.031 .979±.031 .982±.032 .967±.042 .977±.044 .951±.044 .966±.043	.084±.042 054±.055 015±.057 .060±.060 .100±.076 .073±.080 012±.082 .048±.178 .139±.092	.260± .055 .173± .073 .292± .075 .424± .077 .254± .100 .235± .105 .341± .107 .248± .102		.060± .074 .134± .098 .334± .100 .091± .105 .233± .135 .240± .140 .128± .145 .212± .135	5.40 11.69 23.57 17.94 18.81 12.26 24.45 18.54 21.57
Cos 0m²	1.60 1.75 1.85 2.00 2.15 2.30 2.45 2.60 2.90	.996±.019 .987±.025 .990±.025 .992±.026 .980±.034 .985±.036 .992±.037 .978±.035	005±.034 .064±.046 .044±.047 .020±.049 074±.063 053±.067 .030±.070 041±.065 021±.080	.240±.045 .264±.060 .378±.062 .385±.064 .277±.083 .363±.086 .450±.089 .338±.084	.033±.053 .015±.071 022±.073 .017±.073 122±.099 .121±.100 .020±.104 046±.099 .082±.116	.187± .061 .157± .081 .242± .082 .172± .085 .155± .112 .103± .118 .019± .120 .049± .115	14.15 21.61 17.74 12.69 17.15 11.87 6.53 17.62 15.92

Table 11.4 Legendre Polynomial Coefficients from the six pion final state.

()	P _L GeV/c)	P _O (x)	P ₁ (x)	P ₂ (x)	P ₃ (x)	P ₄ (x)	χ ²
Cos θ^+	1.60 1.75 1.85 2.00 2.15 2.30 2.45 2.60 2.90	.994±.020 .984±.025 .991±.024 .993±.025 .990±.030 .992±.029 .993±.030 .992±.026	.101±.035 .053±.044 .005±.042 .046±.043 .082±.052 026±.050 .076±.053 025±.046 013±.056	.035±.045 .058±.057 .081±.055 023±.057 .066±.065 019±.066 .091±.069 .036±.059	.057±.054 .032±.069 093±.066 .017±.068 160±.079 047±.077 009±.083 .051±.071	.042±.062 .006±.079 .076±.074 .128±.079 240±.092 .168±.090 026±.096 161±.083 006±.096	16.57 25.28 17.20 12.59 9.69 11.10 7.93 10.46 15.29
Cos 9 _m -	1.60 1.75 1.85 2.00 2.15 2.30 2.45 2.60 2.90	.996±.016 .995±.020 .995±.019 .993±.020 .989±.024 .990±.023 .993±.025 .994±.022	021±.029 .003±.037 .021±.035 .009±.037 .022±.043 .063±.042 .094±.044 .158±.038 .112±.045	.210±.038 .202±.048 .165±.045 .188±.048 .127±.057 .210±.056 .177±.057 .122±.050	.056± .045 048± .057 056± .052 069± .057 021± .067 076± .066 .015± .068 .017± .059 .042± .069	.114± .052 .022± .065 .038± .061 .054± .065 .166± .077 .225± .076 .036± .079 .150± .068 .167± .079	19.68 13.32 13.61 17.22 19.83 20.40 11.62 13.51 16.07
Cos θ^{π^o}	1.60 1.75 1.85 2.00 2.15 2.30 2.45 2.60 2.90	.986±.028 .982±.035 .985±.033 .987±.035 .969±.042 .975±.040 .973±.042 .985±.037	.022±.049 .046±.062 .069±.058 216±.063 232±.073 399±.073 664±.078 510±.068 489±.077	.062± .064 .103± .078 .037± .076 .177± .079 .050± .092 .225± .095 .324± .102 .261± .086 .206± .099	.034± .076081± .094197± .089160± .095 .086± .108 .000± .113 .043± .118023± .102 .114± .117	.025± .089238± .110 .060± .103146± .110183± .127 .119± .125 .062± .128043± .116 .034± .136	18.39 13.86 13.18 10.43 17.09 15.72 15.33 10.95 11.94

Figure 22. Legendre polynomial coefficients

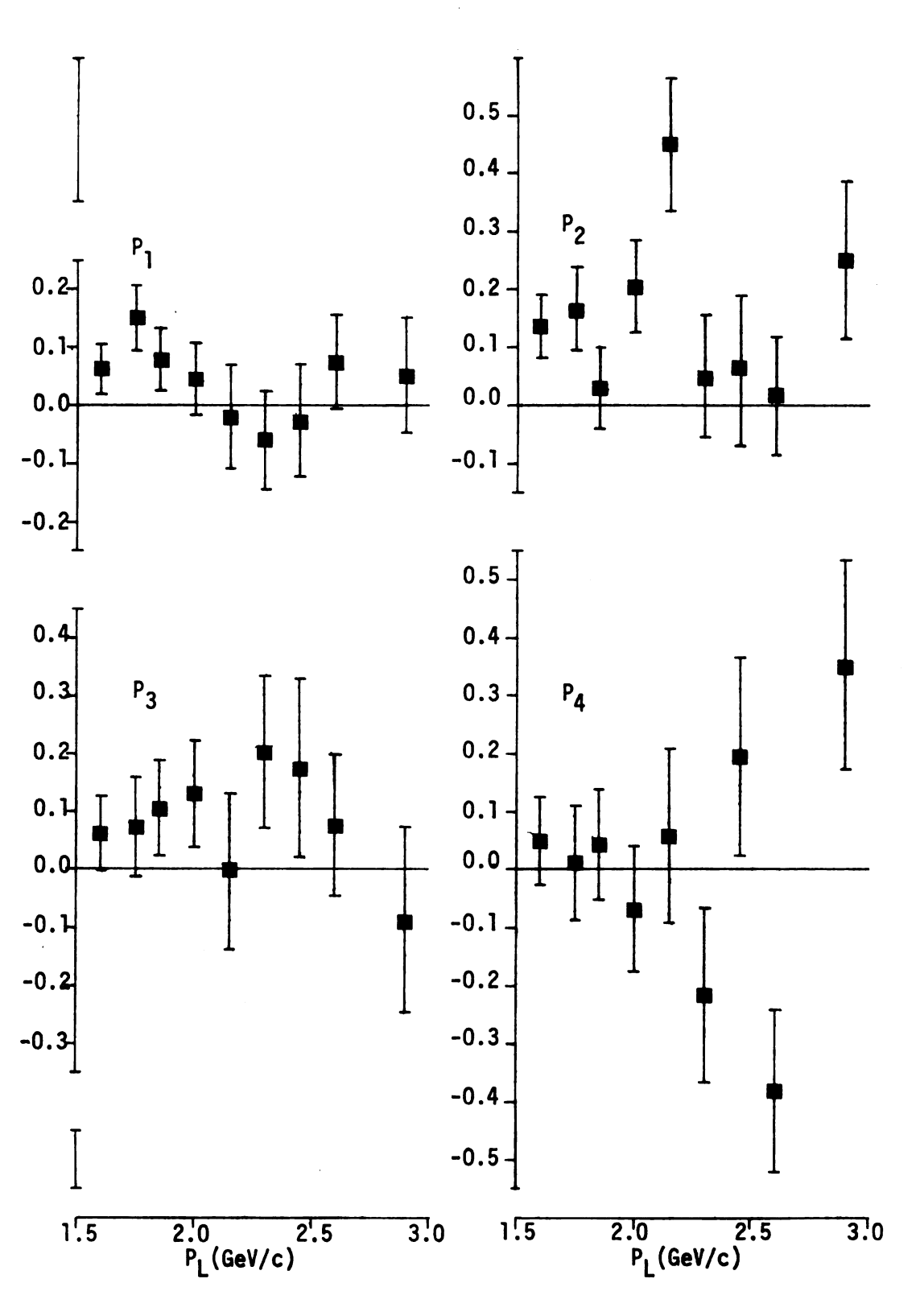
- 22.1 Legendre polynomial coefficients for π^+ from the four pion final state
- 22.2 Legendre polynomial coefficients for π^- from the four pion final state
- 22.3 Legendre polynomial coefficients for π° from the four pion final state
- 22.4 Legendre polynomial coefficients for π^+ from the five pion final state
- 22.5 Legendre polynomial coefficients for π^- from the five pion final state
- 22.6 Legendre polynomial coefficients for π^+ from the six pion final state
- 22.7 Legendre polynomial coefficients for π^- from the six pion final state
- 22.8 Legendre polynomial coefficients for π° from the six pion final state

rom

OM

OM

M



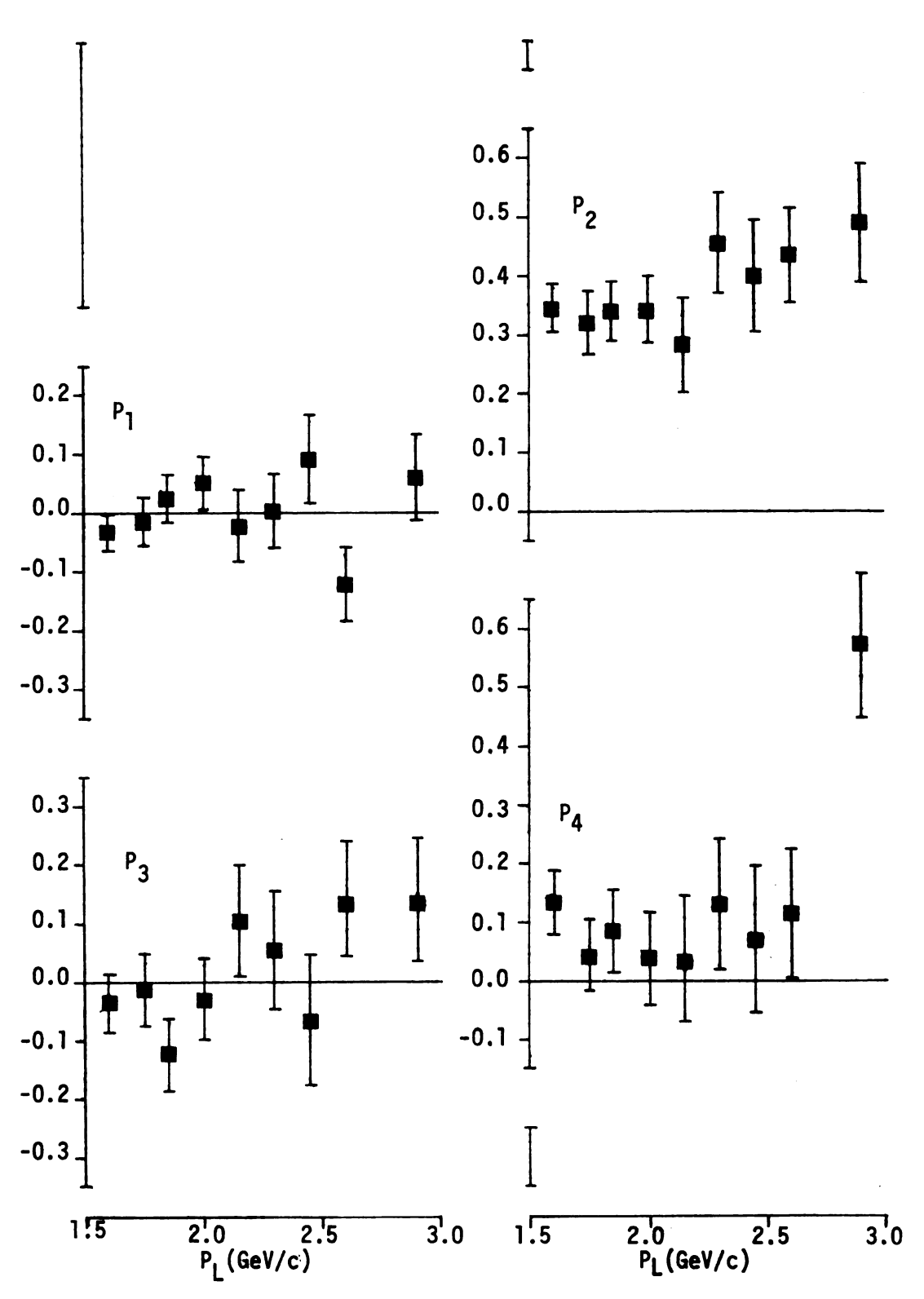


Figure 22.2 Legendre polynomial coefficients for π^- from the four pion final state

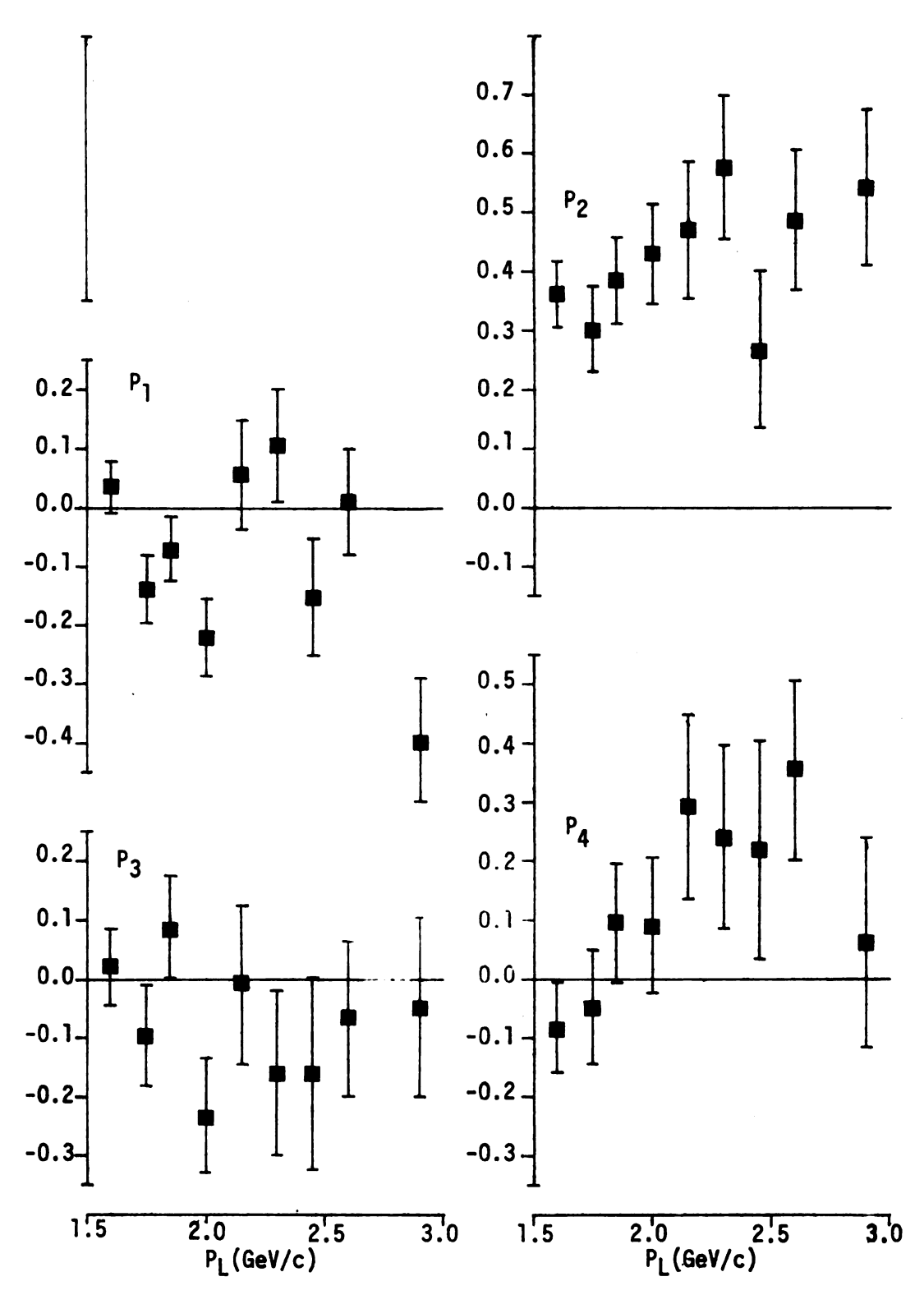


Figure 22.3 Legendre polynomial coefficients for π^{o} from the four pion final state

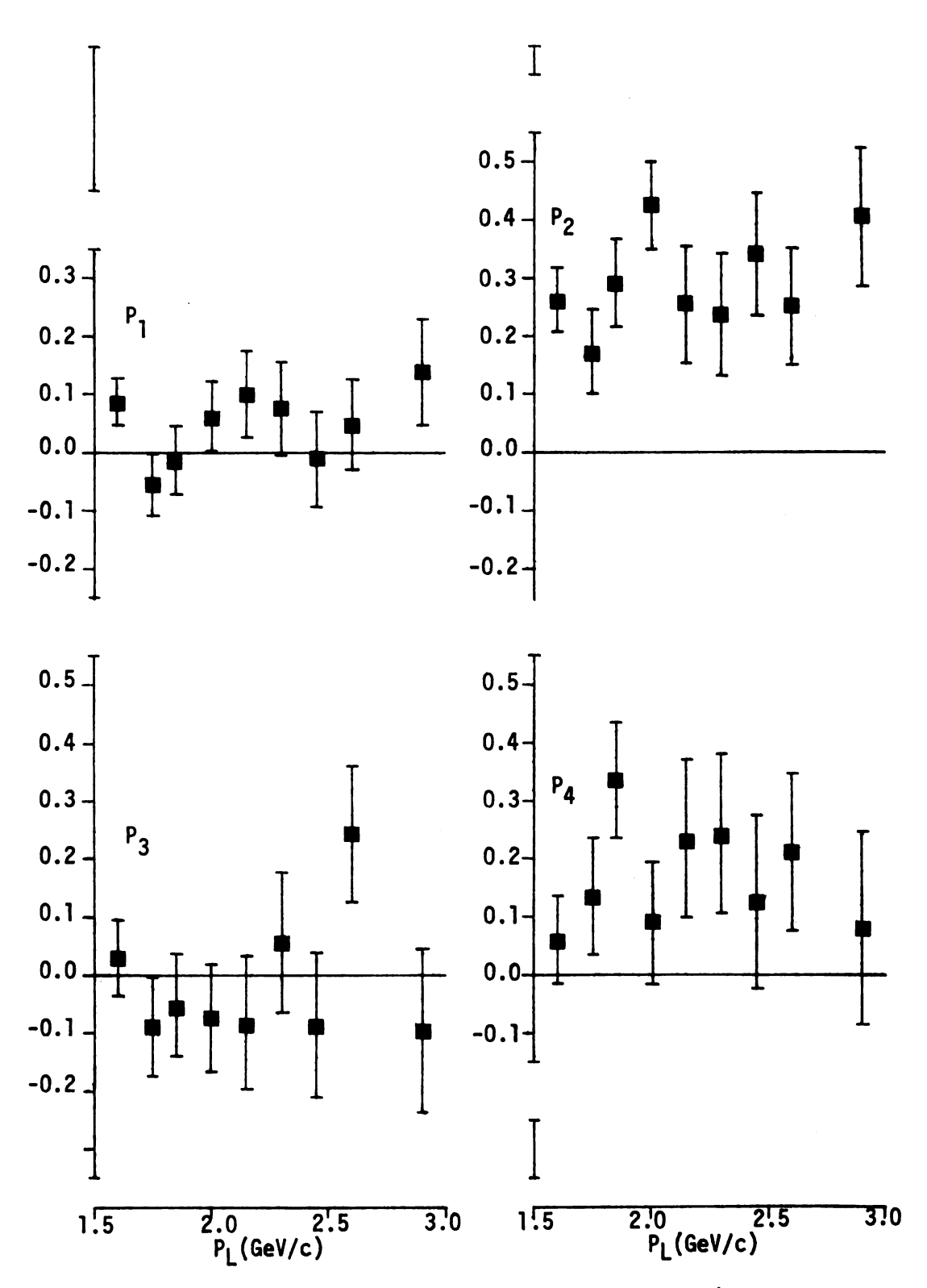


Figure 22.4 Legendre polynomial coefficients for π^{+} from the five pion final state

Figure 22.5 Legendre polynomial coefficients for π^- from the five pion final state

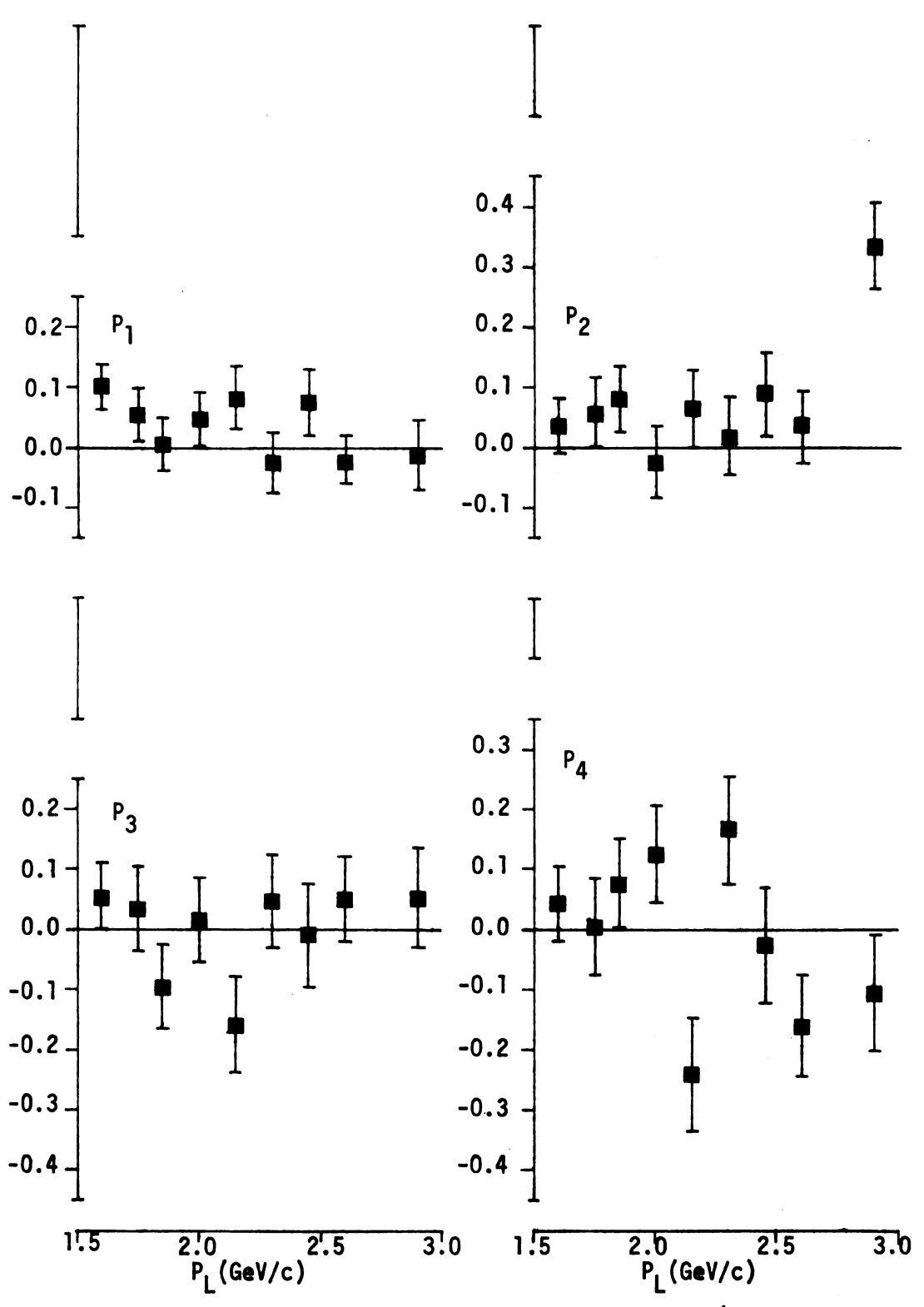


Figure 22.6 Legendre polynomial coefficients for π^{+} from the six pion final state

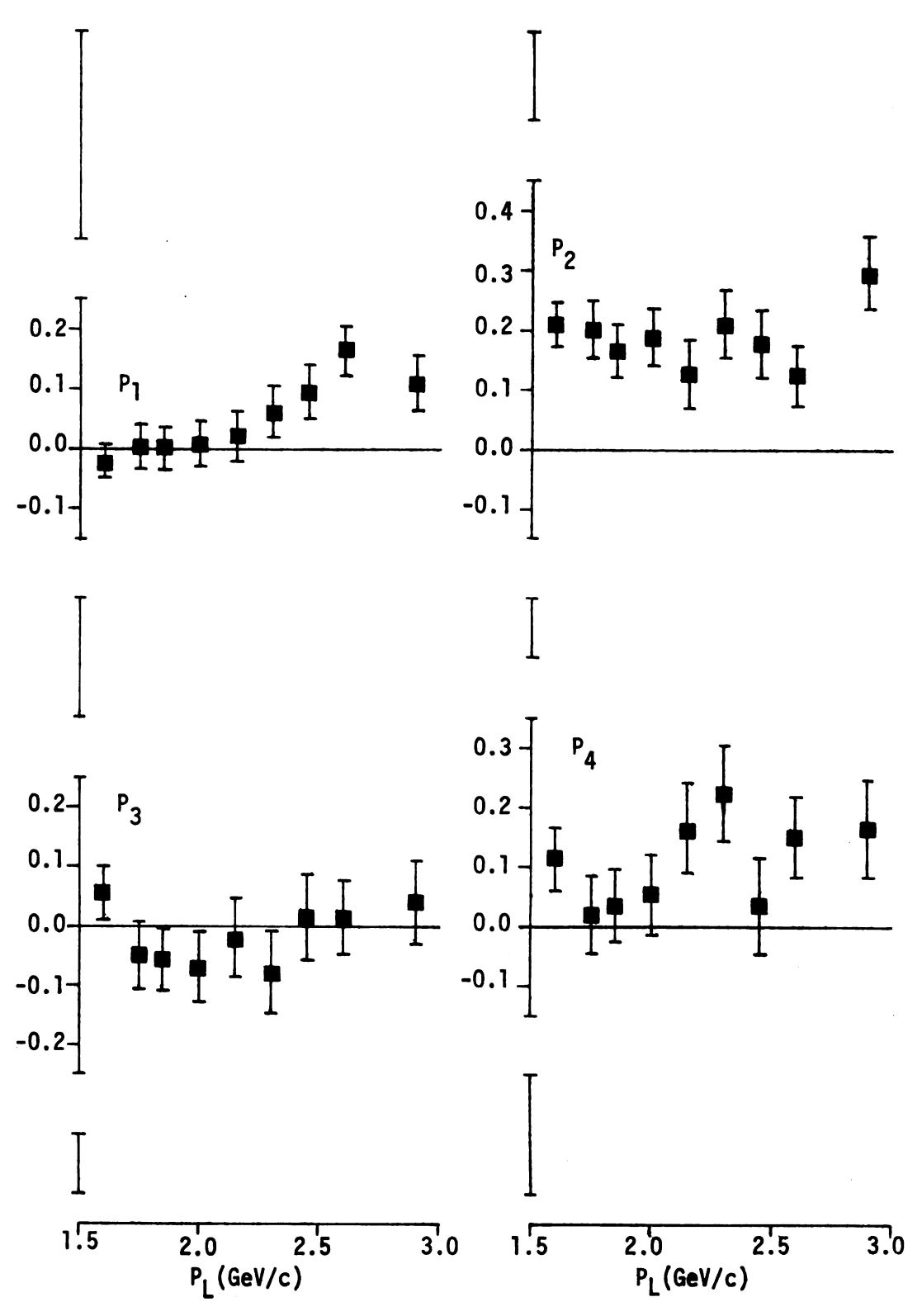


Figure 22.7 Legendre polynomial coefficients for π^- from the six pion final state

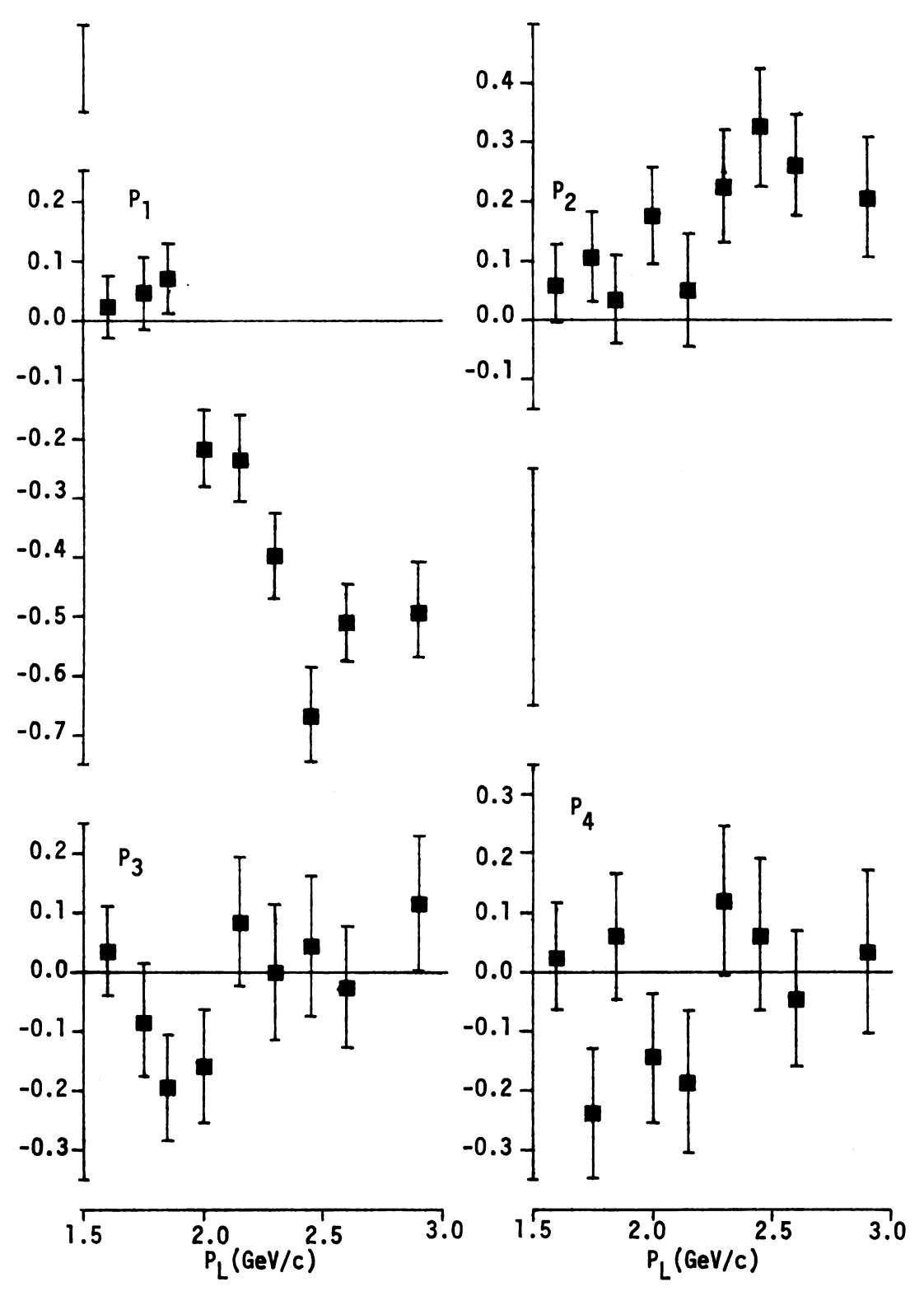


Figure 22.8 Legendre polynomial coefficients for π^{o} from the six pion final state

To discuss the cos $\theta_{\pi_{\mbox{\scriptsize c.m.}}}$ distributions, it is convenient to define the following parameters

asymmetry
$$A = F/B$$
 (17)

collimation
$$C = P/E$$
 (18)

where F is the number of pions going forward in the center-of-mass ($\cos\theta_{\pi}>0$), B is the number going backward ($\cos\theta_{\pi}<0$), and P and E are the number of polar and equitorial pions ($|\cos\theta_{\pi}|>0.5$ and $|\cos\theta_{\pi}|<0.5$ respectively). Unlike $\bar{p}p$ annihilations, in $\bar{p}n$ there is no charge conjugation, coordinate rotation (CR) invariance, thus one charge state cannot be folded into another and each charge state must be investigated independently. The asymmetry and collimation parameters as well as the cosine center-of-mass quadrant values used to calculate them are listed in Table 12 and ploted in Figure 23.

In the three, four, and five pion annihilations, there is very little asymmetry in the $\cos\theta_\pi$ distributions with most of the values being within one standard deviation of unity. In addition, no clear trends are present among the none momenta for any particular charge state. Collimation in these channels is readily apparent but despite the appearance of effects seen visually in the distributions, the only discernable trends are in the $\cos\theta_\pi$ - distributions for the three and five pion channels. In these channels, where all the pions are in a charged state, the collimation of the π^- increases with increasing momentum. As in the four pion annihilations, the collimation of the six pion distributions remains relatively constant as a function of momentum and the asymmetry parameter of the π^+ is nearly unity. However, contrary to the trends at lower multiplicities, the asymmetry of the

Table 12. Asymmetry and collimation parameters

12.1 Parameters for π^+ from the three pion final state. 12.2 Parameters for π^+ from the three pion final state. 12.3 Parameters for π^- from the four pion final state. 12.4 Parameters for π^- from the four pion final state. 12.5 Parameters for π^- from the four pion final state. 12.6 Parameters for π^+ from the five pion final state. 12.7 Parameters for π^- from the five pion final state. 12.8 Parameters for π^- from the six pion final state. 12.9 Parameters for π^- from the six pion final state.

12.10 Parameters for π° from the six pion final state.

Figure 23. Asymmetry and collimation parameters

23.1 Parameters for π^+ from the three pion final state. 23.2 Parameters for π^+ from the three pion final state. 23.3 Parameters for π^- from the four pion final state. 23.4 Parameters for π^- from the four pion final state. 23.5 Parameters for π^+ from the four pion final state. 23.6 Parameters for π^+ from the five pion final state. 23.7 Parameters for π^- from the five pion final state. 23.8 Parameters for π^- from the six pion final state. 23.9 Parameters for π^- from the six pion final state. 23.10 Parameters for π^- from the six pion final state.

Table 12.1 Parameters for π^+ from the three pion final state.

PL	Cos	0 cen	ter-of	-mass	An i mana di sai c	Collimation	
GeV/c	-1 <x<< th=""><th>5<x<< th=""><th>0.0<x<< th=""><th>0.5<x<1< th=""><th>Asymmetry</th></x<1<></th></x<<></th></x<<></th></x<<>	5 <x<< th=""><th>0.0<x<< th=""><th>0.5<x<1< th=""><th>Asymmetry</th></x<1<></th></x<<></th></x<<>	0.0 <x<< th=""><th>0.5<x<1< th=""><th>Asymmetry</th></x<1<></th></x<<>	0.5 <x<1< th=""><th>Asymmetry</th></x<1<>	Asymmetry		
1.60	138.	113.	114.	148.	1.043 +.096/088	1.259 +.118/107	
1.75	63.	49.	63.	77.	1.250 +.171/148	1.250 +.171/148	
1.85	71.	57.	55.	78.	1.039 +.137/121	1.330 +.181/156	
2.00	56.	53.	50.	44.	.862 +.130/114	.970 +.146/127	
2.15	33.	21.	28.	29.	1.055 +.222/182	1.265 +.272/219	
2.30	17.	11.	16.	15.	1.107 +.335/254	1.185 +.362/272	
2.45	22.	15.	8	18.	.702 +.204/164	1.739 +.571/403	
2.60	19.	7.	14.	16.	1.153 +.362/271	1.666 +.578/403	
2.90	11.	8.	8.	11.	1.000 +.387/279	1.375 +.566/383	

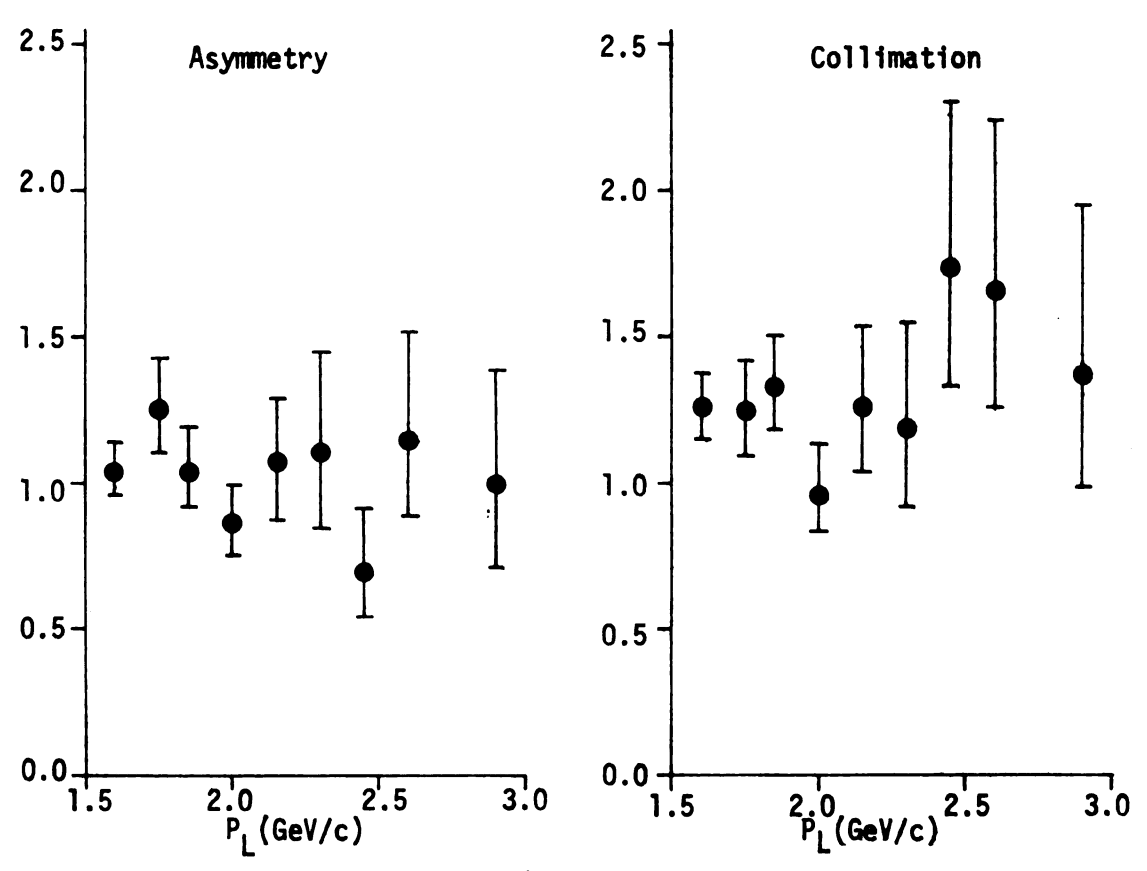


Figure 23.1 Parameters for π^+ from the three pion final state

state, state, state, state tate.

tate. tate. a*te.*

te. ate.

ate. ate. te. te. te.

e. e. .

Table 12.2 Parameters for π^* from the three pion final state.

PL	Cos 0 center-of-mass				As <i>ymme</i> try	Collimation	
GeV/c	-1 <x<< th=""><th>5<x<< th=""><th>0.0<x<< th=""><th>0.5<x<1< th=""><th>Asymile Cry</th><th colspan="2">COTTIMACTOR</th></x<1<></th></x<<></th></x<<></th></x<<>	5 <x<< th=""><th>0.0<x<< th=""><th>0.5<x<1< th=""><th>Asymile Cry</th><th colspan="2">COTTIMACTOR</th></x<1<></th></x<<></th></x<<>	0.0 <x<< th=""><th>0.5<x<1< th=""><th>Asymile Cry</th><th colspan="2">COTTIMACTOR</th></x<1<></th></x<<>	0.5 <x<1< th=""><th>Asymile Cry</th><th colspan="2">COTTIMACTOR</th></x<1<>	Asymile Cry	COTTIMACTOR	
1.60 1.75 1.85 2.00 2.15 2.30 2.45 2.60 2.90	280. 135. 145. 112. 59. 37. 39. 35. 25.	218. 127. 118. 75. 56. 24. 17. 21.	229. 101. 100. 86. 54. 24. 33. 18.	299. 141. 159. 133. 53. 37. 38. 24.	1.060 +.068/064 .923 +.086/079 .984 +.090/082 1.171 +.123/111 .930 +.133/117 .934 +.189/158 1.250 +.250/205 1.000 +.208/172 1.000 +.259/205	1.295 +.085/079 1.210 +.114/103 1.394 +.132/119 1.521 +.168/148 1.018 +.146/128 1.458 +.313/249 1.520 +.318/254 1.871 +.450/343 1.814 +.541/391	

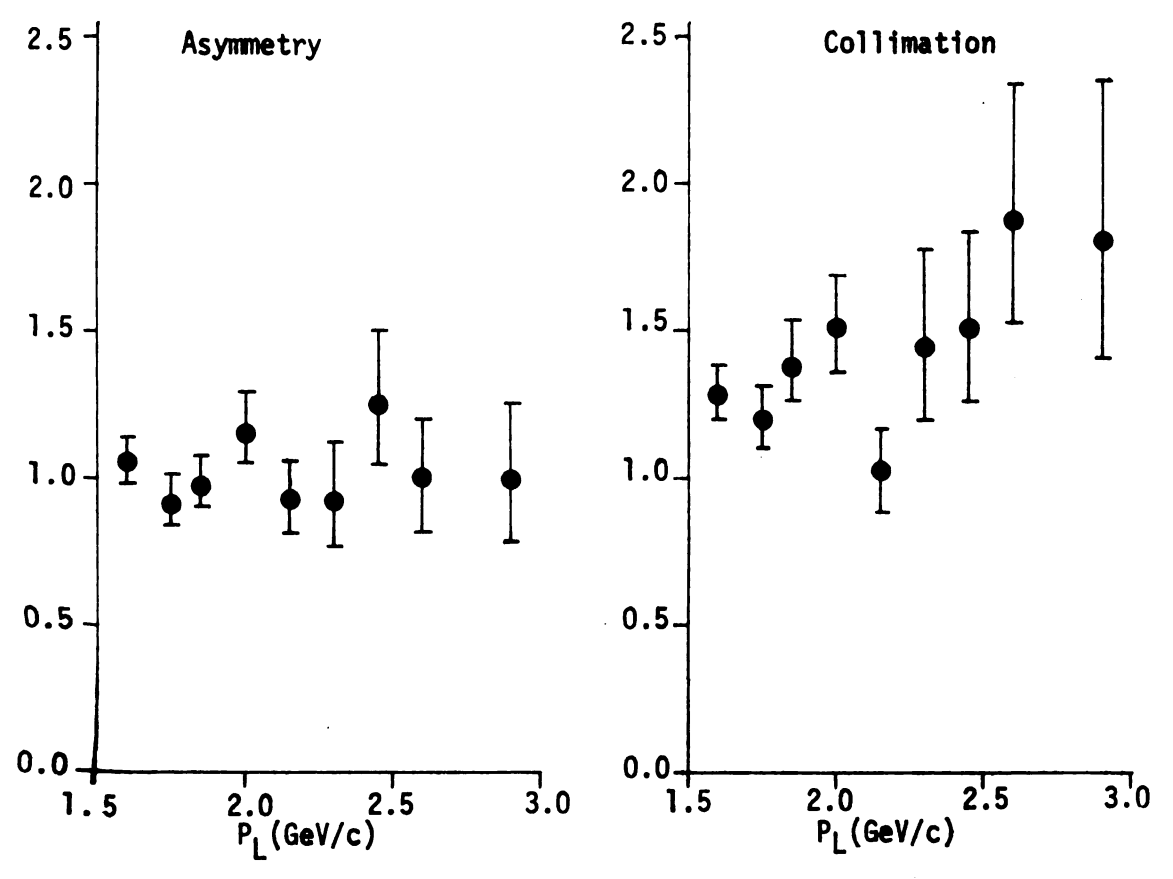


Figure 23.2 Parameters for π^- from the three pion final state

Table 12.3 Parameters for π^+ from the four pion final state.

^{P}L	Cos	9 cen	ter-of	-mass	Acremotes	Collimation	
GeV/c	-1 <x<< th=""><th>5<x<< th=""><th>0.0<x<< th=""><th>0.5<x<1< th=""><th>Asymmetry</th></x<1<></th></x<<></th></x<<></th></x<<>	5 <x<< th=""><th>0.0<x<< th=""><th>0.5<x<1< th=""><th>Asymmetry</th></x<1<></th></x<<></th></x<<>	0.0 <x<< th=""><th>0.5<x<1< th=""><th>Asymmetry</th></x<1<></th></x<<>	0.5 <x<1< th=""><th>Asymmetry</th></x<1<>	Asymmetry		
1.60 1.75 1.85 2.00 2.15 2.30 2.45 2.60 2.90	441. 247. 247. 211. 126. 105. 75. 121.	419. 227. 271. 194. 86. 106. 83. 94. 77.	425. 241. 247. 189. 98. 87. 73. 115.	492. 298. 286. 221. 118. 105. 80. 111.	1.066 +.051/049 1.137 +.074/069 1.029 +.065/061 1.012 +.073/068 1.018 +.103/093 .910 +.095/086 .968 +.116/104 1.051 +.105/095 1.064 +.126/113	1.105 +.053/051 1.164 +.076/071 1.029 +.065/061 1.127 +.082/076 1.326 +.138/123 1.088 +.114/103 .993 +.119/106 1.110 +.111/100 1.038 +.123/110	

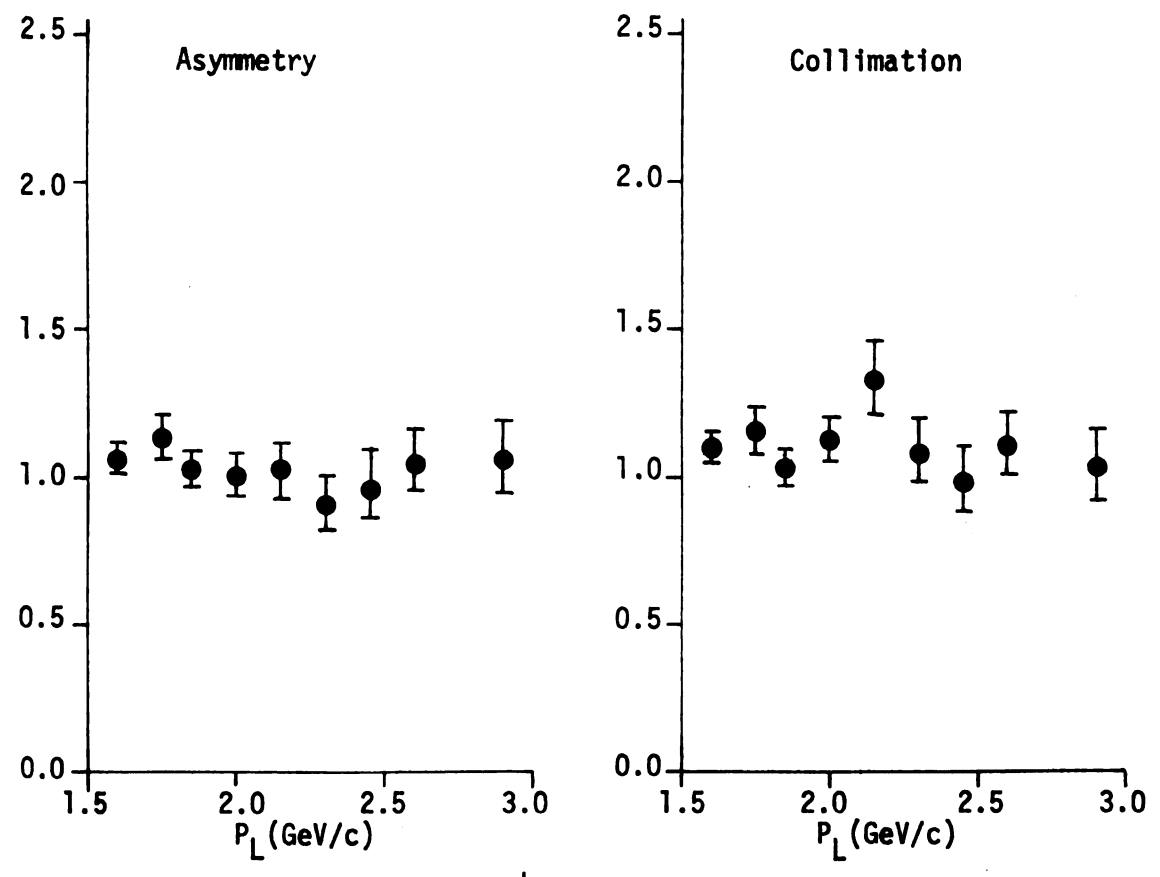


Figure 23.3 Parameters for π^+ from the four pion final state

Table 12.4 Parameters for π^- from the four pion final state.

P_{L}	Cos	θ cer	iter-of	-mass	Asymmetry	Collimation	
G e∀ /c	-1 <x<< th=""><th>5<x<< th=""><th>0.0<x<< th=""><th>0.5<x<1< th=""><th>oo i i ima ci oii</th></x<1<></th></x<<></th></x<<></th></x<<>	5 <x<< th=""><th>0.0<x<< th=""><th>0.5<x<1< th=""><th>oo i i ima ci oii</th></x<1<></th></x<<></th></x<<>	0.0 <x<< th=""><th>0.5<x<1< th=""><th>oo i i ima ci oii</th></x<1<></th></x<<>	0.5 <x<1< th=""><th>oo i i ima ci oii</th></x<1<>		oo i i ima ci oii	
1.60	1027.	778.	773.	976.	.969 +.033/032	1.291 +.044/043	
1.75	574.	447.	450.	555.	.984 +.044/042	1.258 +.058/055	
1.85	573.	448.	495	586.	1.058 +.047/045	1.229 +.055/052	
2.00	430.	381.	339.	480.	1.009 +.051/048	1.263 +.065/061	
2.15	232.	215.	178.	231.	.915 +.064/060	1.178 +.084/078	
2.30	223.	183.	172.	228.	.985 +.071/067	1.270 +.094/087	
2.45	167.	126.	148.	181.	1.122 +.094/086	1.270 +.108/098	
2.60	280.	188.	178.	236.	.884 +.061/058	1.409 +.101/094	
2.90	173.	133.	145.	185.	1.078 +.089/082	1.287 +.108/099	

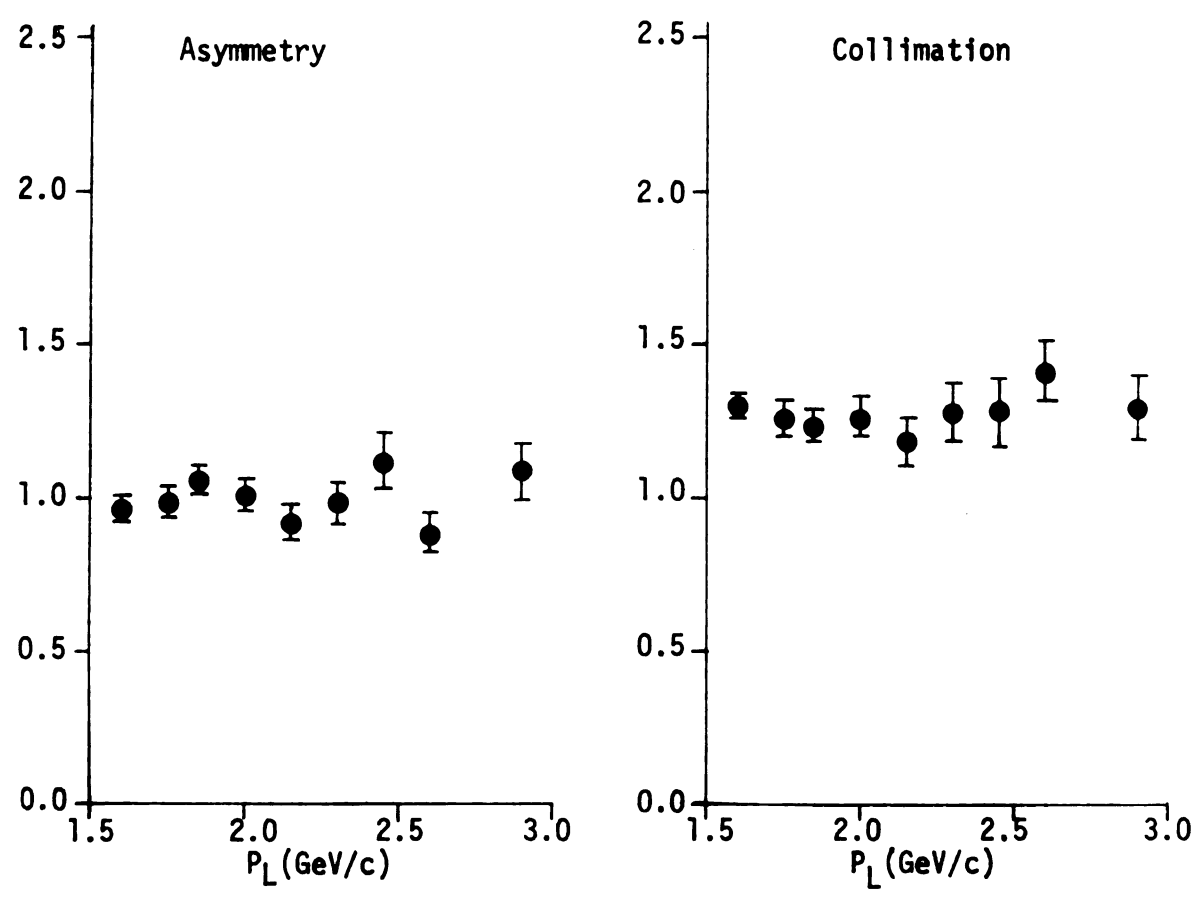


Figure 23.4 Parameters for π^- from the four pion final state

Table 12.5 Parameters for π° from the four pion final state.

PL	Cos	9 cen	ter-of	-mass	A	Collimation	
GeV/c	-1 <x<< th=""><th>5<x<< th=""><th>:0.0<x<< th=""><th>0.5<x<1< th=""><th>Asymmetry</th><th>Collimation</th></x<1<></th></x<<></th></x<<></th></x<<>	5 <x<< th=""><th>:0.0<x<< th=""><th>0.5<x<1< th=""><th>Asymmetry</th><th>Collimation</th></x<1<></th></x<<></th></x<<>	:0.0 <x<< th=""><th>0.5<x<1< th=""><th>Asymmetry</th><th>Collimation</th></x<1<></th></x<<>	0.5 <x<1< th=""><th>Asymmetry</th><th>Collimation</th></x<1<>	Asymmetry	Collimation	
1.60 1.75 1.85 2.00 2.15 2.30 2.45	497. 297. 301. 277. 123. 110. 94.	379. 235. 253. 160. 83. 77.	370. 204. 203. 174. 99. 84.	531 277. 294. 204. 123.	1.028 +.050/047 .904 +.058/058 .897 +.057/053 .865 +.063/059 1.077 +.109/099 1.155 +.122/109	1.372 +.068/064 1.307 +.086/080 1.304 +.085/079 1.440 +.108/100 1.351 +.141/126 1.503 +.166/146	
2.45 2.60 2.90	121. 114.	100. 66.	68. 89. 66.	77. 131. 72.	.873 +.105/094 .995 +.099/090 .766 +.092/083	1.221 +.149/131 1.333 +.137/122 1.409 +.174/152	

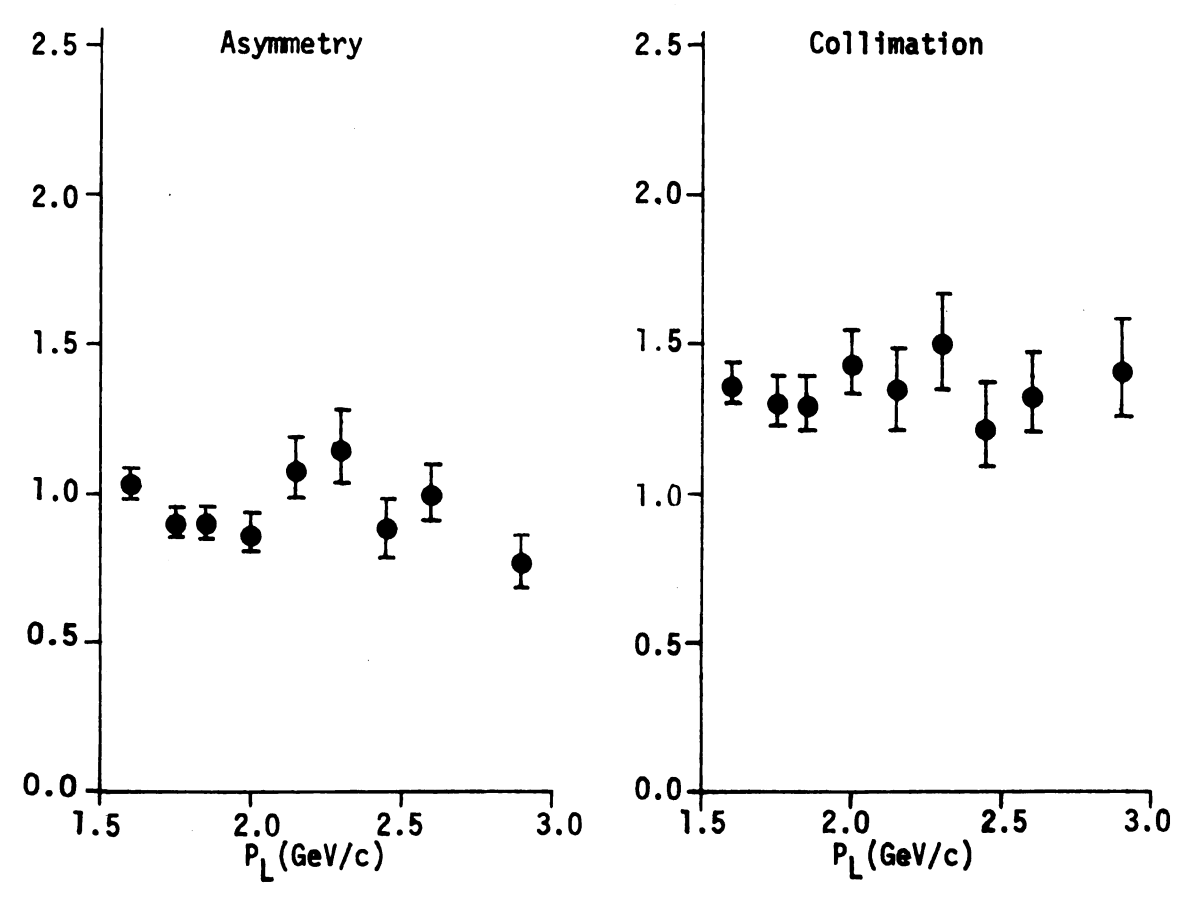


Figure 23.5 Parameters for π° from the four pion final state

Table 12.6 Parameters for π^+ from the five pion final state.

^{P}L	Cos	0 cer	i te r-of	-mass	Asymmetry	Collimation	
GeV/c	-1 <x<< th=""><th>5<x<< th=""><th>0.0<x<< th=""><th>0.5<x<1< th=""><th>COTTINIACTOR</th></x<1<></th></x<<></th></x<<></th></x<<>	5 <x<< th=""><th>0.0<x<< th=""><th>0.5<x<1< th=""><th>COTTINIACTOR</th></x<1<></th></x<<></th></x<<>	0.0 <x<< th=""><th>0.5<x<1< th=""><th>COTTINIACTOR</th></x<1<></th></x<<>	0.5 <x<1< th=""><th>COTTINIACTOR</th></x<1<>		COTTINIACTOR	
1.60 1.75 1.85 2.00 2.15 2.30 2.45 2.60 2.90	476. 285. 273. 268. 136. 124. 136. 132. 97.	421. 232. 242. 183. 121. 120. 103. 131. 80.	428. 264. 232. 230. 140. 116. 119. 116. 95.	541. 255. 277. 279. 157. 146. 128. 147.	1.080 +.051/048 1.003 +.064/060 .988 +.063/059 1.128 +.075/070 1.155 +.103/094 1.073 +.100/091 1.033 +.098/089 1.000 +.091/083 1.214 +.131/117	1.197 +.057/054 1.088 +.070/065 1.160 +.075/070 1.324 +.090/084 1.122 +.100/091 1.144 +.107/097 1.189 +.114/103 1.129 +.103/094 1.240 +.134/119	

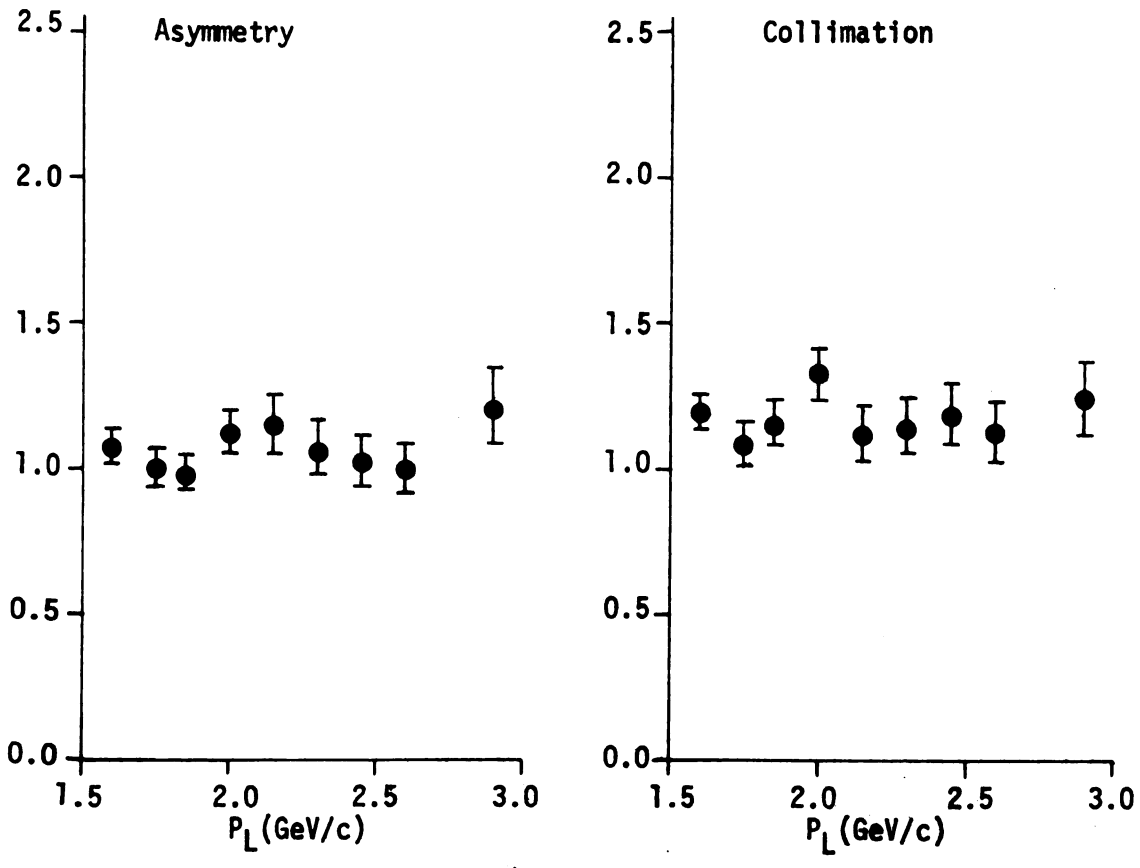


Figure 23.6 Parameters for π^+ from the five pion final state

Table 12.7 Parameters for π^- from the five pion final state.

P_{L}	Cos	0 cer	iter-of	-mass	Asymmetry Asymmetry	Collimation	
GeV/c	-1 <x<< th=""><th>5<x<< th=""><th>0.0<x<< th=""><th>0.5<x<1< th=""><th>COTTINECTOR</th></x<1<></th></x<<></th></x<<></th></x<<>	5 <x<< th=""><th>0.0<x<< th=""><th>0.5<x<1< th=""><th>COTTINECTOR</th></x<1<></th></x<<></th></x<<>	0.0 <x<< th=""><th>0.5<x<1< th=""><th>COTTINECTOR</th></x<1<></th></x<<>	0.5 <x<1< th=""><th>COTTINECTOR</th></x<1<>		COTTINECTOR	
1.60 1.75 1.85 2.00 2.15 2.30 2.45 2.60 2.90	747. 409. 405. 400. 236. 227. 206. 221.	653. 360. 349. 311. 187. 172. 148. 185.	654. 360. 353. 310. 192. 154. 158. 173.	745. 425. 429. 419. 216. 206. 217. 210. 186.	.999 +.038/037 1.020 +.053/050 1.037 +.054/051 1.025 +.055/052 .964 +.069/064 .902 +.068/063 1.059 +.081/075 .943 +.069/065 .960 +.082/076	1.141 +.044/042 1.158 +.060/057 1.188 +.062/059 1.318 +.073/068 1.192 +.086/080 1.328 +.102/094 1.382 +.110/100 1.203 +.090/083 1.648 +.153/137	

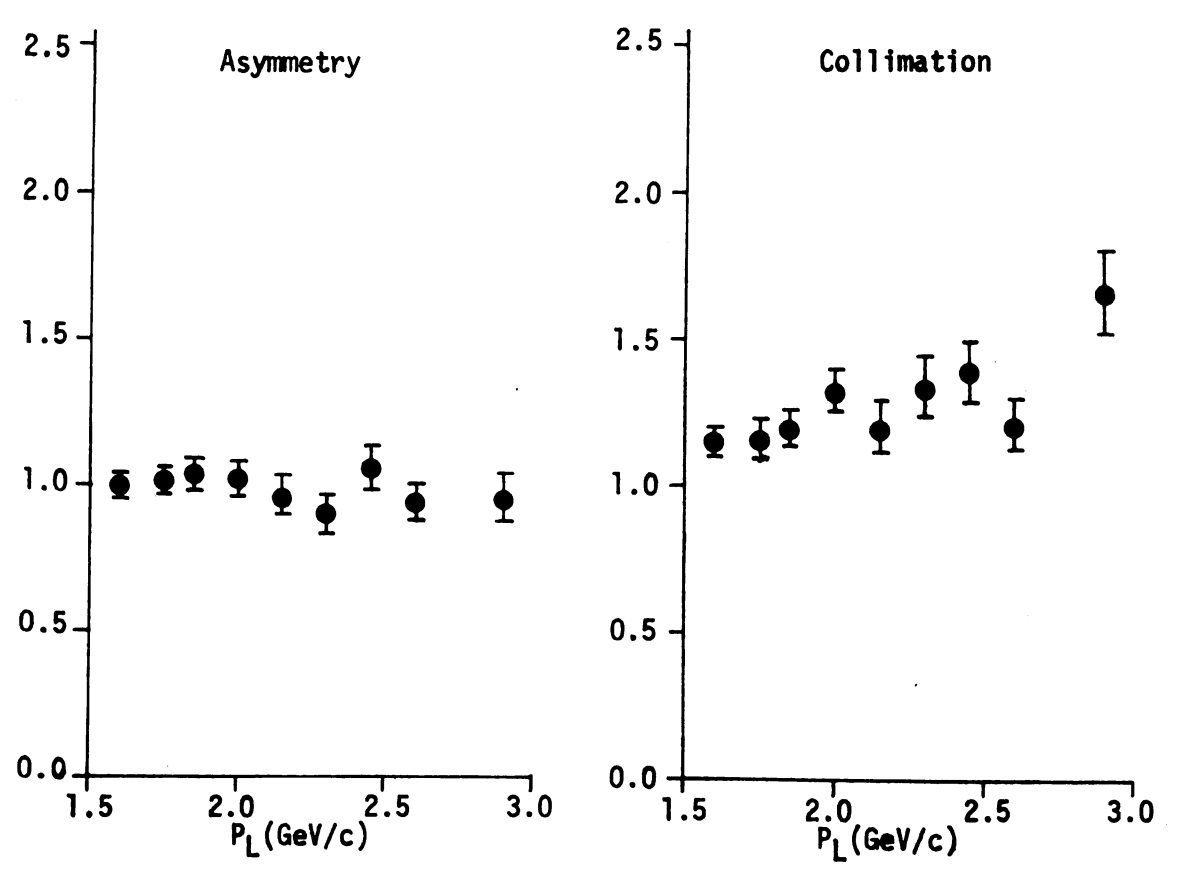


Figure 23.7 Parameters for π^- from the five pion final state

Table 12.8 Parameters for π^+ from the six pion final state.

P_{L}	Cos	0 cen	ter-of	-mass	A a same a bass	Collimation	
GeV/c	-1 <x<< th=""><th>5<x<< th=""><th>0.0<x<< th=""><th>0.5<x<1< th=""><th>Asymmetry</th><th>COTTIMACTOR</th></x<1<></th></x<<></th></x<<></th></x<<>	5 <x<< th=""><th>0.0<x<< th=""><th>0.5<x<1< th=""><th>Asymmetry</th><th>COTTIMACTOR</th></x<1<></th></x<<></th></x<<>	0.0 <x<< th=""><th>0.5<x<1< th=""><th>Asymmetry</th><th>COTTIMACTOR</th></x<1<></th></x<<>	0.5 <x<1< th=""><th>Asymmetry</th><th>COTTIMACTOR</th></x<1<>	Asymmetry	COTTIMACTOR	
1.60 1.75 1.85 2.00 2.15 2.30 2.45 2.60 2.90	585. 391. 445. 382. 276. 312. 265. 372. 313.	621. 378. 420. 395. 241. 304. 257. 343. 235.	616. 391. 456. 418. 280. 305. 260. 350. 232.	688. 420. 451. 397. 315. 295. 306. 357.	1.081 +.044/042 1.054 +.054/051 1.048 +.051/048 1.048 +.054/051 1.150 +.071/067 .974 +.057/054 1.084 +.068/063 .988 +.053/051 .989 +.061/058	1.029 +.041/040 1.054 +.054/051 1.022 +.049/047 .958 +.049/046 1.134 +.070/066 .996 +.058/055 1.104 +.069/065 1.051 +.057/054 1.334 +.085/079	

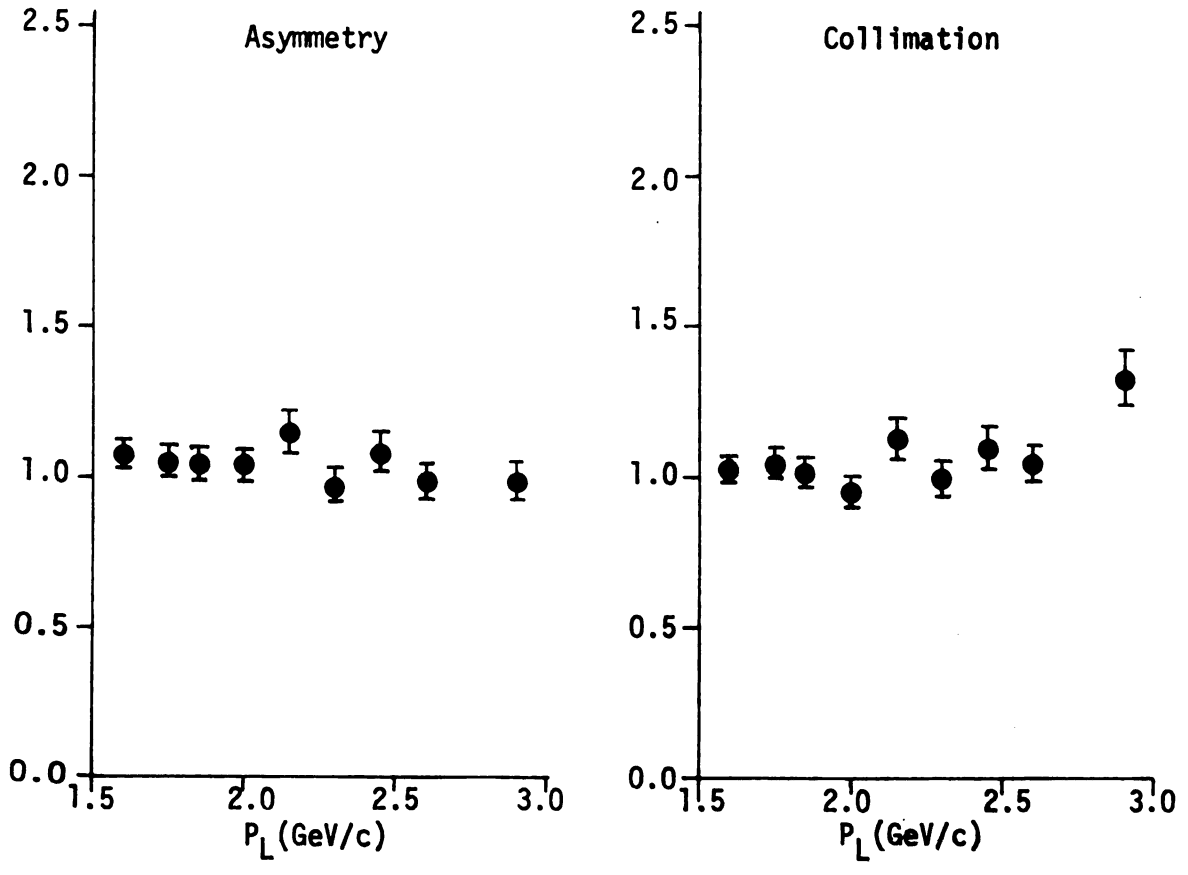


Figure 23.8 Parameters for π^+ from the six pion final state

ti kinga

Table 12.9 Parameters for π^- from the six pion final state.

PL	Cos	θ cer	i te r-of	-mass	A a samue t mos	Collimation	
GeV/c	-1 <x<< th=""><th>5<x<< th=""><th>0.0<x< th=""><th>0.5<x<1< th=""><th>Asymmetry</th></x<1<></th></x<></th></x<<></th></x<<>	5 <x<< th=""><th>0.0<x< th=""><th>0.5<x<1< th=""><th>Asymmetry</th></x<1<></th></x<></th></x<<>	0.0 <x< th=""><th>0.5<x<1< th=""><th>Asymmetry</th></x<1<></th></x<>	0.5 <x<1< th=""><th>Asymmetry</th></x<1<>	Asymmetry		
1.60 1.75 1.85 2.00 2.15 2.30 2.45 2.60 2.90	1012. 627. 710. 637. 426. 461. 400. 475.	886. 564. 602. 532. 394. 400. 385. 504.	860. 546. 643. 593. 421. 452. 378. 541.	1007. 633. 703. 626. 427. 511. 469. 613.	.983 +.032/031 .989 +.041/039 1.025 +.040/039 1.042 +.043/041 1.034 +.052/049 1.118 +.053/051 1.079 +.054/052 1.178 +.052/050 1.107 +.056/053	1.156 +.038/037 1.135 +.047/045 1.134 +.045/043 1.122 +.047/045 1.046 +.052/050 1.140 +.055/052 1.138 +.058/055 1.041 +.046/044 1.239 +.063/060	

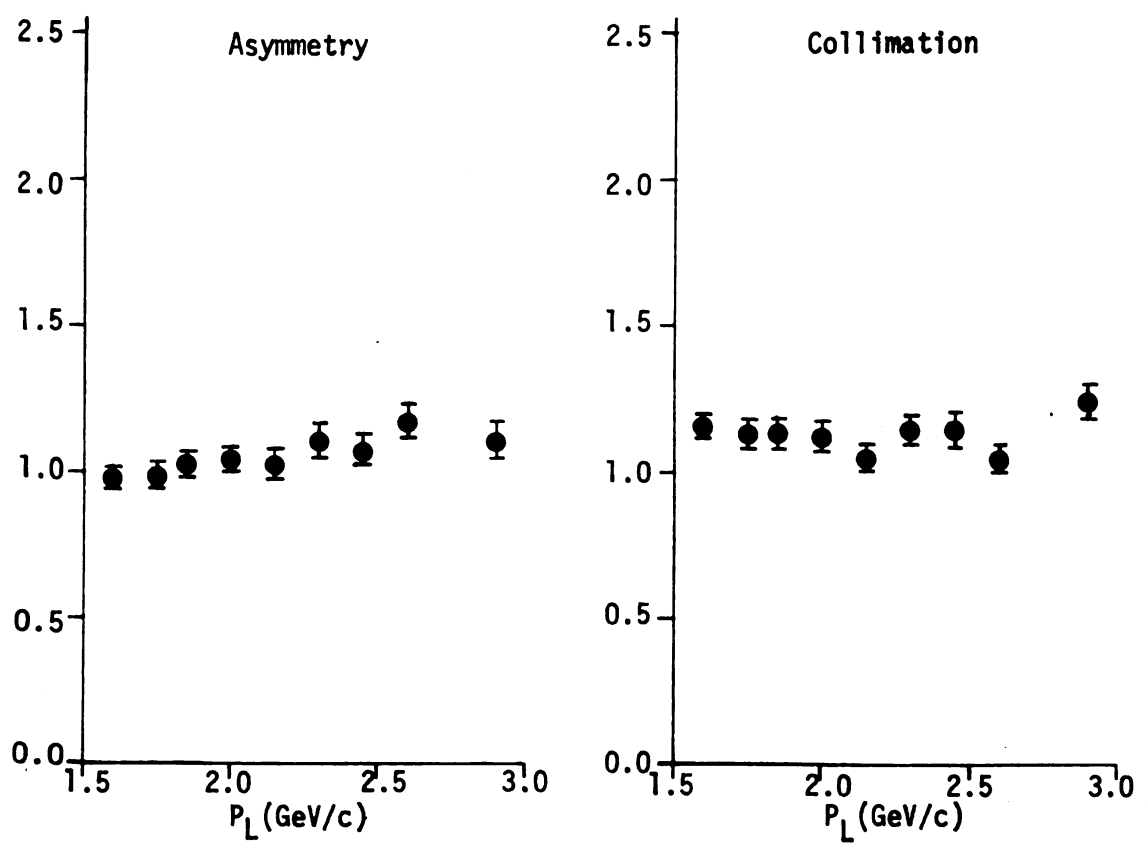


Figure 23.9 Parameters for π^- from the six pion final state

and the second

.

Table 12.10 Parameters for π° from the six pion final state.

P_{L}	Cos	θ cer	iter-of	-mass	Asymmetry	Callimation	
GeV/c	-1 <x<< th=""><th>5<x<< th=""><th>0.0<x<< th=""><th>0.5<x<1< th=""><th>Collimation</th></x<1<></th></x<<></th></x<<></th></x<<>	5 <x<< th=""><th>0.0<x<< th=""><th>0.5<x<1< th=""><th>Collimation</th></x<1<></th></x<<></th></x<<>	0.0 <x<< th=""><th>0.5<x<1< th=""><th>Collimation</th></x<1<></th></x<<>	0.5 <x<1< th=""><th>Collimation</th></x<1<>		Collimation	
1.60 1.75 1.85 2.00 2.15 2.30 2.45 2.60 2.90	325. 206. 220. 257. 168. 210. 209. 265. 200.	302. 179. 188. 177. 144. 163. 161. 178. 143.	307. 195. 252. 186. 124. 121. 90. 143. 104.	321. 210. 226. 176. 120. 114. 84. 125. 98	1.001 +.058/055 1.051 +.077/072 1.171 +.082/076 .834 +.061/057 .782 +.070/064 .630 +.055/052 .470 +.047/044 .605 +.049/046 .588 +.056/052	1.060 +.061/058 1.112 +.082/076 1.013 +.070/065 1.192 +.088/082 1.074 +.095/087 1.140 +.097/089 1.167 +.105/096 1.215 +.096/088 1.206 +.109/099	

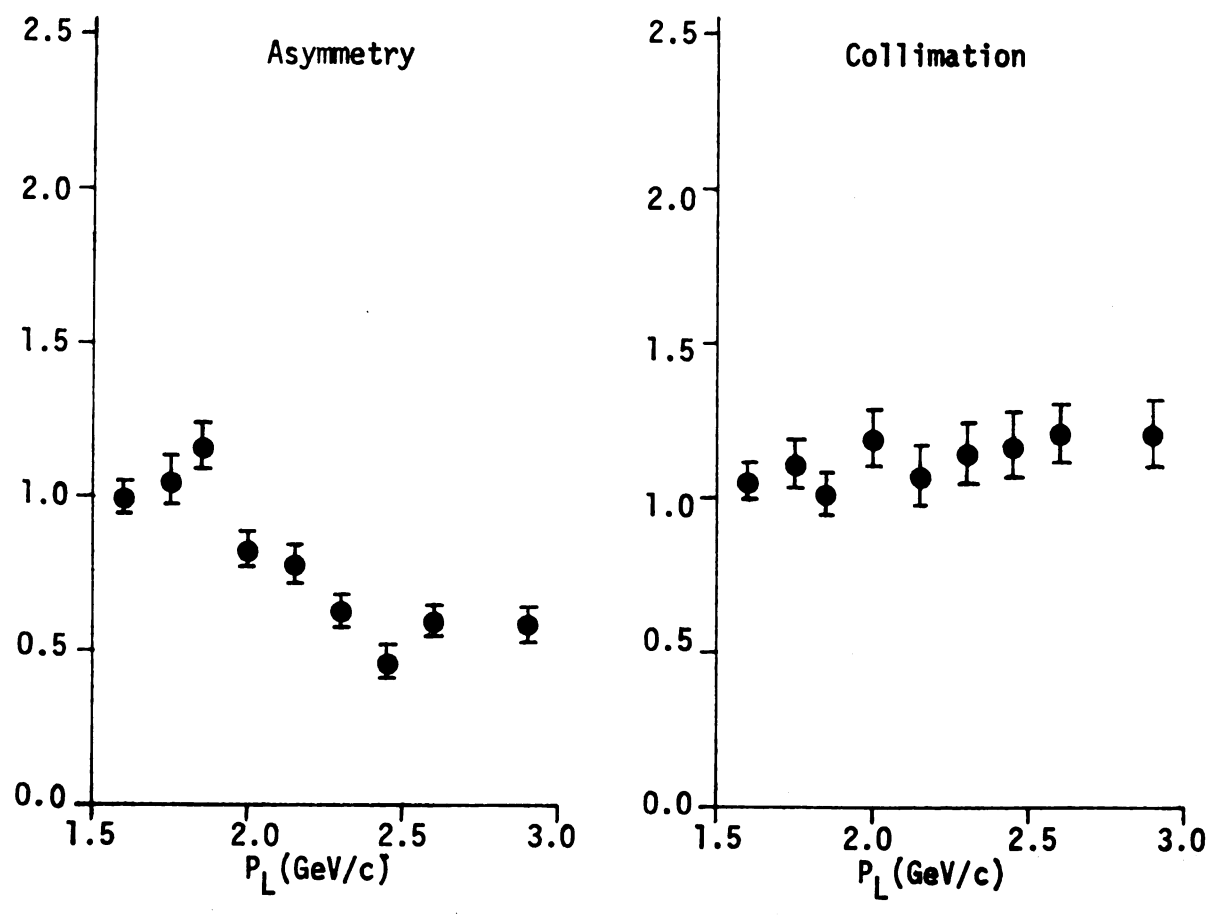


Figure 23.10 Parameters for π° from the six pion final state

 π^{-} and π° distributions is not constant but exhibits an increasing preference for forward and backward production as the incident beam momentum increases.

The center-of-mass longitudinal momentum and transverse momentum distribution for the three through six pion annihilations, are shown in Figure 24. The dashed curves in Figure 24 represent fits of the centerof-mass longitudinal momentum, \boldsymbol{p}_{l} , and the transverse momentum, \boldsymbol{p}_{T} , to functions of the form³⁶:

$$\frac{dN}{dp_1} = N_t \alpha_{ij} e^{-\alpha_{jj} P_L}$$
 (19)

$$\frac{dN}{dp_{L}} = N_{t} \alpha_{ii} e^{-\alpha_{ii} P_{L}}$$

$$\frac{dN}{dp_{T}} = N_{t} (\frac{2}{3 \pi}) \alpha_{L}^{5/2} p_{T}^{3/2} e^{-\alpha_{L} p_{T}}$$
(20)

where N_{t} is the total number of pions. Although these functions, based on a statistical model, were used by D. B. Smith et al. 37 to describe the momentum spectra of charged pions produced in pp interactions between 13 GeV/c and 28.5 GeV/c and adequately describe the transverse momentum distributions, they fail to account for the asymmetry and the collimation of the pn interactions as is evidenced by the poor fit to the $\pi^{\circ}_{\text{C.m.}}$ longitudinal momentum distributions from the six pion annihilations.

- Figure 24. Center-of-mass longitudinal and transverse momentum distributions. The solid curves are fits to statistical model predictions
 - 24.1 Longitudinal momentum distributions from three pion final states between 1.60 and 2.00 GeV/c
 - 24.2 Transverse momentum distributions from three pion final states between 1.60 and 2.00 GeV/c
 - 24.3 Longitudinal momentum distributions from four pion final states between 1.60 and 2.00 GeV/c
 - 24.4 Transverse momentum distributions from four pion final states between 1.60 and 2.00 GeV/c
 - 24.5 Longitudinal momentum distributions from four pion final states between 2.15 and 2.90 GeV/c
 - 24.6 Transverse momentum distributions from four pion final states between 2.15 and 2.90 GeV/c
 - 24.7 Longitudinal momentum distributions from five pion final states between 1.60 and 2.00 GeV/c
 - 24.8 Transverse momentum distributions from five pion final states between 1.60 and 2.00 GeV/c
 - 24.9 Longitudinal momentum distributions from five pion final states between 2.15 and 2.90 GeV/c
 - 24.10 Transverse momentum distributions from five pion final states between 2.15 and 2.90 GeV/c
 - 24.11 Longitudinal momentum distributions from six pion final states between 1.60 and 2.00 GeV/c
 - 24.12 Transverse momentum distributions from six pion final states between 1.60 and 2.00 GeV/c
 - 24.13 Longitudinal momentum distributions from six pion final states between 2.15 and 2.90 GeV/c
 - 24.14 Transverse momentum distributions from six pion final states between 2.15 and 2.90 GeV/c

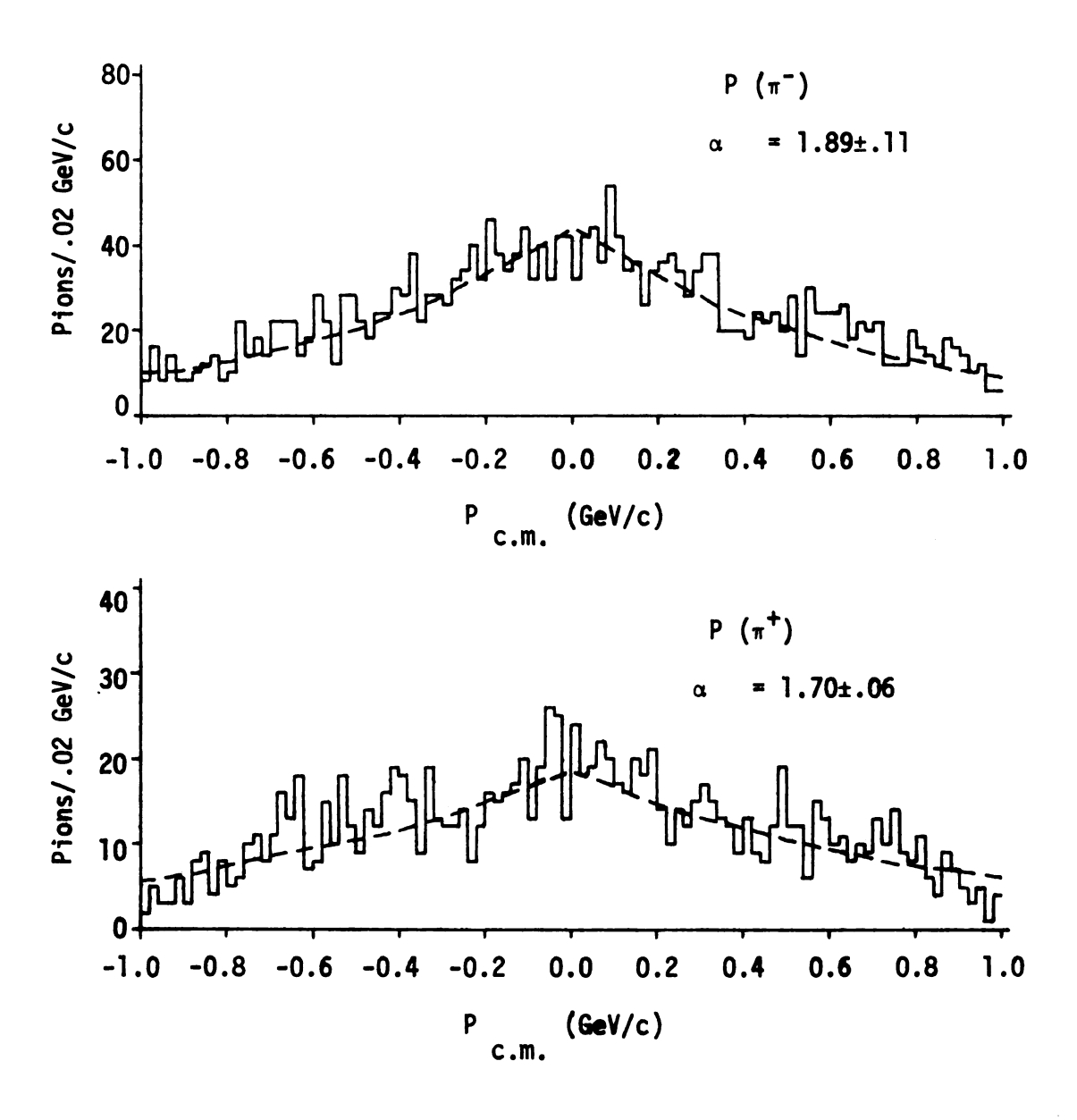
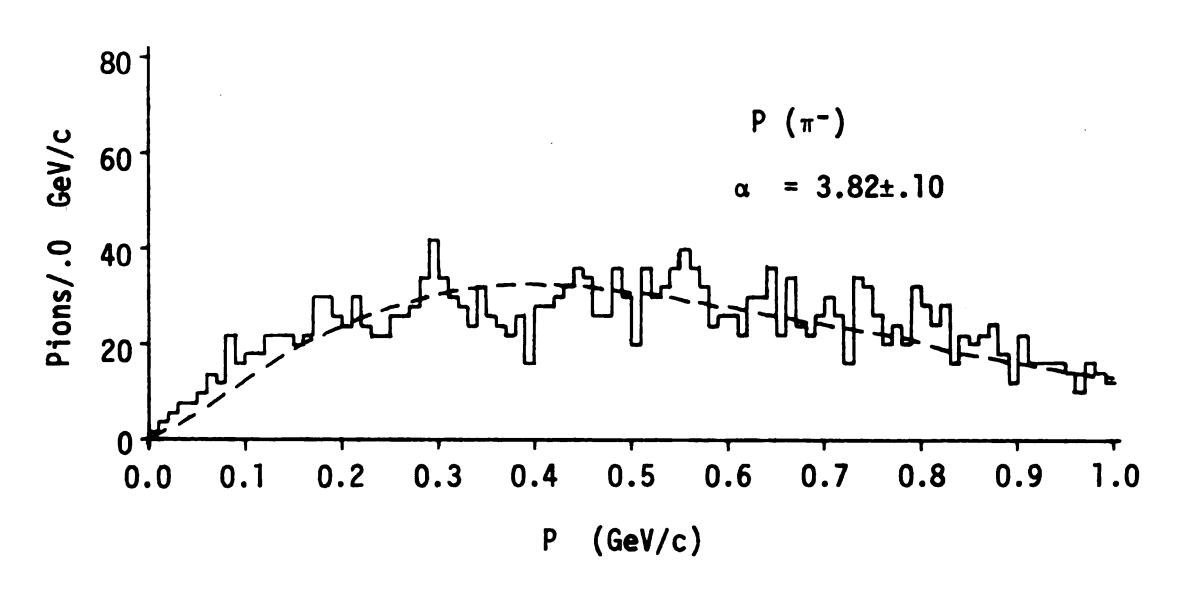


Figure 24.1 Longitudinal momentum distributions from three pion final states between 1.60 and 2.00 GeV/c



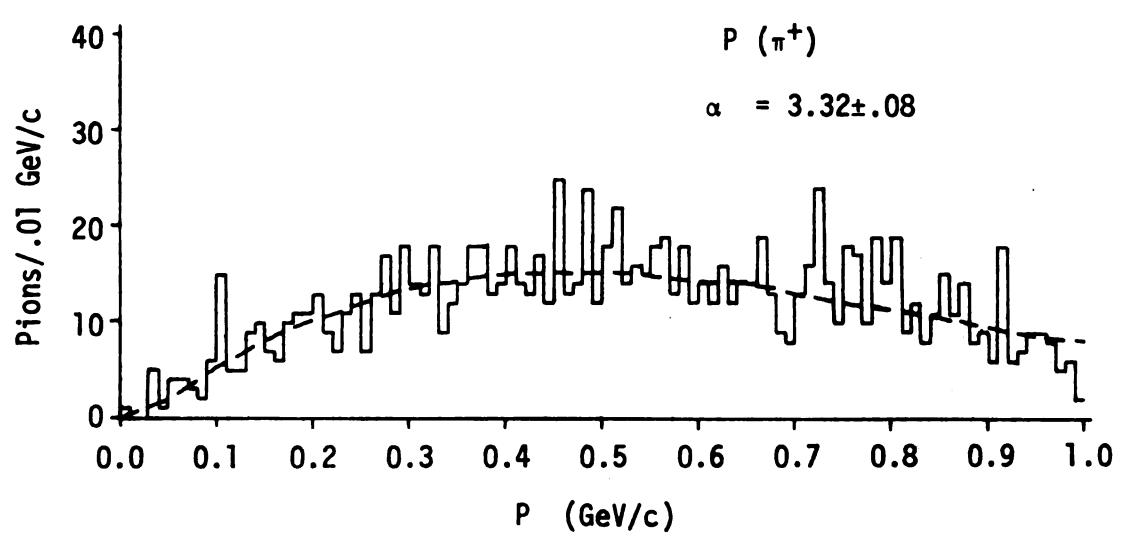


Figure 24.2 Transverse momentum distributions from three pion final states between 1.60 and 2.00 GeV/c

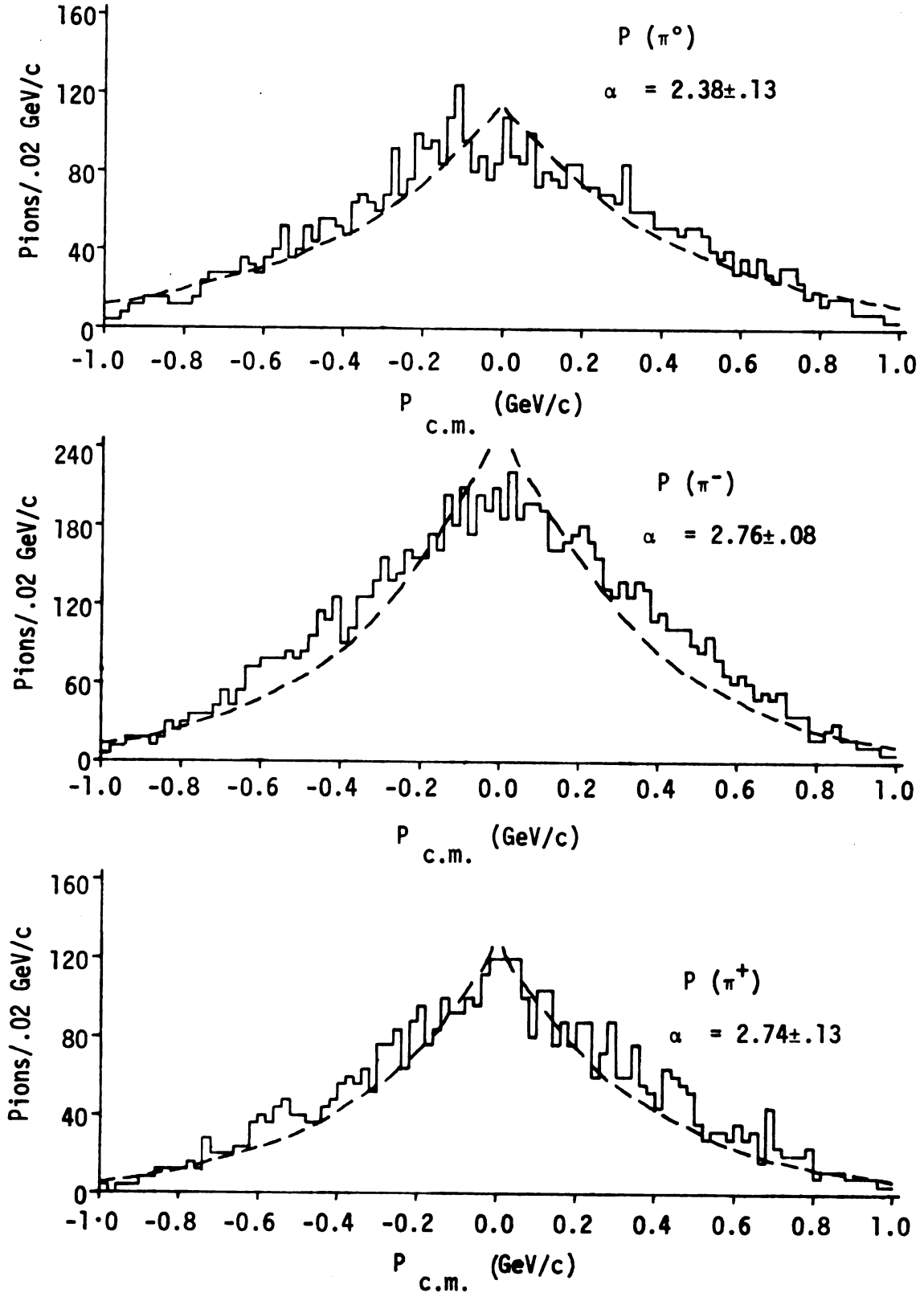


Figure 24.3 Longitudinal momentum distributions from four pion final states between 1.60 and 2.00 GeV/c

; udition

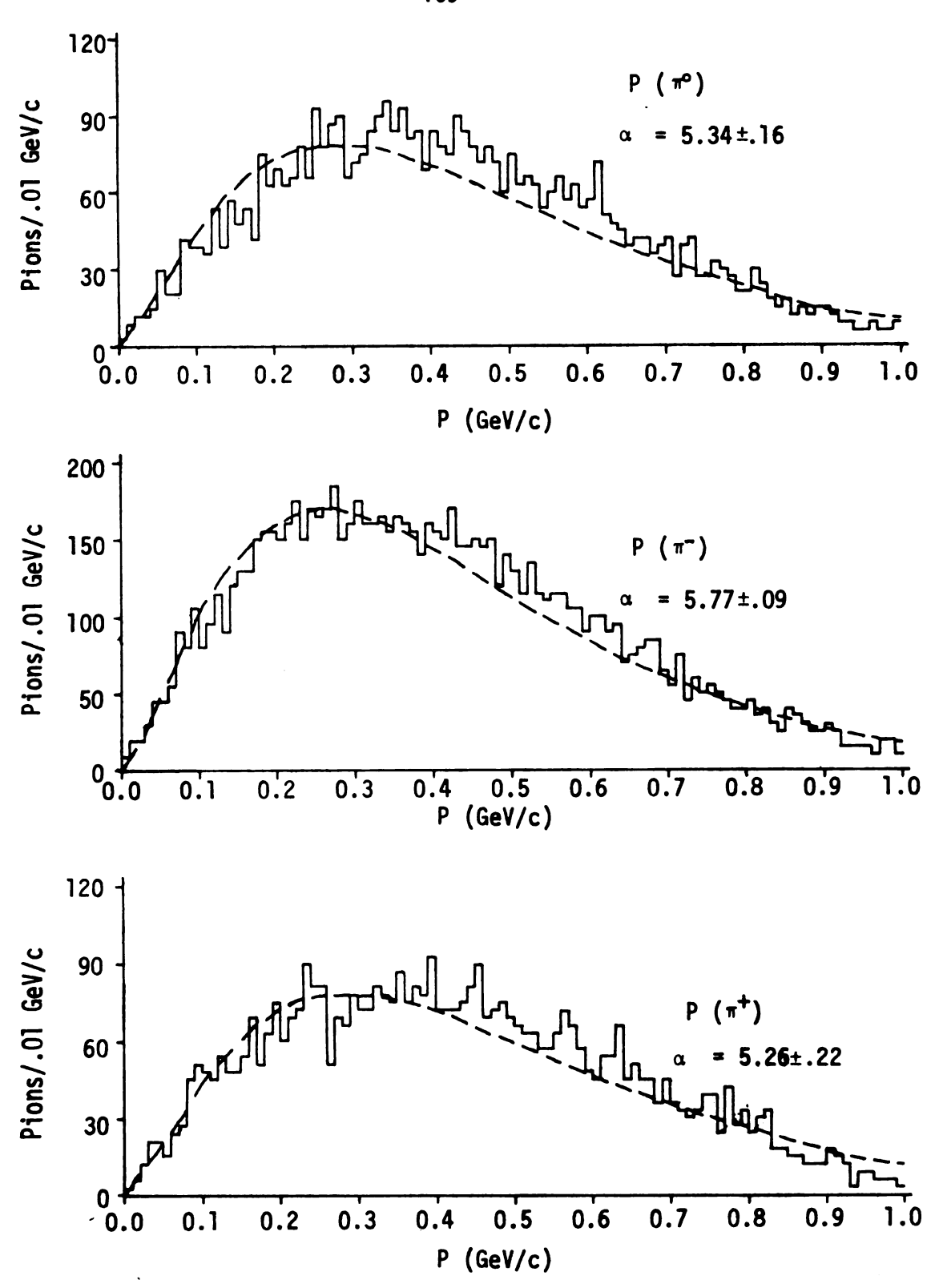


Figure 24.4 Transverse momentum distributions from four pion final states between 1.60 and 2.00 GeV/c

in the second

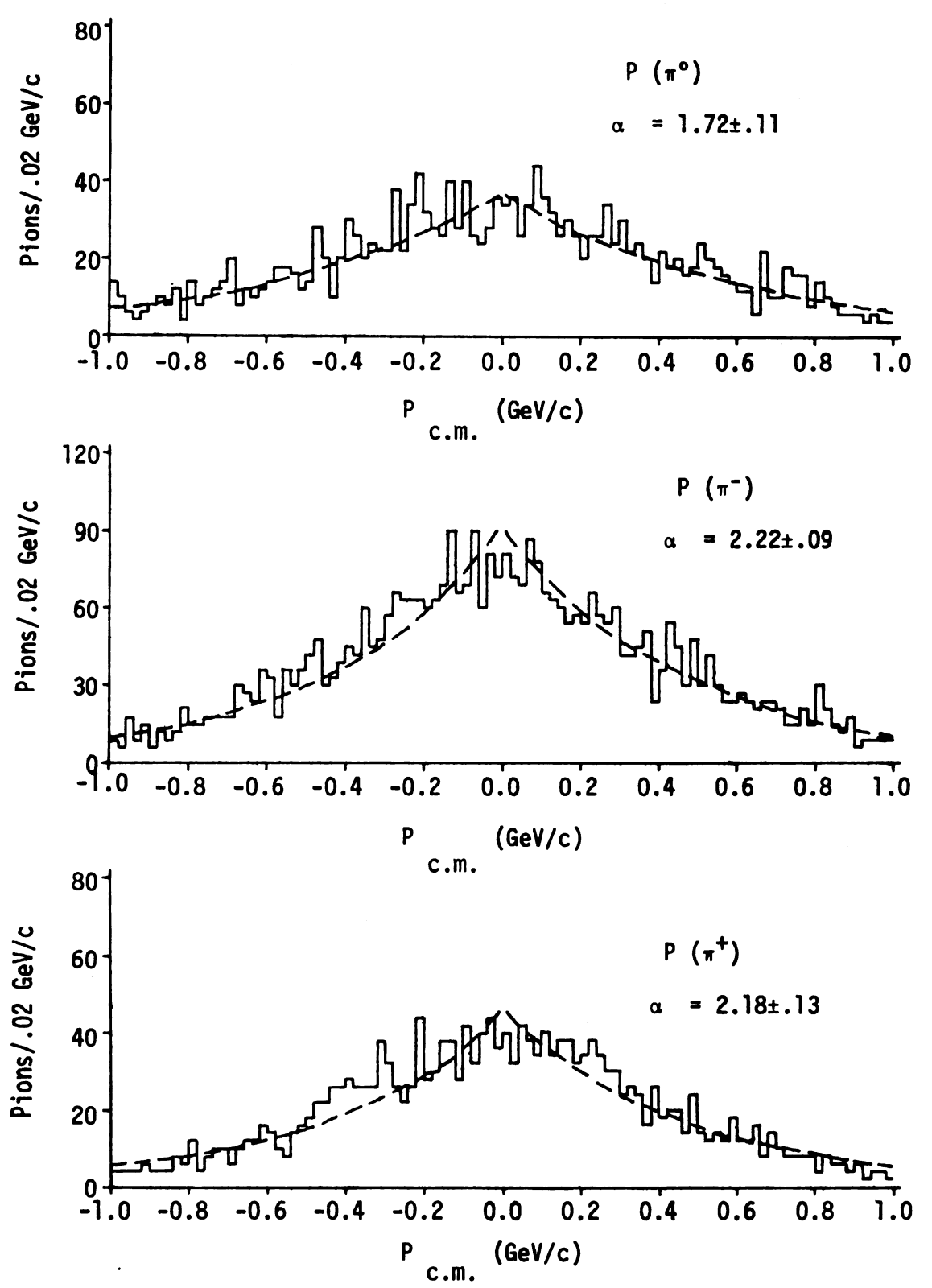


Figure 24.5 Longitudinal momentum distributions from four pion final states between 2.15 and 2.90 GeV/c

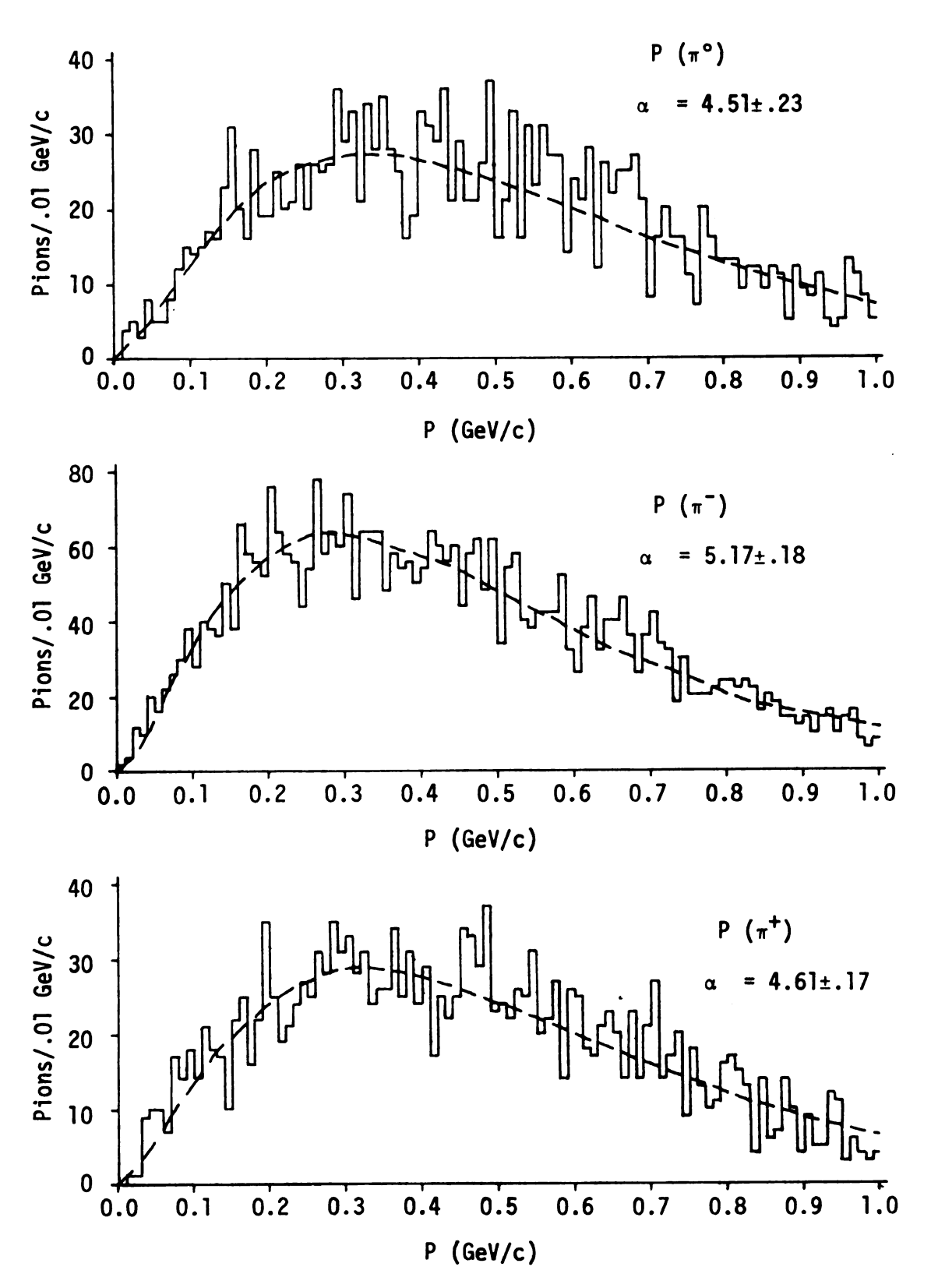


Figure 24.6 Transverse momentum distributions from four pion final states between 2.15 and 2.90 GeV/c

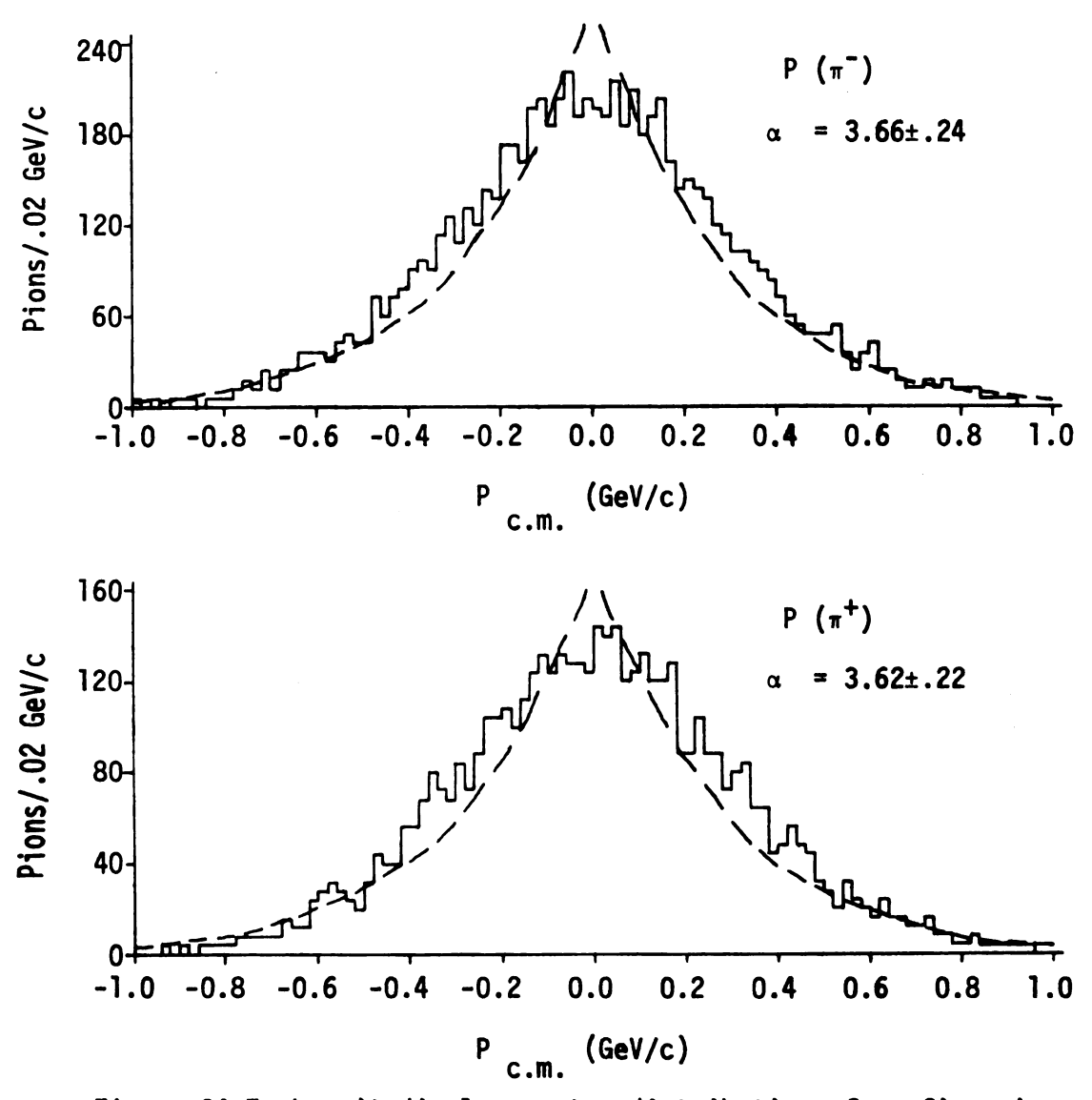
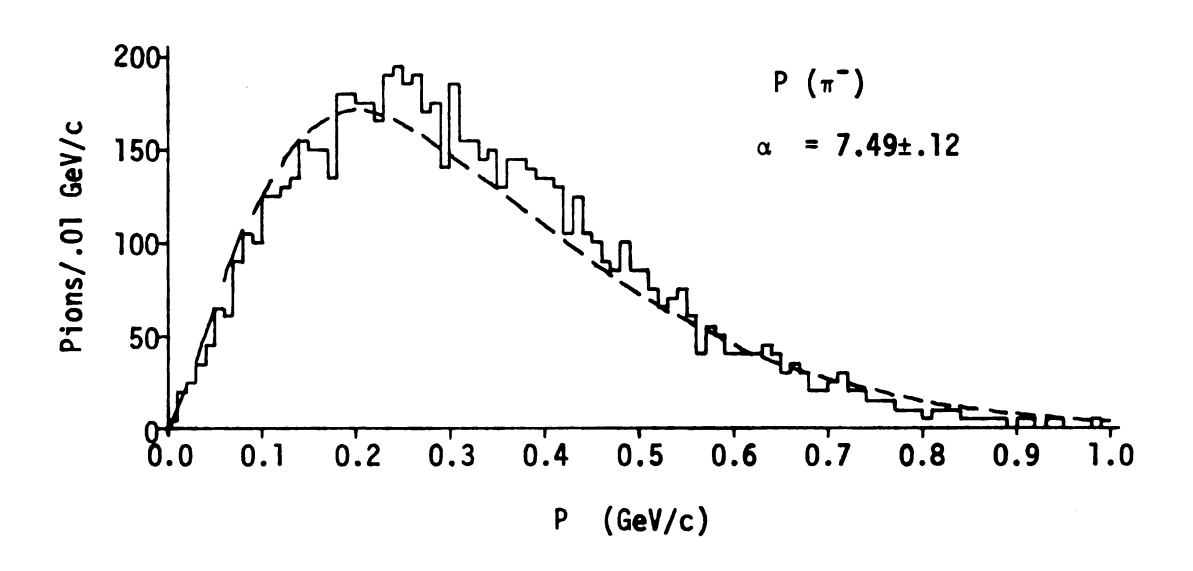


Figure 24.7 Longitudinal momentum distributions from five pion final states between 1.60 and 2.00 GeV/c



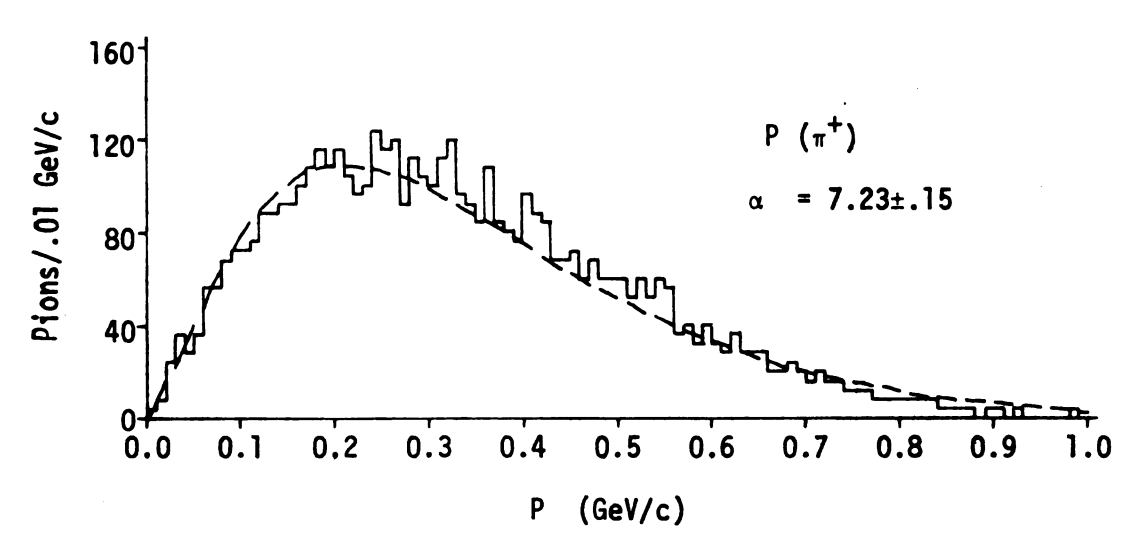
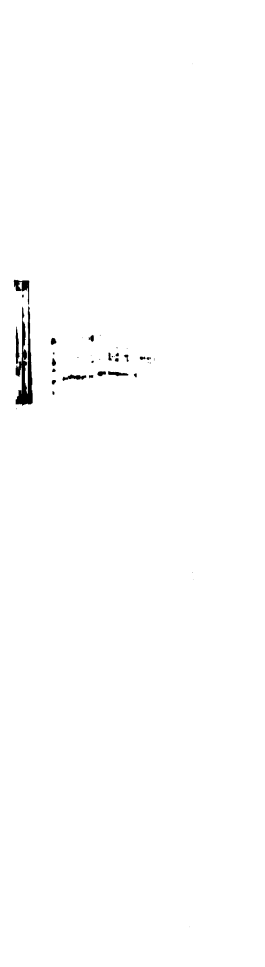


Figure 24.8 Transverse momentum distributions from five pion final states between 1.60 and 2.00 GeV/c



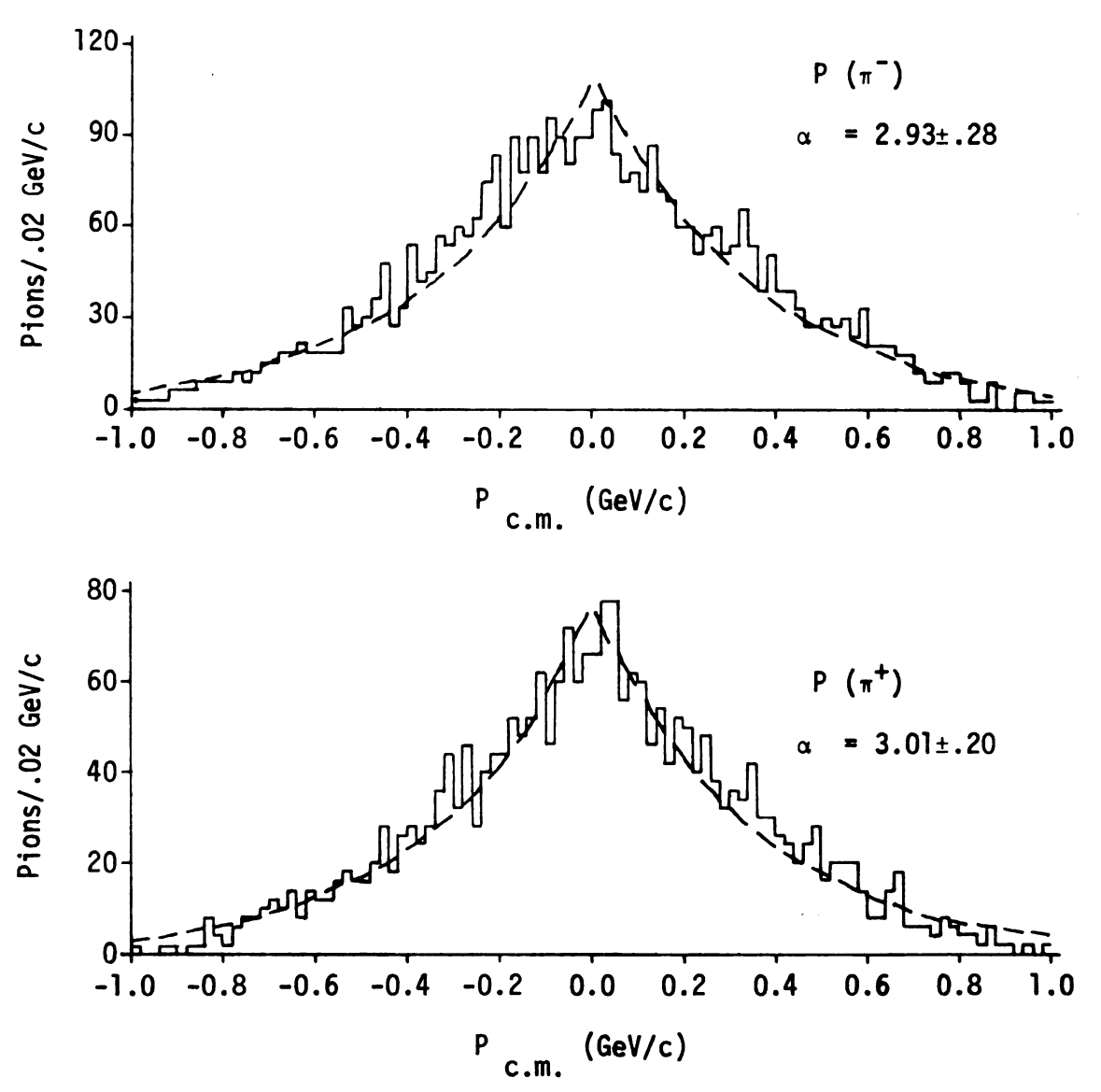
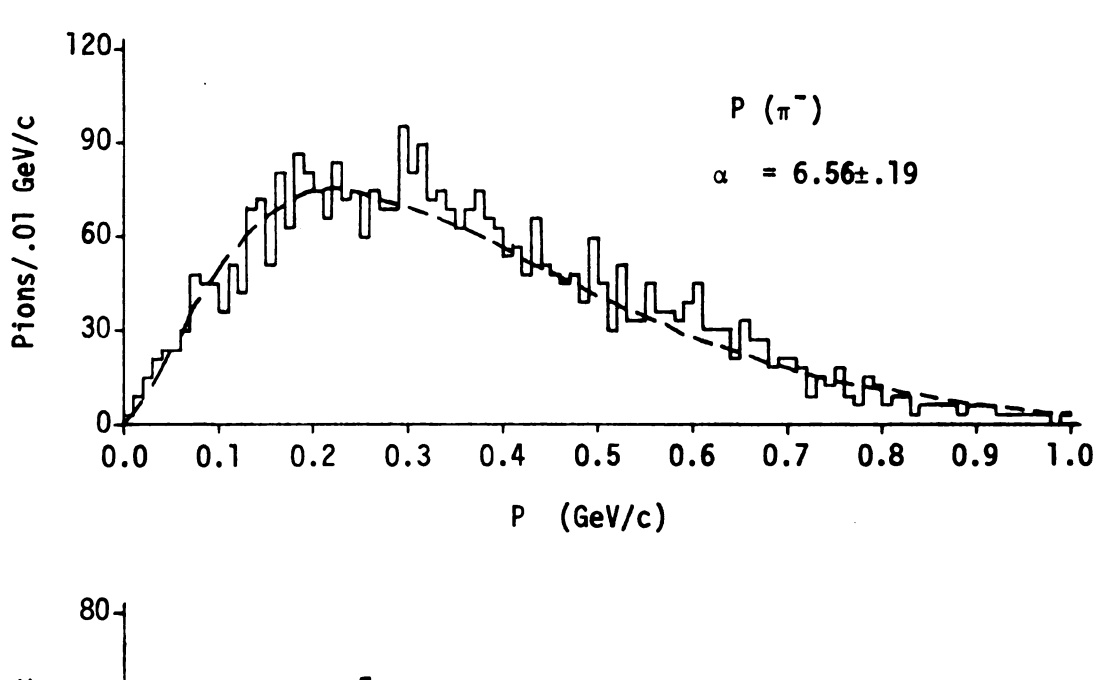


Figure 24.9 Longitudinal momentum distributions from five pion final states between 2.15 and 2.90 GeV/c

22 779



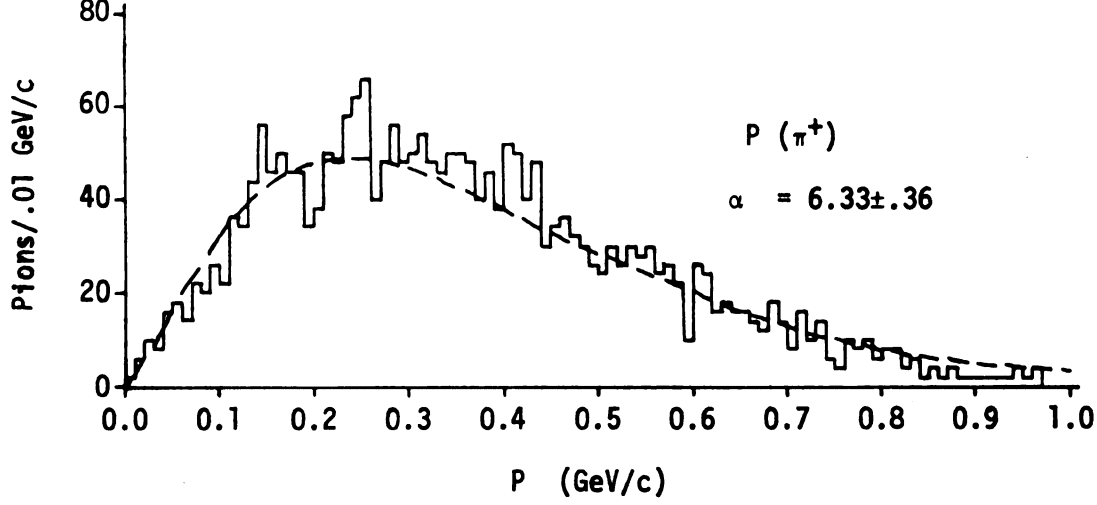


Figure 24.10 Transverse momentum distributions from five pion final states between 2.15 and 2.90 GeV/c

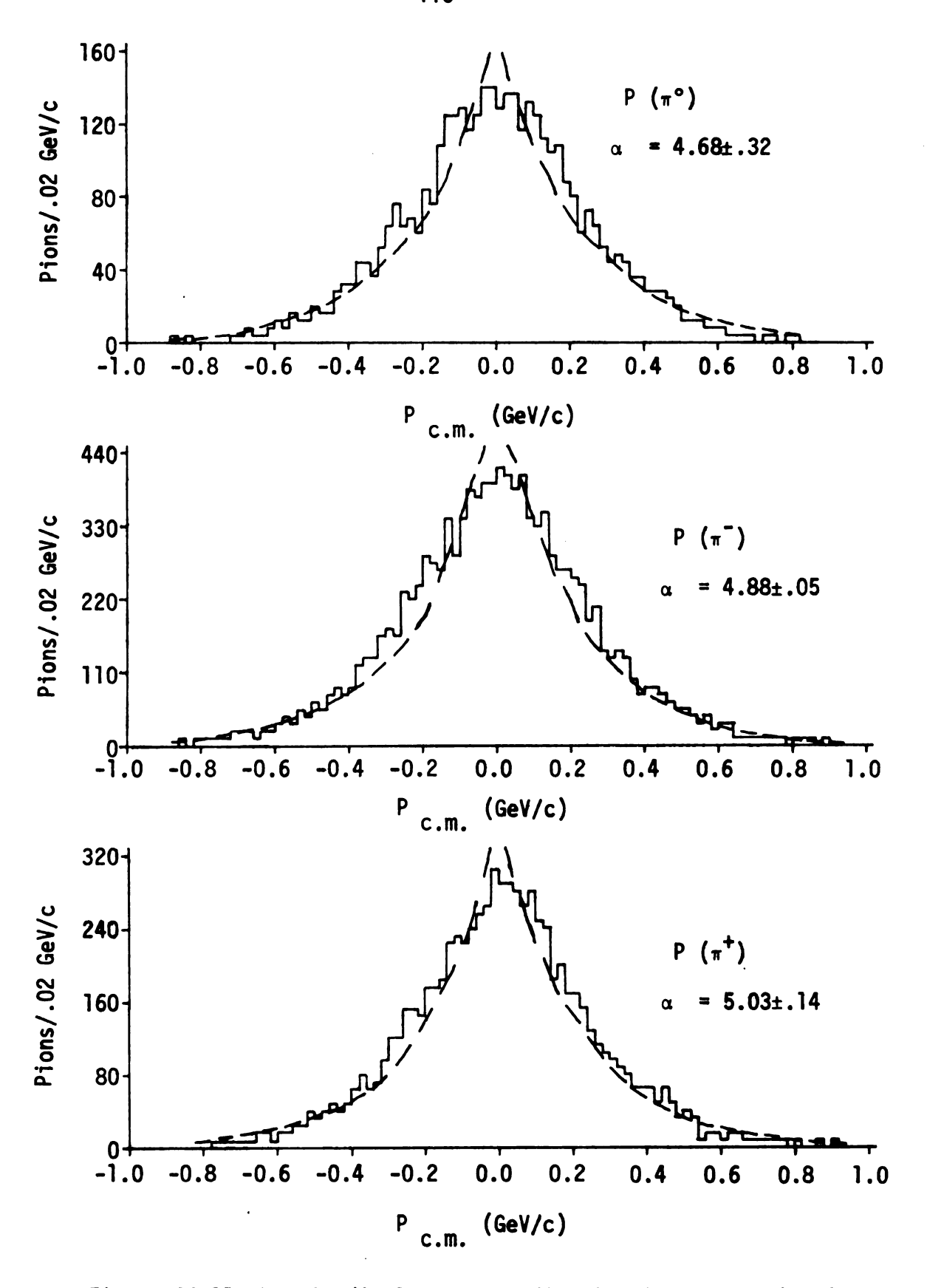


Figure 24.11 Longitudinal momentum distributions from six pion final states between 1.60 and 2.00 GeV/c

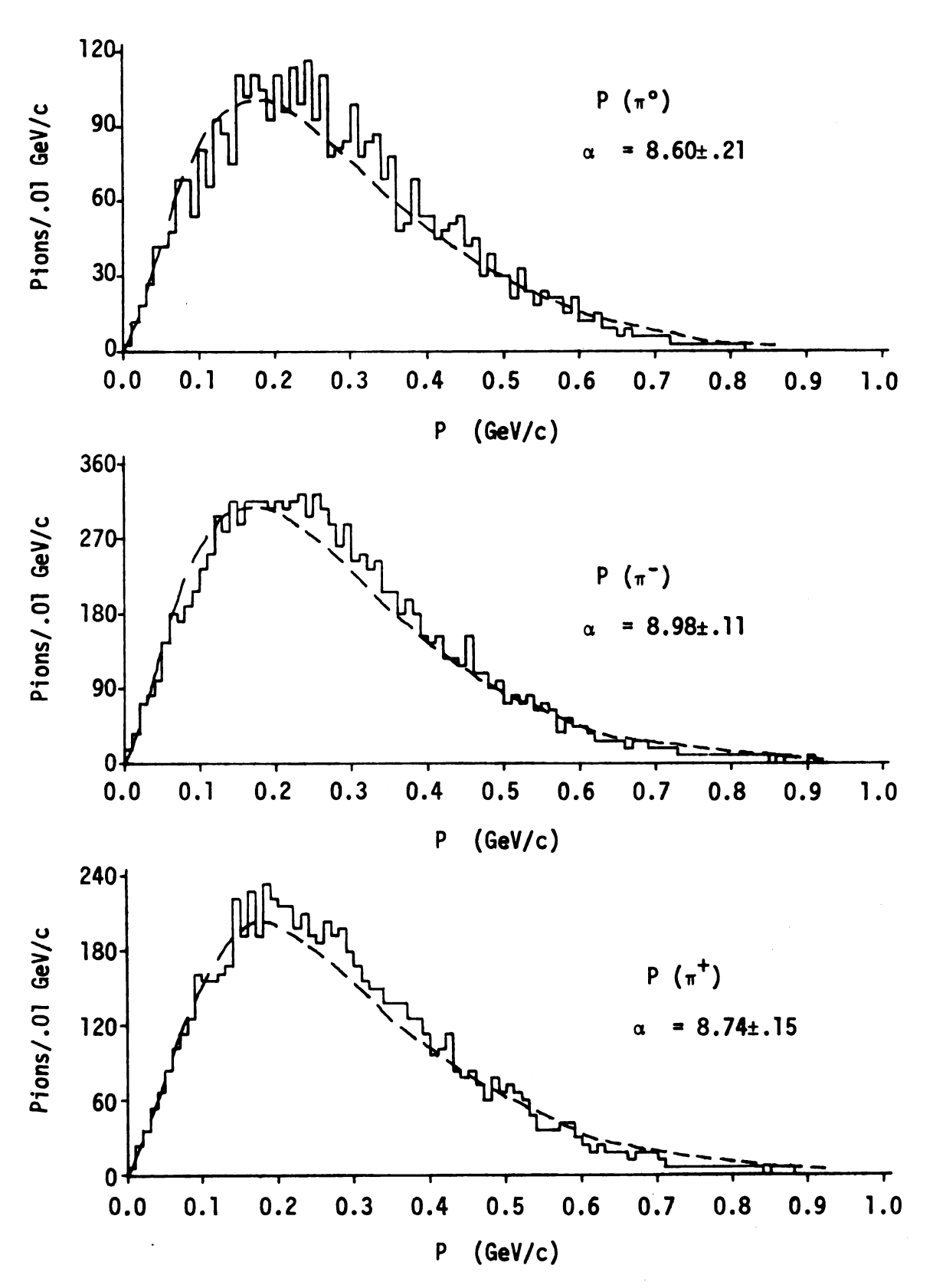
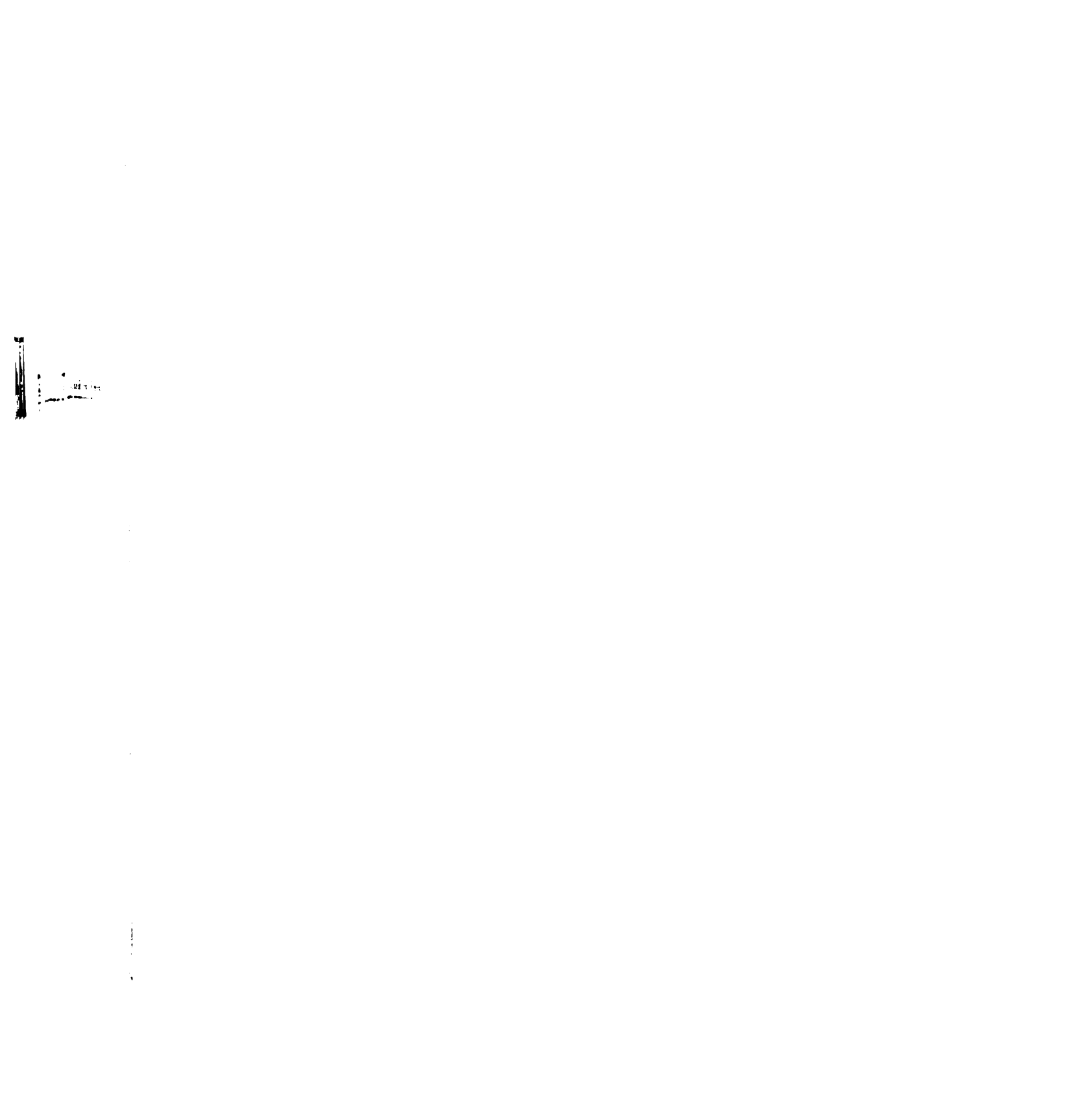


Figure 24.12 Transverse momentum distributions from six pion final states between 1.60 and 2.00 GeV/c



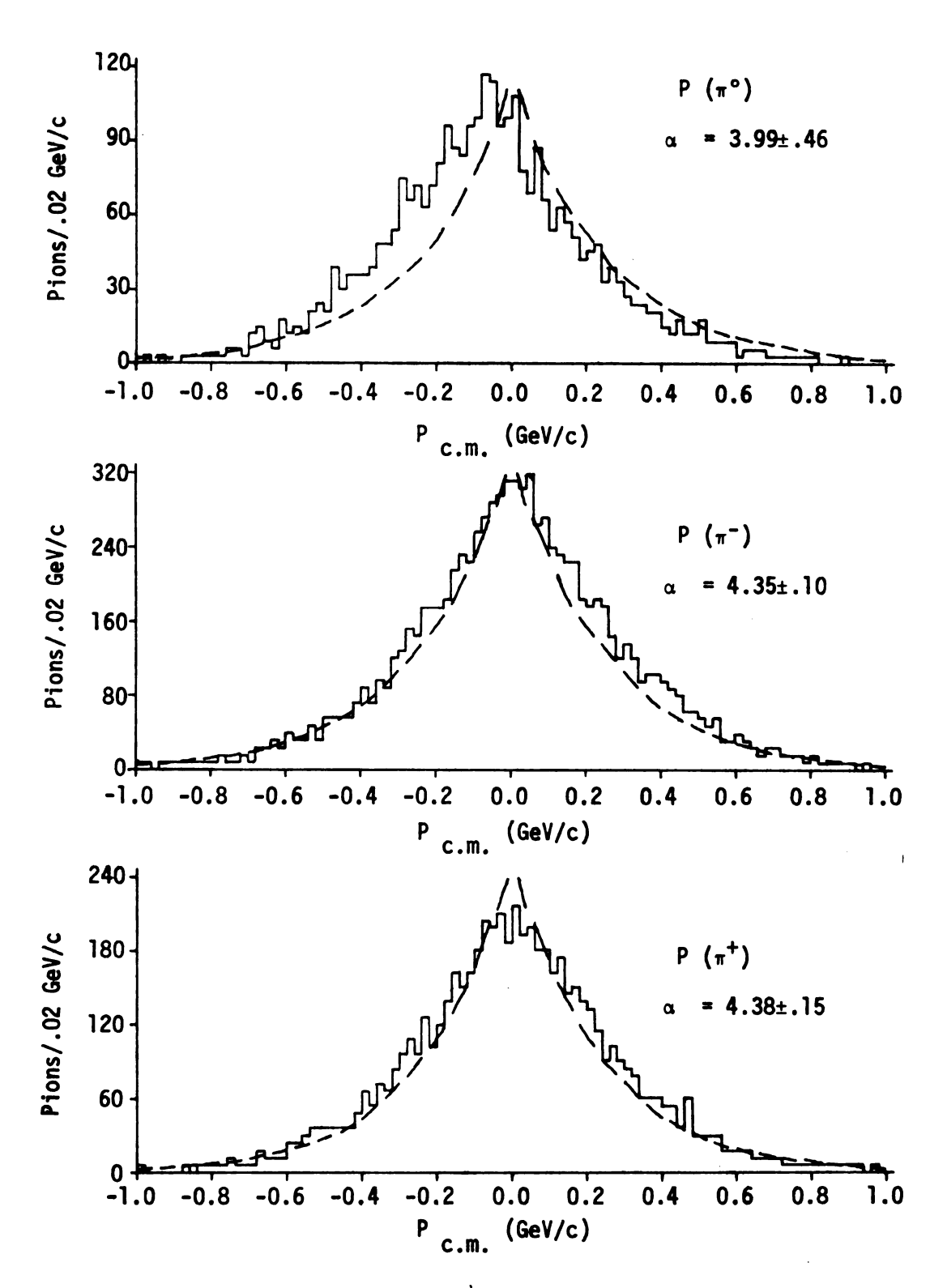


Figure 24.13 Longitudinal momentum distributions from six pion final states between 2.15 and 2.90 GeV/c

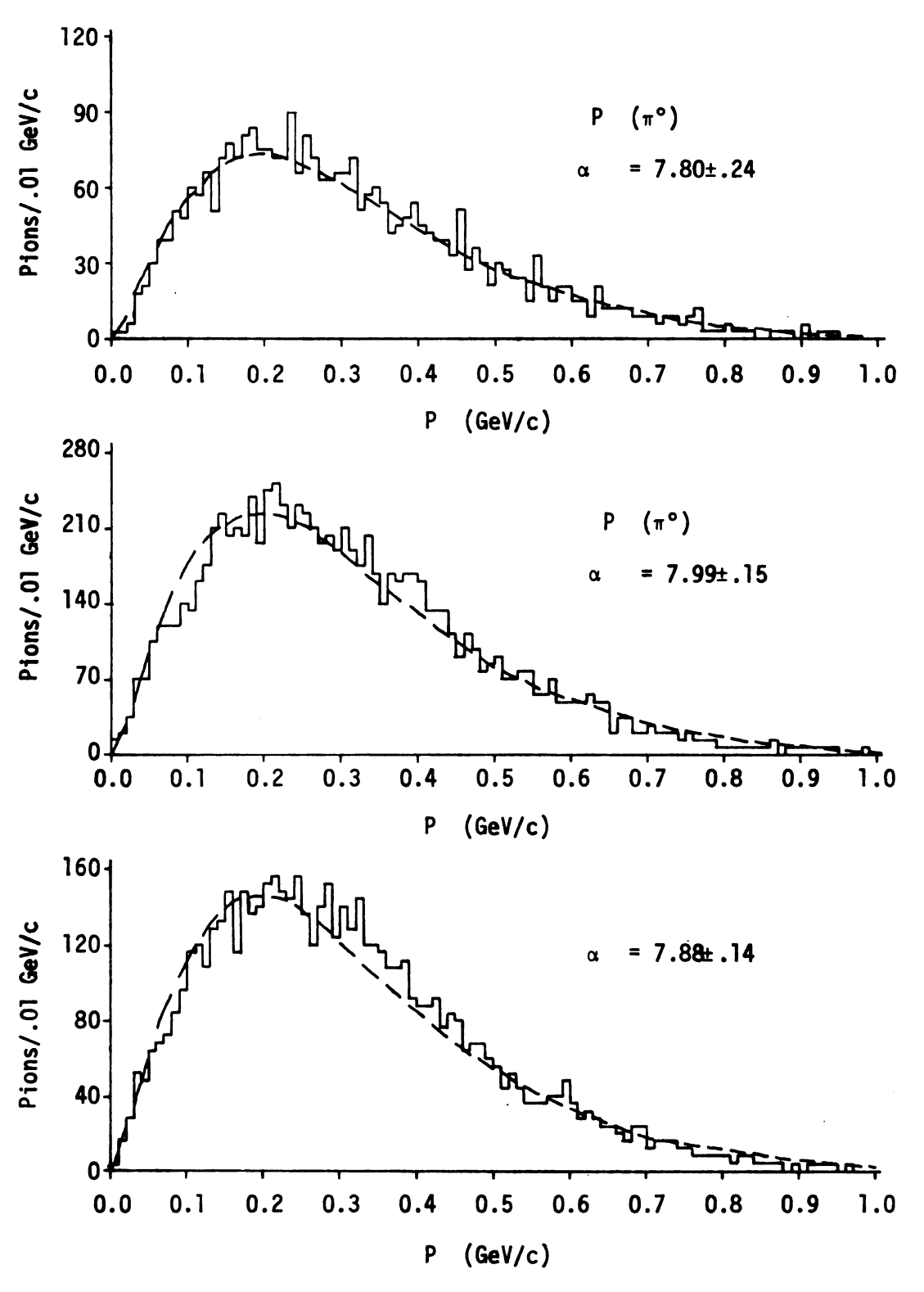


Figure 24.14 Transverse momentum distributions from six pion final states between 2.15 and 2.90 GeV/c

CHAPTER 8

MODELS FOR NUCLEON-ANTINUCLEON ANNIHILATIONS

A Reggeized multiperipheral model for high energy multiple particle reactions has been proposed by Chan, Loskiewicz, and Allison³⁸, hereafter referred to as CLA. Many attempts have been made at applying the CLA model to nucleon-antinucleon interactions, although, to date, none of these attempts have made any explicit calculations for the antiproton-neutron annihilations. Several features of the CLA model are independent of the charge of the initial particles, requiring only that the interaction be a nucleon-antinucleon annihilation and these features will be discussed.

Chen³⁹, using the CLA model, calculated the total cross sections as a function of incident momentum for various multiplicities of proton-antiproton annihilations into pions. Each multiple-production process

$$A + B \rightarrow 1 + 2 + ... + n$$
 (21)

was calculated from incoherently superimposed amplitudes of the form

$$|A| \propto \frac{n-1}{i-1} \left(\frac{g_i s_i + ca}{s_i + a} \right) \left(\frac{s_i + a}{a}^{\alpha_i} \right) \left(\frac{s_i + b_i}{b_i} \right)^{\beta_i t_i}$$
 (22)

where a, b_i , c, and g_i are constant parameters, α_i and β_i are the intercept and slope of the i^{th} Regge pole trajectory, and s_i and t_i are

defined by

$$s_i = (p_i + p_{i+1})^2 - (m_i + m_{i+1})^2$$
 (23)

$$t_i = (p_A - \sum_{r=1}^i p_r)^2$$
 (24)

 $\mathbf{p}_{\mathbf{A}}$ being the center-of-mass momentum of the beam particle.

In the case of nucleon-antinucleon annihilations into pions, only the N and Δ trajectories are allowed to exchange. It is well known 40 that the coupling strength of the Δ -trajectory is about one order of magnitude weaker than the coupling strength of the N-trajectory. Therefore, only the N-trajectory was used in the calculation and the independent amplitudes needed for each multiplicity are shown in Figure 25. In the reaction $\bar{p}n \rightarrow m\pi$, there is only a single amplitude which contributes to the odd multiplicity, m, reactions while there are m numerically equal but physically distinct amplitudes needed for each even multiplicity reaction.

Equation 22 was simplified by Chen to

$$|A| = C_{m_{i=1}}^{m-1} (1 + \frac{h}{(1 + s_{i/a})}) (1 + s_{i/a})^{\alpha} (1 + s_{i/b})^{\beta t_{i}}$$
 (25)

where c/g - 1 was replaced by h and the value 0.077 corresponding to the c/g ratio determined by CLA was used. The Regge parameters, α and β of the linear nucleon trajectory, were fixed at -0.38 and 0.88 respectively. The energy scale factors of a=0.1 and b=3.0 were found by Chen to give the best fits to available data from the reaction $\bar{pp} \rightarrow m\pi$ for multiplicities between 2 and 9. The overall normalization,

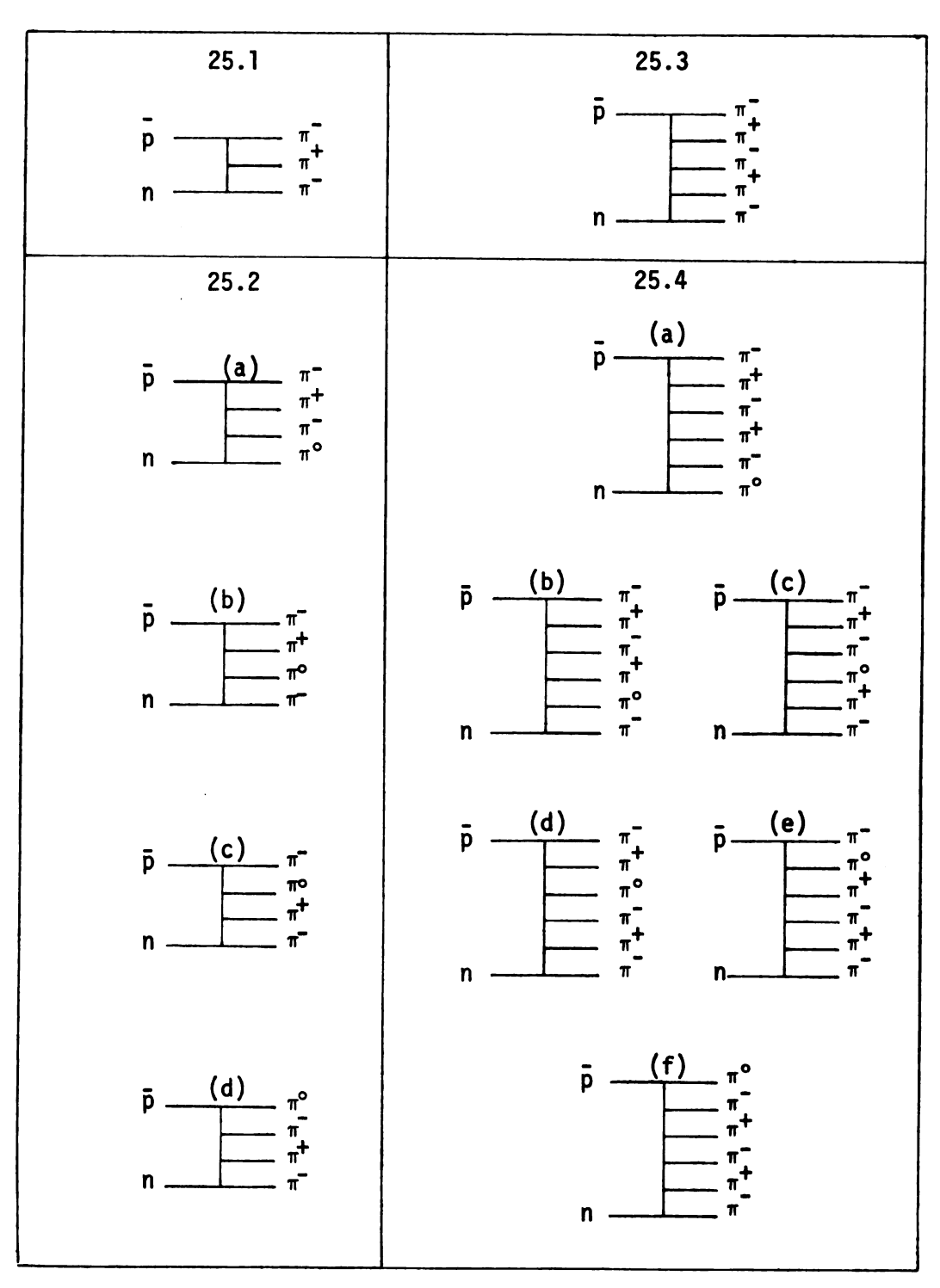


Figure 25. Regge diagrams with nucleon exchange used in the CLA model

- 25.1 Three pion final state
- 25.2 Four pion final state
- 25.3 Five pion final state
- 25.4 Six pion final state

 $\mathbf{C}_{\mathbf{m}}$, was then adjusted to give the best fit to the cross sections for a given multiplicity.

Since the cross sections of the CLA model as applied by Chen to proton-antiproton annihilations, are only dependent upon the parameters of the nucleon trajectory for their physical significance, they can easily be compared with the cross sections from antiproton-neutron annihilations. To compare the cross sections of pp with those from pn. it is only necessary to scale the overall normalization for a given multiplicity. A comparison between an arbitrarily scaled pp prediction and the pn data is shown in Figure 26 along with a similarly renormalized comparison of the predictions of the statistical model calculated by G. van Kuek 41. The scaled pp agrees quite well with the data at all four multiplicities, however, the scale factors for the three through six pion annihilations of 0.64, 3.1, 0.30 and 4.9 are somewhat different from the values of 0.33, 4.0, 0.20 and 6.0 respectively, calculated solely from the number of contributing diagrams. This discrepancy is not surprising since there was some disagreement between the calculated and fitted $\mathrm{C_m}$'s of Chen and also since the CLA model used by Chen does not include resonant production which is highly prevalent in the multipion annihilations.

Due to the lack of CR invariance in p̄n reactions, no direct comparison of the angular and momentum distributions can be made with the predictions from p̄p. However, certain features of the model can be readily deduced and compared with the data. Since the CLA model assumes that all diagrams contribute equally (i.e. the same number of distinct couplings occur in each diagram), it is apparent from the diagrams in

Figure 26. Comparison of the multipion annihilations with the multiperipheral and statistical models. Solid (dashed) curves are predictions of the multiperipheral (statistical) model

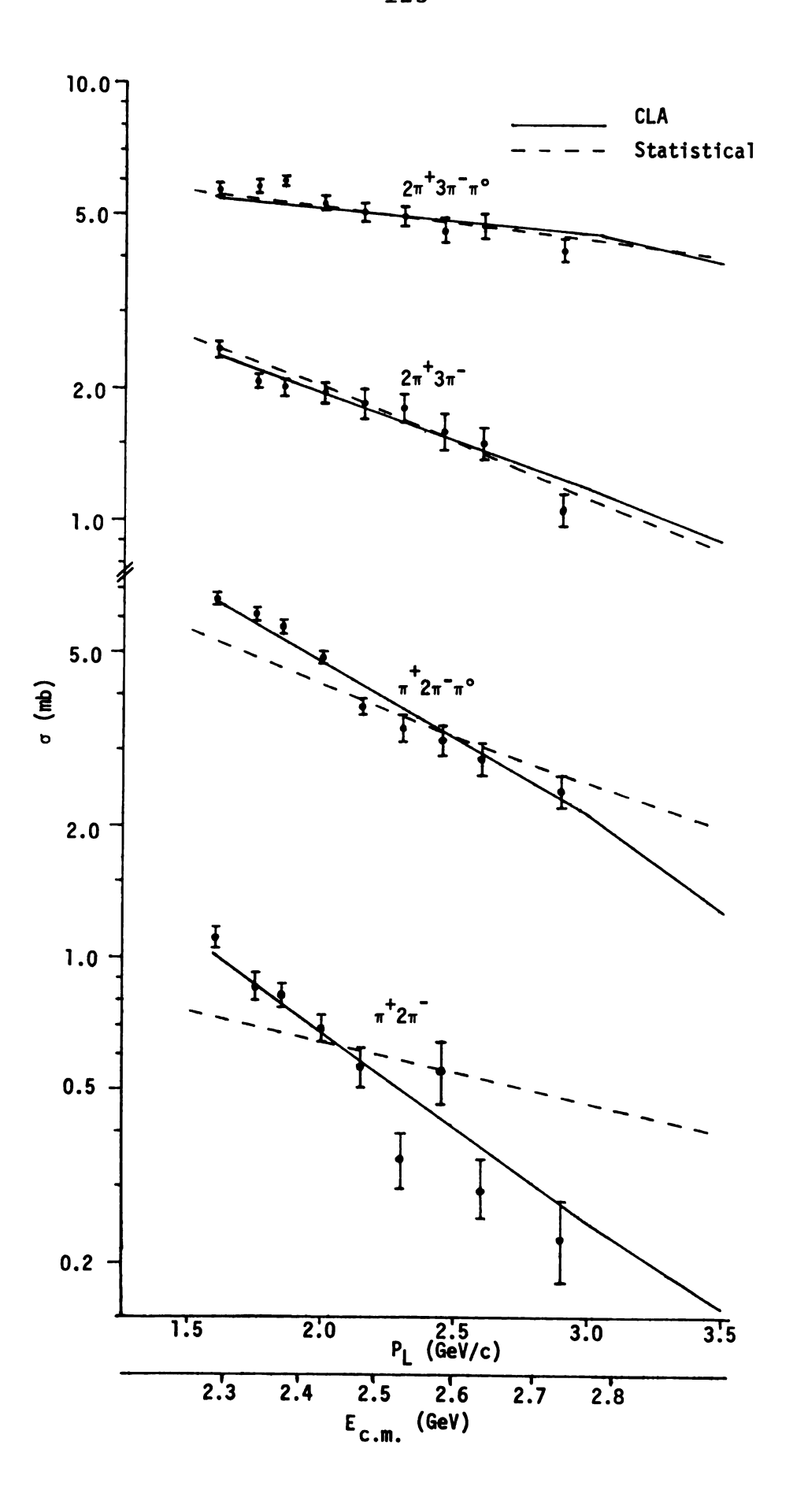


Figure 25 that there should be no asymmetry in the cos $\theta_{\text{c.m.}}$ distributions in any particular charged particle state since each allowed final configuration may be reflected to form another allowed configuration. The three, four and five pion final states are consistent with this prediction, however, there is a definite asymmetry which is increasing with increasing beam momentum in the π^- and π° charge states of the six pion annihilations. Thus, rather than all diagrams contributing equally, there appears to be an emerging dominance of diagram 25.4a over the others. This asymmetry can be attributed to a charge following effect of the leading particles. A similar effect may be seen in the four pion annihilations where the asymmetry values of the π° mirror those of the π^- . It is not clear whether or not diagram 25.2a is becoming dominant at the higher momenta and additional experiments above 3.0 GeV/c are needed to confirm any definite trend.

Collimation on the other hand, is independent of CR invariance and therefore independent of the folding used in $\bar{p}p$ analysis. Although their results differ significantly, both Chen and Roberts 43 predict that the collimation values should be increasing with momentum in the 1.5 GeV/c to 3.0 GeV/c momentum range. They also find that the rate of increase is less as the multiplicity increases. Since the CLA model for nucleon-antinucleon annihilations is essentially a series of peripheral processes without double charge exchange, it is natural to expect that the particles on the ends of the chain will make the greatest contribution to the deviation of the collimation parameters from unity. In a manner similar to $\bar{p}p$ the collimation parameters for for π^- in the three and five pion final states in $\bar{p}n$ exhibit an

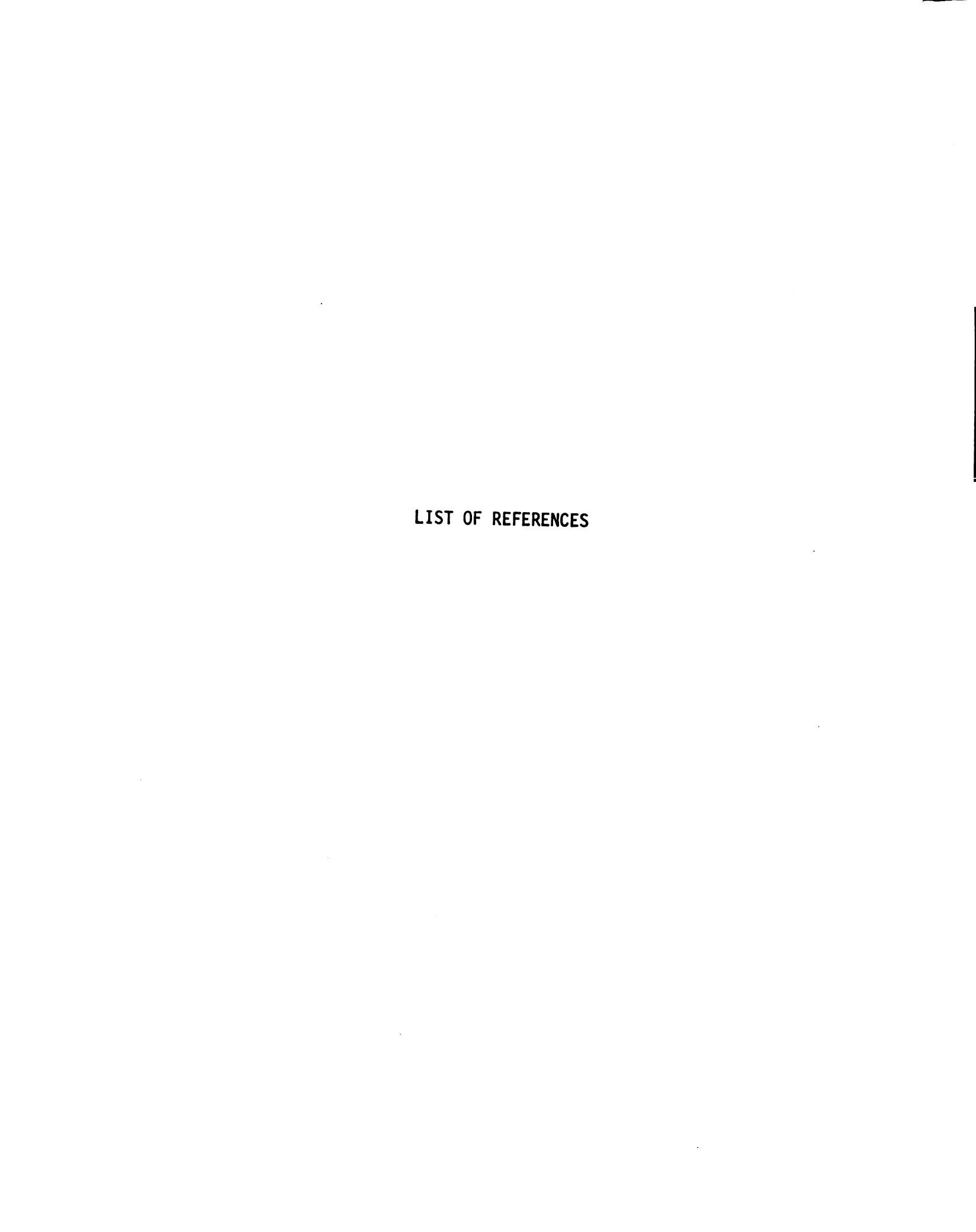
increase with increasing momentum and with a slope which is less in the five pion final state than in the three pion final state. Likewise, the collimation parameters for the π^+ , which barring double charge exchange, are always internal to the chain, are consistently smaller than the corresponding parameters for the π^- and π° in all multiplicities. While the collimation parameters for the π^- and π° in the four and six pion final states exhibit the decrease in magnitude with increasing multiplicity, they fail to show the momentum dependence seen in $\bar{p}p$ as well as in the three and five pion final states of $\bar{p}n$.

CHAPTER 9

SUMMARY AND CONCLUSIONS

Topological and reaction cross sections for antiprotons interacting with deuterons and resonant production cross sections for antiproton-neutron annihilations into three through six pions have been determined for incident momenta between 1.60 GeV/c and 2.90 GeV/c. The cross sections for single and double pion production without annihilation as well as the cross sections for the hydrogen like, pp, reactions are in good agreement with other experiments lending confidence in the procedure used to analyze the data. The overall momentum to momentum dependence of the topological cross sections fail to show enhancements sufficient to explain the structures in the isospin one total cross sections, although their errors do not rule out such structure in any particular topology. The reaction cross sections, where any enhancement may be more noticeable, similarly fail to show evidence for any significant structure with the exception of the cross section for the reactions $\bar{p}d \rightarrow p\pi^{+}2\pi^{-}\pi^{\circ}$ and $\bar{p}d \rightarrow p2\pi^{+}3\pi^{-}\pi^{\circ}$ which exhibit turnovers in the region of the isospin one structure at 2350 MeV center-ofmass energy. These turnovers, which may be reflected in the resonance production reactions $\bar{p}d \rightarrow p\omega^{\circ}\pi^{-}$, $\bar{p}d \rightarrow p\omega^{\circ}\pi^{+}2\pi^{-}$ and remotely $\bar{p}d \rightarrow p\omega^{\circ}p^{\circ}\pi^{-}$, cannot be conclusively determined to be contributing to the structure without further investigation at lower energies. Particular emphasis may be given to the resonance production channel $\omega^{\circ}\pi^{+}\pi^{-}\pi^{-}$ which appears to follow the general trends of the $\bar{p}d \rightarrow p2\pi^+3\pi^-\pi^\circ$ reaction cross section. Investigation of the resonance production cross sections in the annihilation channels has yielded no evidence for contributions to the I=1 structures with the exception of a K*K enhancement at 2360 MeV seen both in this experiment and in a $\bar{p}p$ experiment. The resonance production cross sections for $\bar{p}n + \rho^{\circ}\rho^{\circ}\pi^{-}$ have been investigated for a possible relation to the $\rho^{\circ}\rho^{\circ}\pi^{\circ}$ enhancement from $\bar{p}p$ annihilations at 1.32 GeV/c (2190 MeV center-of-mass energy) reported by Kalbfleisch et. al.⁴. If this enhancement from the pp annihilations is reflected in the $\bar{p}n$ annihilations, the apparent width is much greater than the Γ < 80 MeV/c² reported by the authors of reference 4.

The general features of the multipion annihilations and their angular and momentum distributions have been compared with various models. The multiperipheral multi-Regge model of CLA far more accurately describes the slopes of the cross sections for the multipion annihilations than does the statistical model. Although no direct calculation of either model was made, it was observed that some modification is necessary to include the effects of charge following.



LIST OF REFERENCES

- 1) R. J. Abrams et al., Phys. Rev. D1 (1970) 1917.
- 2) R. L. Cool et al., Phys. Rev. D1 (1970) 1887.
- 3) W. A. Cooper et al., Phys. Rev. Letters, 20 (1968) 1059.
- 4) G. Kalbfleisch, R. Strand and V. Vanderburg, Phys. Letters <u>29B</u> (1969) 259.
- 5) G. Chikovani et al., Phys. Letters 22 (1966) 233.
- 6) E. W. Anderson et al., Phys. Rev. Lett. 22 (1969) 1390.
- 7) M. N. Focacci et al., Phys. Rev. Lett. 17 (1966) 890.
- 8) B. Y. Oh et al., Phys. Rev. Lett. 24 (1970) 1257.
- 9) Z. Ming Ma and G. A. Smith, Phys. Rev. Lett. 27 (1971) 344.
- 10) D. L. Parker, Ph.D. Thesis, Michigan State University (1971).
- 11) F. T. Solmitz <u>et al.</u>, Lawrence Radiation Laboratory, Alvarez Programming Group Note #117 (1966).
- 12) O. I. Dahl <u>et al.</u>, Lawrence Radiation Laboratory, Alvarez Programming Group Note #126 (1966).
- 13) Nathan, W. Dean, Phys. Rev. Lett. <u>27</u> (1971) 276.
- 14) M. J. Moravcsik, Nuc. Phys. <u>7</u> (1958) 113.
- 15) R. J. Glauber, Phys. Rev. <u>100</u> (1955) 242.
- 16) V. Franco and R. J. Glauber, Phys. Rev. 142 (1966) 1195.
- 17) H. Nicholson et al., Phys. Rev. Lett. 23 (1969) 603.
- 18) J. W. Chapman <u>et al.</u>, Phys. Rev. Lett. <u>21</u> (1968) 1718.
- 19) H. Braun <u>et al</u>., Phys. Rev. <u>D2</u> (1970) 488.

- 20) T. C. Bacon et al., Phys. Rev. 139 (1965) B1420.
- 21) T. C. Bacon et al., Phys. Rev. <u>162</u> (1967) 1320.
- 22) T. C. Bacon et al., Phys. Rev. <u>D2</u> (1970) 463.
- 23) J. Friedman, Lawrence Radiation Laboratory, Alvarez Programming Group Note #156 (1966).
- 24) J. D. Jackson, Nuovo Cimento 34 (1964) 1644.
- 25) G. Goldhaber et al., Phys. Rev. 120 (1960) 302.
- 26) M. Abramovich et al., Nuc. Phys. <u>B20</u> (1970) 209.
- 27) W. W. M. Allison et al., Phys. Rev. Lett. 24 (1970) 618.
- 28) S. M. Flatte et al., Phys. Rev. 145 (1966) 1050.
- 29) S. M. Flatte, Phys. Rev. <u>155</u> (1967) 1517.
- 30) S. M. Flatte, Phys. Rev. <u>D1</u> (1970) 1.
- 31) G. Goldhaber et al., Phys. Rev. Lett. 23 (1969) 1351.
- 32) J. E. Agustin et al., Lett. Nuovo Cimento 2 (1969) 214.
- 33) P. J. Biggs et al., Phys. Rev. Lett. 24 (1970) 1197.
- 34) H. Alvensben et al., Phys. Rev. Lett. 27 (1971) 888.
- 35) H. Pilkuhn: The Interactions of Hadrons, John Wiley & Sons, Inc., New York (1967).
- 36) J. W. Elbert et al., Phys. Rev. Lett. 20 (1968) 124.
- 37) D. B. Smith, R. J. Sprafka and J. A. Anderson, Phys. Rev. Lett. 23 (1969) 1064.
- 38) Chan Hong-Mo, J. Loskiewicz, and W. W. Allison, Nuovo Cimento 57A (1968) 93.
- 39) Fong-Ching Chen, Nuovo Cimento 62A (1969) 113.
- 40) V. Barger and D. Cline, Phys. Rev. Lett. <u>21</u> (1968) 392.
- 41) G. van Kuek, DESY Preprint 68/10, "Zur Anwendung des Statistischen Modells mit Drehimpulserhaltung," 1968.

- 42) J. Benecke et al., Phys. Rev. 188 (1969) 2159.
- 43) R. G. Roberts, Nuc. Phys. <u>B13</u> (1969) 662.
- 44) Bettini et al., Nuovo Cimento <u>1A</u> (1971) 333.

